



Adaptive EAF online control based on innovative sensors and comprehensive models for improved yield and energy efficiency

(AdaptEAF)

FINAL REPORT

Adaptive EAF online control based on innovative sensors and comprehensive models for improved yield and energy efficiency (AdaptEAF)

European Commission

Directorate-General for Research and Innovation

Directorate D - Industrial Technologies

Unit D.4 — Coal and Steel

Contact Hervé Martin

E-mail RTD-PUBLICATIONS@ec.europa.eu

European Commission

B-1049 Brussels

Manuscript completed in 2019.

This document has been prepared for the European Commission however it reflects the views only of the authors, and the Commission cannot be held responsible for any use which may be made of the information contained therein.

More information on the European Union is available on the internet (<http://europa.eu>).

Luxembourg: Publications Office of the European Union, 2019

PDF

ISBN 978-92-79-98359-7

ISSN 1831-9424

doi: 10.2777/1906

KI-NA-29-547-EN-N

© European Union, 2019.

Reuse is authorised provided the source is acknowledged. The reuse policy of European Commission documents is regulated by Decision 2011/833/EU (OJ L 330, 14.12.2011, p. 39).

For any use or reproduction of photos or other material that is not under the EU copyright, permission must be sought directly from the copyright holders.

All pictures, figures and graphs © VDEh-Betriebsforschungsinstitut GmbH (BFI), RFSP-CT-2014-00004 AdaptEAF

European Commission

Research Fund for Coal and Steel

Adaptive EAF online control based on innovative sensors and comprehensive models for improved yield and energy efficiency

(AdaptEAF)

B. Kleimt, R. Pierre, T. Kordel
VDEh-Betriebsforschungsinstitut GmbH (BFI)
Sohnstr. 65, 40237 Düsseldorf, Germany

T. Rekersdrees, L. Schlinge, O. Hellermann, S. Elsabagh
Georgsmarienhütte GmbH (GMH)
Neue Hüttenstraße 1, 49124 Georgsmarienhütte, Germany

V. Haverkamp, S. Gogolin
Helmut-Schmidt-Universität (HSU)
Holstenhofweg 85, 22043 Hamburg, Germany

Grant Agreement RFSP-CT-2014-00004
01.07.2014 – 30.06.2017

Final report

Directorate-General for Research and Innovation

2019

EUR 29547 EN

Table of contents

1.	Final Summary	5
1.1	Overall project objectives	5
1.2	Consortium	5
1.3	Summary of obtained results	6
1.4	Concluding overview	15
2.	Scientific and technical description of results	17
2.1	Scientific project objectives	17
2.2	Description of activities and discussion	17
2.2.1	<i>WP 1: Application of new measurement devices</i>	17
2.2.2	<i>WP 2: Industrial campaigns to derive additional process information from new measurement devices</i>	46
2.2.3	<i>WP 3: Enhancement of existing process models by using information from newly applied measurement systems</i>	60
2.2.4	<i>WP 4: Application of process control tools based on newly implemented measurement systems and advanced dynamic process models</i>	83
2.2.5	<i>WP 5: Extensive plant trials for online test and evaluation of process control tools</i>	92
3.	Final conclusions	101
4.	Exploitation and impact of the results	103
5.	List of figures	105
6.	List of tables	109
7.	List of References	111

1. Final Summary

1.1 *Overall project objectives*

The main objective of this Pilot & Demonstration project was to set up a new adaptive on-line control for the EAF depending on the properties of the actually charged materials, to optimise the efficiency of the chemical energy input and thus to reduce the total energy consumption and to improve the metallic yield.

Novel sensors and measurement methods for online acquisition of bath level, steel and slag amount, and scrap melting behaviour were to be applied. This additional process information was to be used to enhance the performance and prediction accuracy of previously developed dynamic and statistical models for online monitoring of the process status. Furthermore relevant information on the efficiency of the different energy inputs and the metallic yield of the charged scrap were to be derived.

The on-line information on bath level, steel and slag amount, scrap melting progress and energetic behaviour was to be used for model-based on-line control of scrap charging as well as chemical energy input via burners and oxygen injectors, aiming at:

- Balanced electrical and chemical energy inputs for optimised energetic performance
- Maximised metallic yield of the charged materials (avoiding yield losses by excessive oxidation)
- Optimised furnace practise regarding scrap charging, steel bath level and slag amount

The tools for monitoring, control and technical management of the EAF process were to be implemented, tested and validated at a well-equipped and instrumented 140 t DC electric arc furnace, to demonstrate the energetic, metallurgical and economic benefits.

1.2 *Consortium*

This Pilot & Demonstration project was performed at the DC EAF of the **Georgsmarienhütte GmbH (GMH)**. GMH in Georgsmarienhütte, Germany, is a producer of high-grade construction and quality engineering steel grades, in particular carbon steels, bearing and spring steels as well as low-alloyed and micro-alloyed steels. The annual production is about 900.000 ton of billets. The steel plant is equipped with a 140 t DC furnace, which is well-equipped with different sources of chemical energy input as well as already instrumented with various sensors and a comprehensive process data acquisition system.

Furthermore it involves the two applied research centres **VDEh-Betriebsforschungsinstitut (BFI)** and the **Institute of Automation Technology of Helmut-Schmidt-University (HSU)**, both having broad knowledge and practical experience in the installation of measurement equipment and process control models at the EAF.

In general the research institutes were responsible for the extension and application of the measurement systems and the process models, whereas the steel producer provided production facilities for plant trials and the practical knowledge needed for the installation of the measurement systems and control tools at the EAF.

1.3 Summary of obtained results

1.3.1 WP 1: Application of new measurement devices

Work package 1 dealt with the development and application of new measurement devices and models for assessment of liquid bath level, slag amount and scrap basket filling degree, as well as for monitoring of the scrap melting evolution.

Liquid bath level assessment

Within the project two different measurement systems to assess the liquid bath level before tapping and the hot heel level after tapping were applied at the EAF of GMH:

- o A bath level and slag thickness dip sensor (Heraeus Delta Dist L)
- o A camera-based system in combination with image analysis to determine the bath level at open EAF furnace after tapping

The Delta Dist sensor is a commercially available dip sensor to measure the thickness of the remaining slag and the steel bath level after EAF deslagging, just before EAF tapping. **Figure A** shows a sketch of the Delta Dist probe and the measurement procedure.

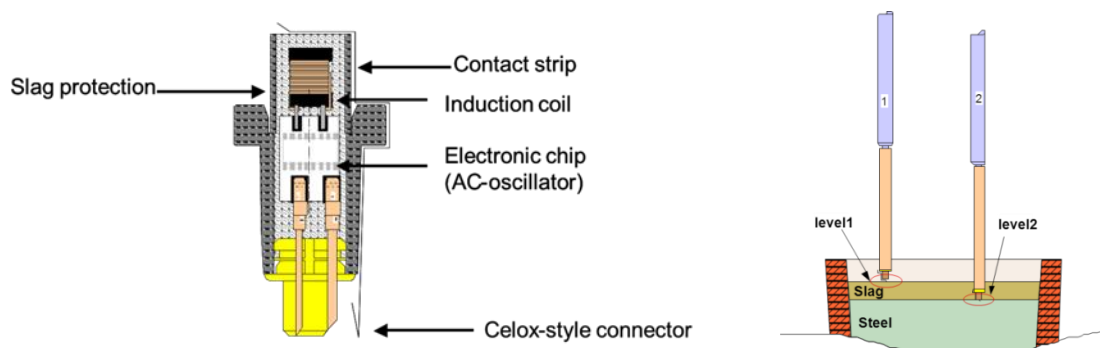


Figure A: Sketch and measurement procedure of the Delta Dist sensor

For immersing the Delta Dist sensor into the steel bath, an already existing lance manipulator is used. The measurement procedure takes about one minute, is performed for every third heat and allows to track the evolution of the hot heel amount. The Delta Dist sensor was calibrated and tested in several trial campaigns. Overall the measurement results were reasonable, only for few heats no measurement value for the slag thickness could be obtained. The steel bath level value is related to the level of the bottom anode after the installation of a new anode, whereas the slag thickness value is an absolute value. The standard deviation, which can be regarded as a value for the accuracy of the measurement, is 11 mm for the steel bath level (corresponding to a weight accuracy of 2.2 t), and 65 mm for the slag thickness (corresponding to a weight accuracy of 3.3 t).

In addition three CCD cameras were mounted in a protective housing and installed above the furnace to monitor the furnace with open roof. An image analysis software was developed to determine the liquid bath level after tapping. **Figure B** shows the view of one of the cameras into the open furnace, and a corresponding grey value image with detection of the hot heel level.

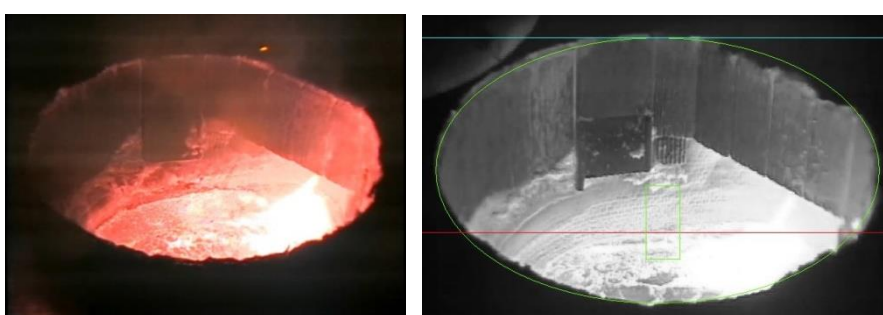


Figure B: View from the position of camera no. 3 into the furnace shell with hot heel level

Slag amount assessment

For monitoring of deslagging an IR camera with side view on the slag tapping stream was mounted at the GMH furnace. The detection of liquid steel carry-over during deslagging based on IR image analysis was investigated and results of camera based steel detection were compared to operator findings. Camera position and exemplary IR images are shown in **Figure C**.

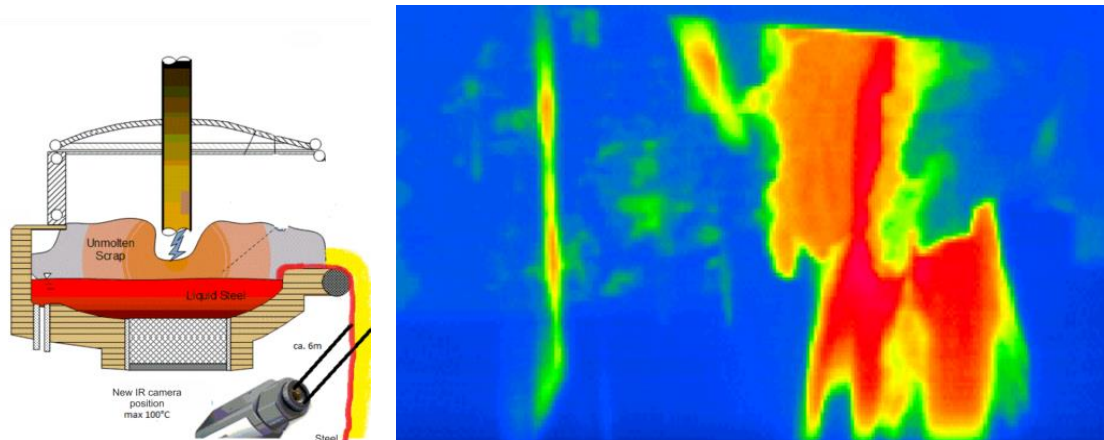


Figure C: Position of IR camera for slag tapping supervision and example IR image

In addition process data for set up of a slag balance calculation, comprising slag analyses and slag former additions for a larger amount of heats treated at the GMH furnace were provided.

Scrap basket filling level assessment

For assessment of the scrap basket filling degree, images of the basket were acquired right before charging into the EAF together with information on the mass of the different loaded scrap types. The scrap filling level was quantified by a suitable image analysis, as shown in **Figure D**.



Figure D: Image of scrap baskets with detection of filling degree

The mean scrap density in the basket was derived from the filling level and the loaded scrap mass. By means of a regression calculation, also the effective density of individual scrap types was determined. In addition a laser based line scanner was tested to assess the filling degree of the scrap baskets, however it was found that it could not provide reliable information, and also the maintenance effort was too high.

Scrap meltdown behaviour assessment

For the assessment of scrap meltdown behaviour vibration sensors and an already existing spectrometer system were tested. Two piezoelectric vibration sensors for two directions were installed at the EAF furnace shell and connected to a data acquisition system for frequency spectrum analysis. **Figure E** shows the position and the mounting of the sensors at the GMH furnace shell.



Figure E: Positions and mounting of the vibration sensors at the GMH furnace

A spectrometer system had previously been installed inside a water-cooled box inside one cooling panel of the GMH DC furnace. The set-up is drafted in **Figure F**. It consisted of two spectrometers with different viewing angles. Despite of first promising results regarding the detection of the level of unmolten scrap in the furnace, it was later decided to unmount the devices due to its considerable maintenance and repair effort.

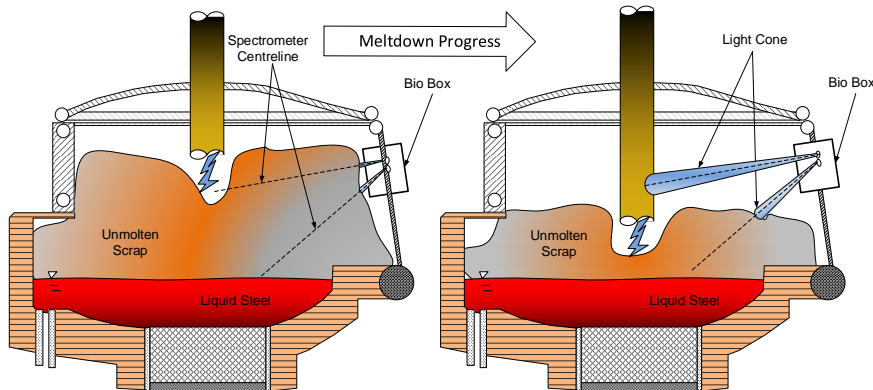


Figure F: Observation of the meltdown progress using a spectrometer system

1.3.2 WP 2: Industrial campaigns to derive additional process information from new measurement devices

Work Package 2 dealt with the derivation of additional process information from the new measurement devices regarding hot heel and slag amount as well as melting behaviour of the scrap.

Determination of hot heel amount

The amounts of steel weight and hot heel were estimated on the basis of the Delta Dist dip measurements and metallic yield calculations. To transfer the liquid bath level measurement into the liquid steel weight, a simple model of the furnace volume, considering the refractory wear during a furnace campaign between two changes of the bottom anode was used. **Figure G** shows the evolution of liquid steel and hot heel amount for a longer sequence of heats. The values coming from the level measurements are indicated by dots. For heats without measurements the follow-up of the amounts was performed according to the expected metallic yield of the charged materials.

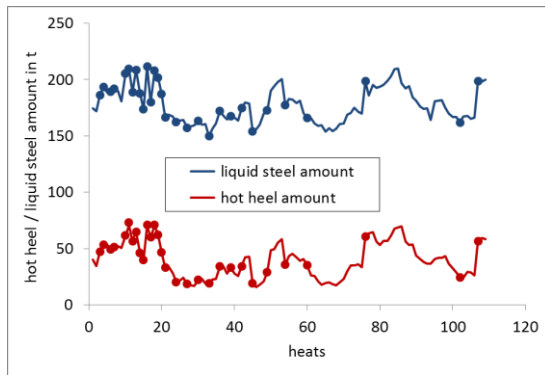


Figure G: Follow-up of liquid steel and hot heel amount at the GMH furnace

The amount of the hot heel was also estimated on the basis of an analysis of the images taken after EAF tapping. As shown in **Figure H**, both methods were compared, with a reasonable correlation. For comparison the dip sensor measurement needs to be corrected by the tapping weight which imposes an uncertainty on the measurement results. On the other hand the image analysis has an accuracy of about 5 pixels which corresponds to about 10 cm in height. Nevertheless, the accuracy of the methods was found to be sufficient to control the hot heel at a constant level.

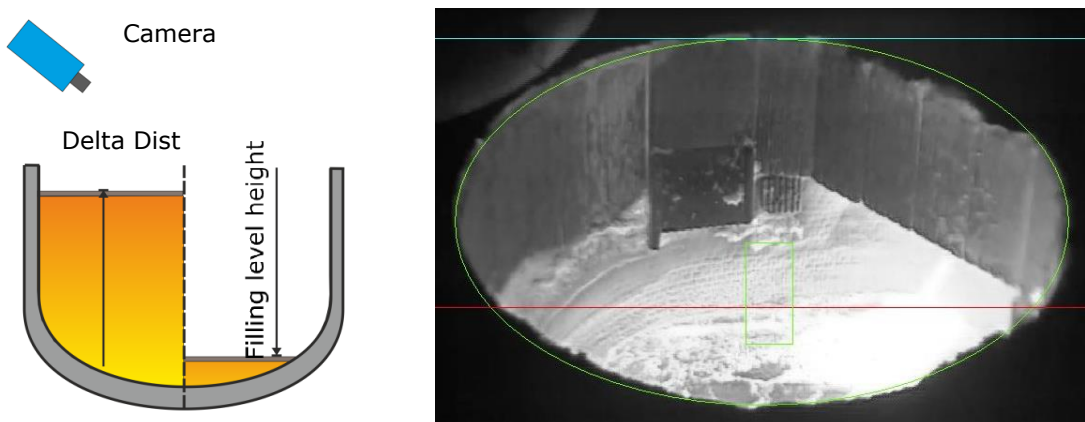


Figure H: Hot heel level measurement with Delta Dist sensor and image analysis

Determination of slag amount

The slag amount has been estimated from the provided GMH process data on the basis of a CaO balance, delivering reliable results. The calculated slag weights were compared to the measured ones derived from the slag pot weight. The remaining slag amount at the beginning of the following heat can be estimated based on the dip measurements. **Figure I** shows the evolution of the remaining slag weight together with the measured values pointed out by dots. The trend of the slag weight shows significant variations in a range between 0 and 30 t.

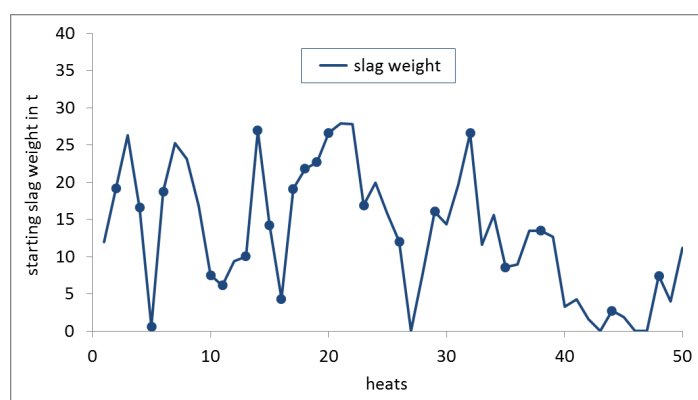


Figure I: Evolution of the remaining slag in the furnace for a trial campaign

Monitoring of scrap melting behaviour

The monitoring of the scrap melting behaviour was performed via the newly installed vibration sensors, the permanently installed off-gas analysis system based on a mass spectrometer, and – in the beginning of the project – by the existing spectrometer system. **Figure J** exemplarily shows the overall vibration RMS signals of the two installed sensors during one complete melt. The scrap basket charging process is indicated by high peaks, during bore down and main meltdown phases the vibration levels quickly rise, afterwards they slowly decline along the progress of meltdown. During the liquid bath phase almost constant low levels are observed. For some heats, in parallel the signals from the spectrometer were recorded (right part of **Figure K**). Towards the end of the first basket's meltdown phase, the spectrometer signal starts to rise. This indicates that the solid scrap has collapsed so that electric arc radiation arrives at the spectrometer lens. Despite these promising results, the spectrometer system was removed from the furnace as explained above.

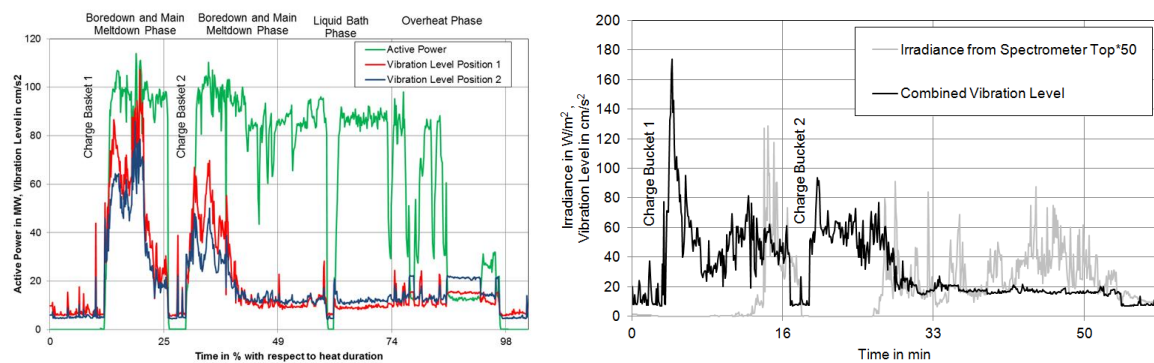


Figure J: Vibration Levels (left), spectrometer signal (right) and Active Power during an EAF melt

For better graphical representation and for modeling a dimensionless logarithmic vibration number was defined, as shown in the left part of **Figure K**. The right hand part of Figure K shows the reduction of the vibration levels at the beginning and at the end of the first basket's meltdown phase. On this basis, a signal was generated to indicate the completion of the meltdown phase of the first basket and thus the optimal point of time for charging of the second basket.

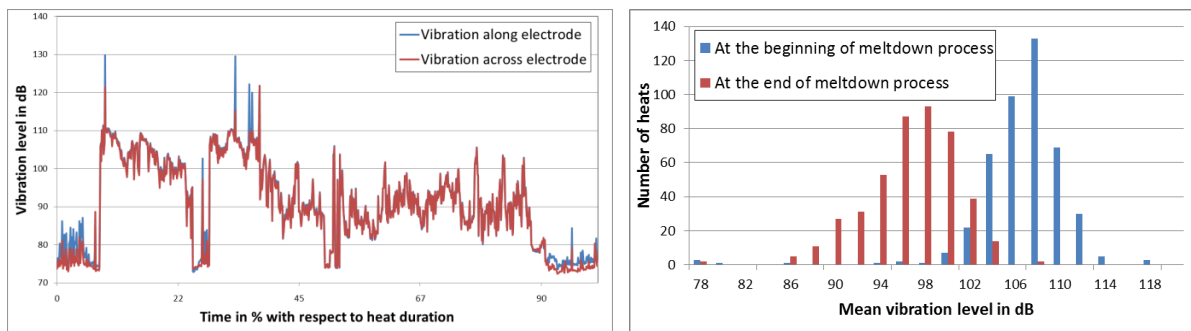


Figure K: Vibration level for one heat and mean value level during first basket meltdown process

Instead of the spectrometer signals the electrode path which is measured by a distance measurement system was analysed. The trend of the electrode path signal after ignition as well as the corresponding vibration level signal are exemplarily shown in **Figure L**. In addition the offgas analysis values were evaluated with reference to the meltdown behaviour of different charge mix clusters. It was found that different scrap mixes show different levels of CO and H₂ in the off-gas, depending on the amounts of charge coke, pig iron skulls and turnings. Scrap mixes including these materials to a larger extend should be treated with an increased oxygen input for post-combustion.

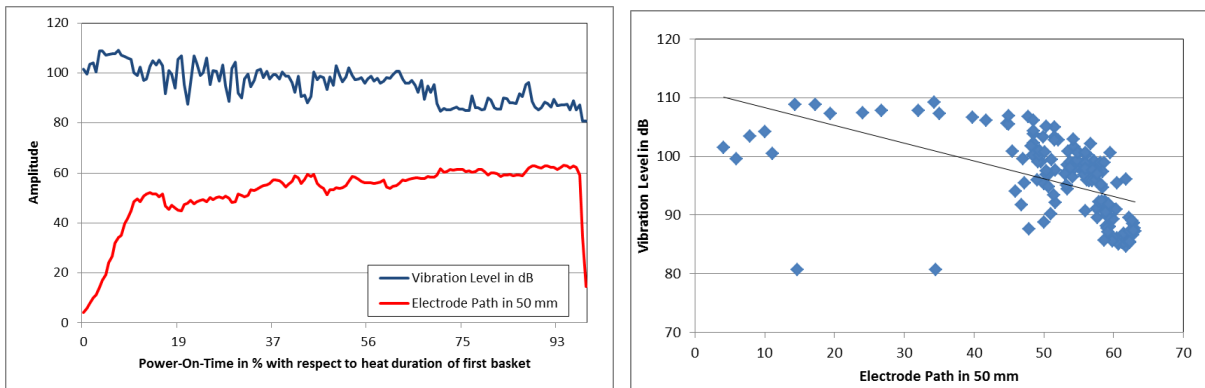


Figure L: Vibration Level and Electrode Path during First Basket Meltdown Process

1.3.3 WP 3: Enhancement of existing process models by using information from newly applied measurement systems

Work Package 3 dealt with the integration and visualisation of additional process information in a process data base, and their utilisation for process modelling and control. The corresponding PCs collecting and pre-processing the new sensor data were attached to the data exchange network and then to a process data base. Existing statistical models have been used, together with estimated slag weights and slag analyses, to determine and to track metallic yield and composition of the different scrap types. The additional calculation of element oxidation, considering the slag amount and composition, provides accurate and comprehensive information on the varying scrap composition. An existing dynamic process model has been extended by a detailed slag balance calculation, which allows, besides the on-line calculation of melt temperature as well as carbon and oxygen content, to monitor the concentration of oxidisable elements and of slag composition, as shown exemplarily in **Figure M**.

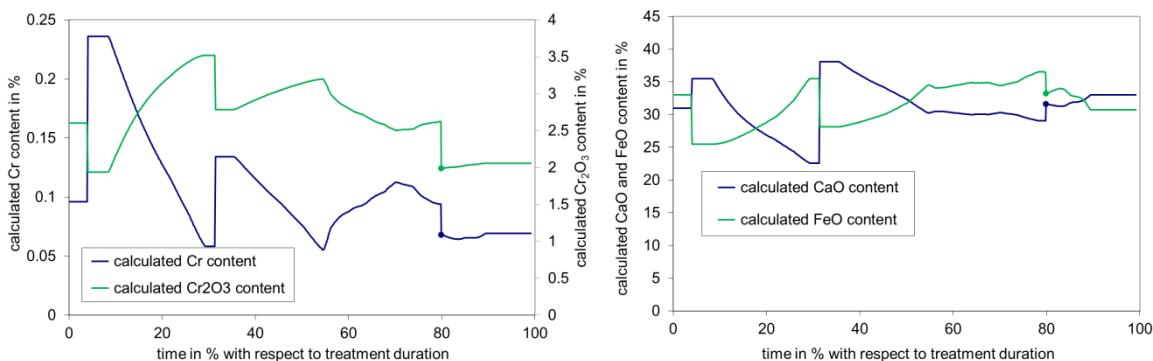


Figure M: Calculated Cr and slag Cr₂O₃, CaO and FeO content evolution for example heat of GMH

Assessment of energetic melting behaviour

Based on the information of the vibration sensors (P2) and the calculations with an energy and mass balance model (P3), an on-line control model to determine the optimal time for charging the second basket was developed. An additional geometric measure for supporting this model calculation was derived from the position of the foot of the electric arc (P1), which can be estimated from the electrode position and the basket filling level derived from the image analysis, which gives an estimation of the starting height at arc ignition. A scheme of the model and exemplary results of correlation are shown in **Figure N**. The basic principle of this model is to predict the free volume in the furnace vessel with respect to the melting progress of the first scrap basket, and to compare this value to the volume required for the scrap load of the second basket.

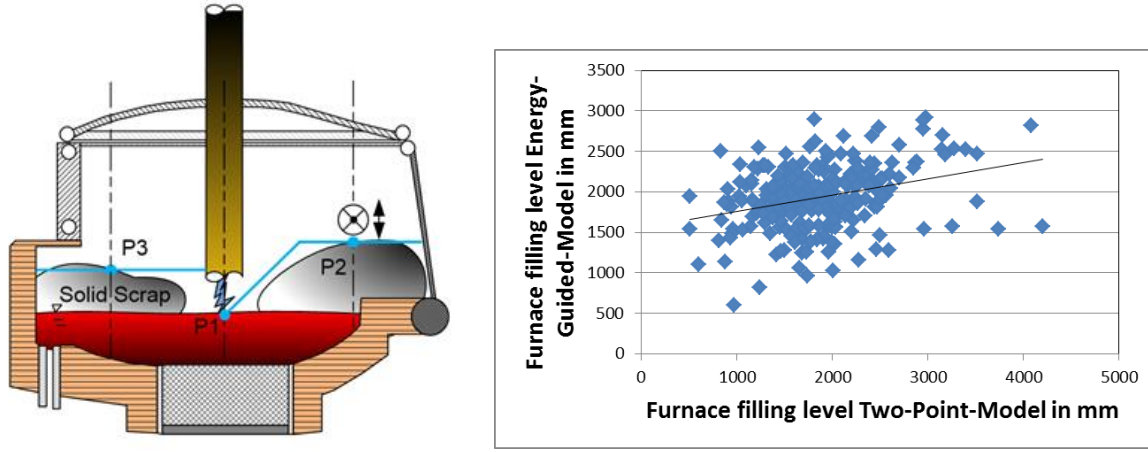


Figure N: Two point scrap index model and correlation to energy balance

Implementation of a display for new measurements and enhanced modelling results

For display of the extended process information, user interfaces and operator displays were designed. **Figure O** shows the display for the scrap basket filling level (left), as well as vibration signals and model calculations rights, which are both available in the EAF control room.

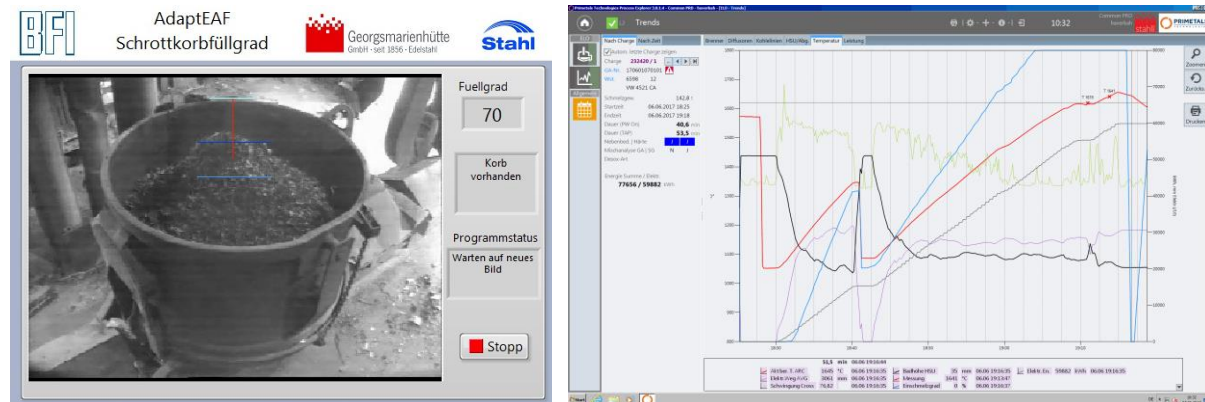


Figure O: Display for scrap basket filling level and model results

1.3.4 WP 4: Application of process control tools based on newly implemented measurement systems and advanced dynamic process models

Heat-individual control of the chemical energy inputs

For scrap mix dependent control of the chemical energy input via the natural gas burners dedicated operating patterns have been set up and corresponding plant trials with extended overstoichiometric operation have been performed. An improved energetic performance of the furnace due to the increased post-combustion degree and thus an increased efficiency of the chemical energy input has been achieved. Thus the chemical energy input via burners and injectors can be controlled according to clustering of the actual scrap mix and selecting an adapted operating pattern, which provides sufficient oxygen for effective post-combustion.

Besides the melt temperature also the steel carbon content has to be adjusted during the refining treatment. The dynamic process model calculates the current carbon content and the remaining treatment time needed for decarburization to reach the target value. Furthermore the chemical energy input by oxygen injection into the steel bath is considered for calculating the remaining time to reach the target tapping temperature. **Figure P** illustrates this concept for end-point control which is integrated within the dynamic process model. Based on the current melt status, heat

individual set-points for the optimal input of oxygen and electrical energy are calculated to achieve the target values at the same time.

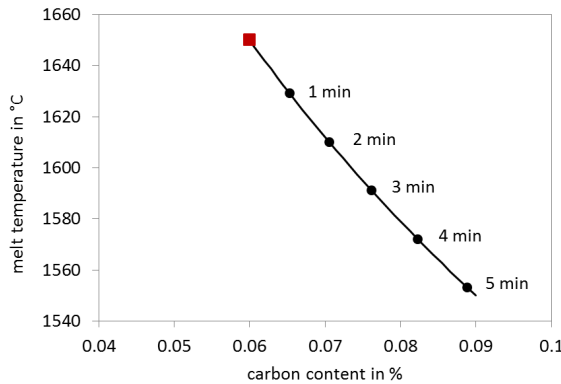


Figure P: Evolution of end-point control for tapping temperature and steel carbon content

Determination of the optimal time for charging the second scrap basket

The optimal charging time for the second scrap basket can be determined by the model described under WP3, taking into account vibration signals and the electrode path in combination with mass and energy balance calculations, considering the filling degree of both scrap baskets. The model has been validated on the basis of irregular charging procedures which indicate a too early charging of the second basket. In normal operation about 20 % of the charging processes are delayed because the second basket does not fit into the furnace and has to be flattened. The two histograms in **Figure Q** show the calculated lack of space in the furnace for charging the second basket. The heats where the second basket fits into the furnace are listed in the left diagram, heats with flattening of the second basket are listed in the right one. Negative values mean more free volume than needed, indicating a too late charging of the second basket. Positive values indicate that there is not enough free volume in the furnace for the scrap load of the next basket.

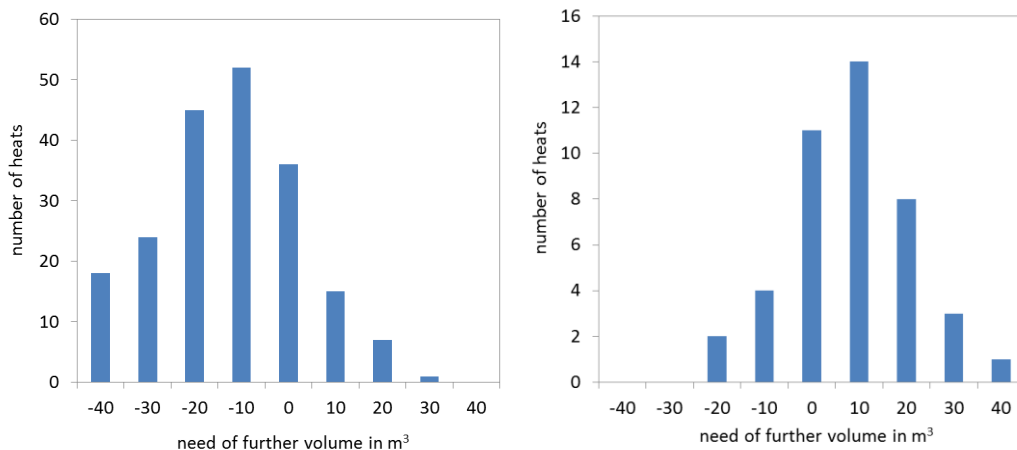


Figure Q: Histograms of calculated lack of volume for heats where the second basket fits into the furnace (left) and where the scrap has been flattened after charging (right)

About 80 % of the charging processes which required a flattening of scrap after charging are detected correctly by the model. For heats without problems during the charging procedure the model predicts for about 75 % a negative volume which indicates an undisturbed charging procedure.

Control of the steel bath level and the remaining slag after tapping

The steel bath level can be controlled using the information from the delta dist sensor for steel and slag level detection. **Figure R** shows the dip-sensor measurements performed at the GMH furnace for about one year, covering in total three furnace campaigns.

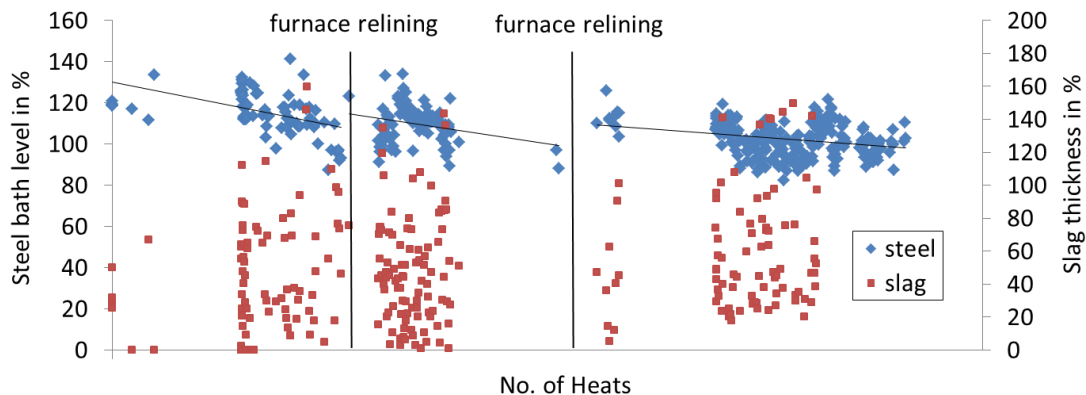


Figure R: Dip sensor measurements for three furnace campaigns at GMH

The decreasing trend of the steel bath level due to the furnace wear, which was observed throughout the first two campaigns, has been reduced by an improved control of the steel bath level so that it was nearly constant during the last campaign. The operator uses the dip sensor information on the bath level to modify the scrap load and the tap weight if necessary. In contrast to that, the measured slag thicknesses still shows a wide scattering, as the deslagging process depends on other uncertainties.

Consideration of quality-dependent constraints at EAF tapping

For consideration of quality-dependent constraints for the EAF end-point control, an analysis of quality dependent target values for tapping temperature and carbon content was performed.

1.3.5 WP 5: Extensive plant trials for online test and evaluation of process control tools

Long term plant trials for validation of the on-line adaptive control tools

Long term plant trials with extensive process data collection and evaluation have been performed to validate the main functions of the new process control tools, with focus on control of chemical energy input and end-point control, charging time of the second basket and the steel bath level.

Evaluation of performance of applied measurement techniques

The accuracy and the reliability of the different sensor technologies applied in the industrial surrounding were evaluated. The delta dist sensor and the camera system to determine the hot heel, the IR camera to monitor deslagging, the image analysis for scrap basket filling level and the vibration sensor to monitor the melting progress are in continuous operation, are working reliably and are well accepted by the operators. The laser scanner to determine the scrap basket filling level and the spectrometer to detect the free burning arc to derive the melting degree of the scrap were too difficult to install or maintain.

Benefits of on-line application of adaptive EAF process control

The overall benefits of application of an adaptive process control were finally assessed. Throughout the project duration, the electrical energy consumption of the EAF at GMH was decreased by about 10 kWh/t and the tap-to-tap time was decreased by 3 minutes. A further decrease of about 5 kWh/t and 2 minutes can be achieved for about 10 % of the heats when applying the recommendation for optimal time of charging the second scrap basket.

1.4 Concluding overview

Within the Pilot & Demonstration project AdaptEAF, different novel and existing sensors were successfully developed, installed and applied at the DC EAF of GMH, to acquire additional process information regarding steel bath level, slag amount, scrap basket filling degree and scrap meltdown progress. This additional process information has been used to extend existing and to develop new process models. Based on the newly implemented measurement systems and advanced process models, on-line applicable process control tools for chemical energy input, end-point control, charging time of the second scrap basket and bath level were developed, tested and validated.

Applying the developed adaptive on-line control tools allows to adapt the operating conditions of the EAF process to the strongly varying properties of the actually charged materials. The economic potential for the use of the project results lies mainly in savings of chemical and electrical energy input as well as in the improvement of productivity by reduced tap-to-tap times.

The applied measurement technologies and extended process models are relatively easy transferable to further EAFs.

2. Scientific and technical description of results

2.1 Scientific project objectives

The overall objective of the Pilot & Demonstration project AdaptEAF was to complement modern EAF process control by integrating novel and existing sensors and advanced process modelling tools. The adaptive EAF on-line process control was to be tested and evaluated under industrial conditions at the well-equipped 140 t DC electric arc furnace of **Georgsmarienhütte (GMH)** with the following key data:

Average oxygen input	40 Nm ³ /t
Oxygen gas burners	5
Oxygen jets	3
PC oxygen injectors	3
C injectors	3
Door lances	2xO ₂ , 1xC
Carbon content at tapping	0.04 - 0.1 %
Off-gas measurement	CO, CO ₂ , O ₂ , H ₂ , CH ₄ , Ar, N ₂ , T, Flow rate
Steel temp. and composition	Thermocouple, CELOX, Sample analysis
Slag composition	Sample analysis

Furthermore the project involved the two applied research centres **VDEh-Betriebsforschungsinstitut (BFI)** and the **Institute of Automation Technology of Helmut-Schmidt-University (HSU)**, both having broad knowledge and practical experience in the installation of measurement equipment and process control models at the EAF. The research institutes were responsible for development, extension and application of measurement systems and process models, with focus on the installation of novel sensors and the revision of existing sensors, aiming to provide additional online measurement data regarding steel and slag amounts, scrap basket filling degree and scrap density, as well as the scrap meltdown behaviour. The additional EAF process information was to be exploited for enhancement of existing process models and for development of on-line process control tools, which were to be validated within industrial trial campaigns.

2.2 Description of activities and discussion

The activities and achieved results of the project are described with reference to the work packages and tasks, as defined in the technical annex to the contract.

2.2.1 WP 1: Application of new measurement devices

Task 1.1: Application of measurement systems to assess the liquid bath level (BFI, GMH)

Within the project two different measurement systems to assess the liquid bath level before tapping and the hot heel level after tapping were applied at the EAF of GMH:

- An already preliminarily installed bath level and slag thickness dip sensor (Heraeus Delta Dist L)
- A camera-based system in combination with image analysis to determine the bath level at open EAF furnace after tapping

The combination of these two measurements allowed to provide reliable information on liquid steel and also slag levels in the furnace.

Delta Dist Dip Sensor (GMH)

With the help of the already commercially available dip sensor Heraeus Delta Dist L [1] the thickness of the remaining slag and the steel bath level can be measured after EAF deslagging, just before EAF tapping. **Figure 1** shows a photo and a sketch of the Delta Dist probe.

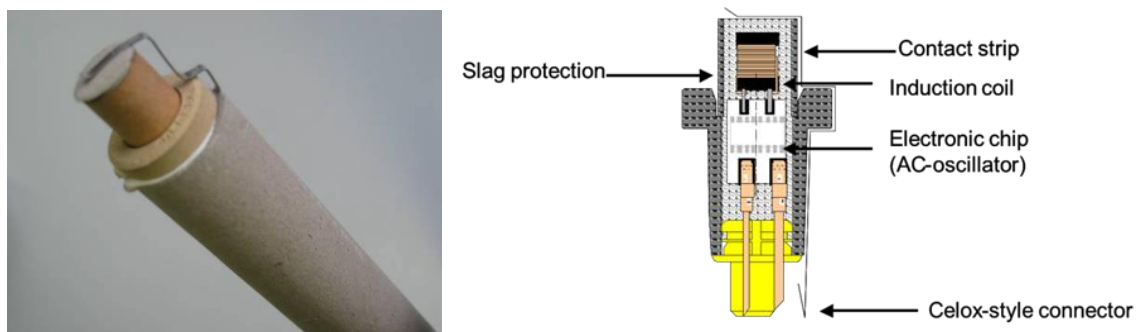


Figure 1: Photo and sketch of the Delta Dist Dip sensor of Heraeus Electronite [1]

The measurement with the Delta Dist L sensor is performed in two steps (see **Figure 2**):

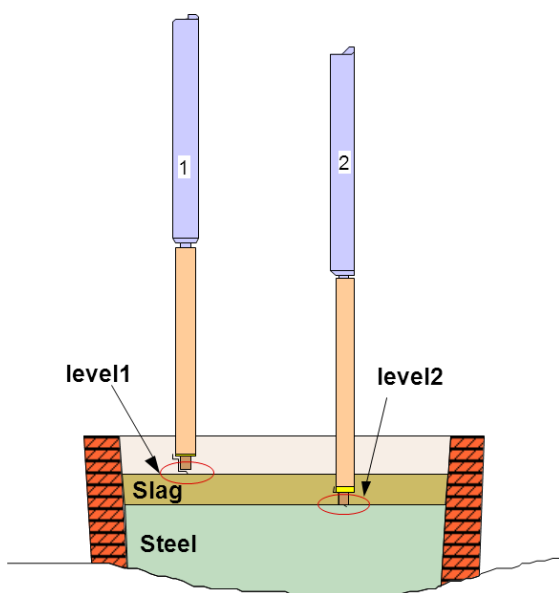


Figure 2: Measurement procedure with the Delta Dist sensor

In a first step, by moving down the lance with the dip sensor, the slag level is detected by the use of a small steel strip mounted at the tip of the sensor (see Figure 1). This steel strip provides an electrical contact (see **Figure 3**) and thus, by recording the position of the sensor, gives information on the slag level.

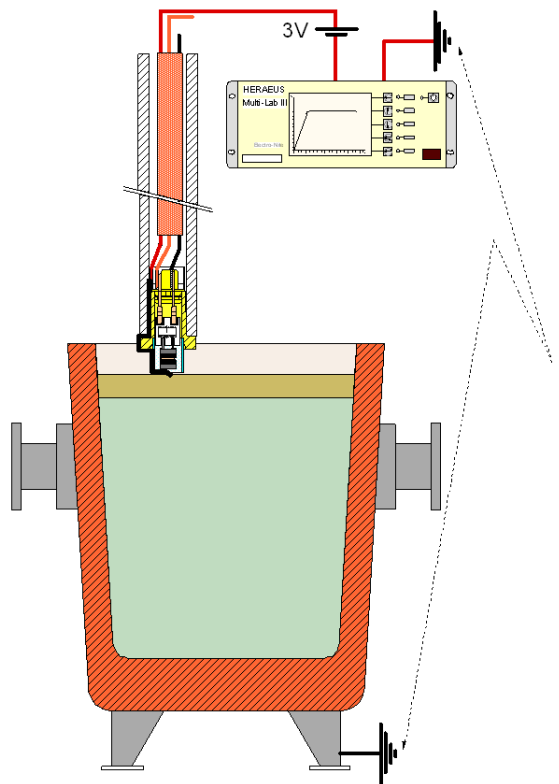


Figure 3: Measurement of the slag level by electrical contact at the tip of the Delta Dist sensor

As the probe continues on its way down into the melt, it penetrates the slag. When crossing the slag / steel interface (step 2 in Figure 2), this is recognised by a small current-carrying coil inside the sensor (see Figure 4). As due to the eddy current effect the characteristics of the current changes dramatically by the presence of steel, the steel level and thus also the slag thickness can be detected by recording the position of the sensor.

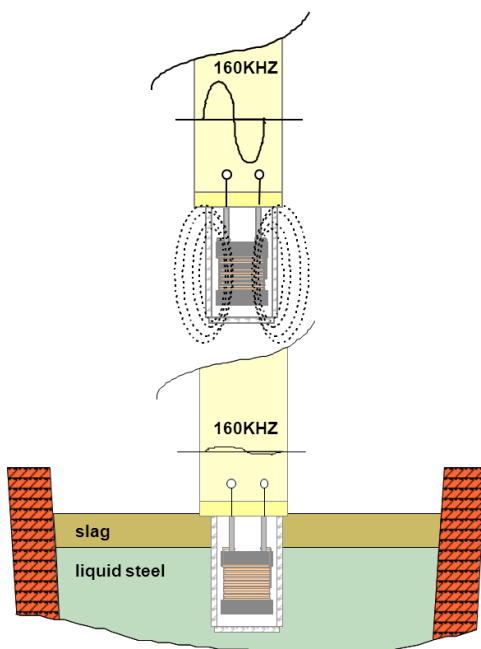


Figure 4: Measurement of the liquid steel level by eddy current change in a coil inside the sensor

For immersing the Delta Dist sensor into the steel bath, an already existing lance manipulator at the GMH furnace was used. With this manipulator, a lance is automatically immersed through the slag door. This lance can either carry a probe for a Celox measurement, for steel sampling or the probe of the Delta Dist measurement. This is displayed in the operating screen of the lance ma-

nipulator shown in Figure 5. Under item 4 of the screen the selected measurement probe is indicated. Items 0, 1 and 2 show the validity of the Delta Dist measurement. Under item 5 the absolute steel bath level is indicated, item 6 shows the slag thickness. Item 7 gives the absolute position of the lance, which is automatically recorded and used for determining the liquid steel bath level and the slag thickness. The signals of the Delta Dist sensor are connected to the Celox measurement device by a standardised plug (see also on the right hand side of Figure 1).

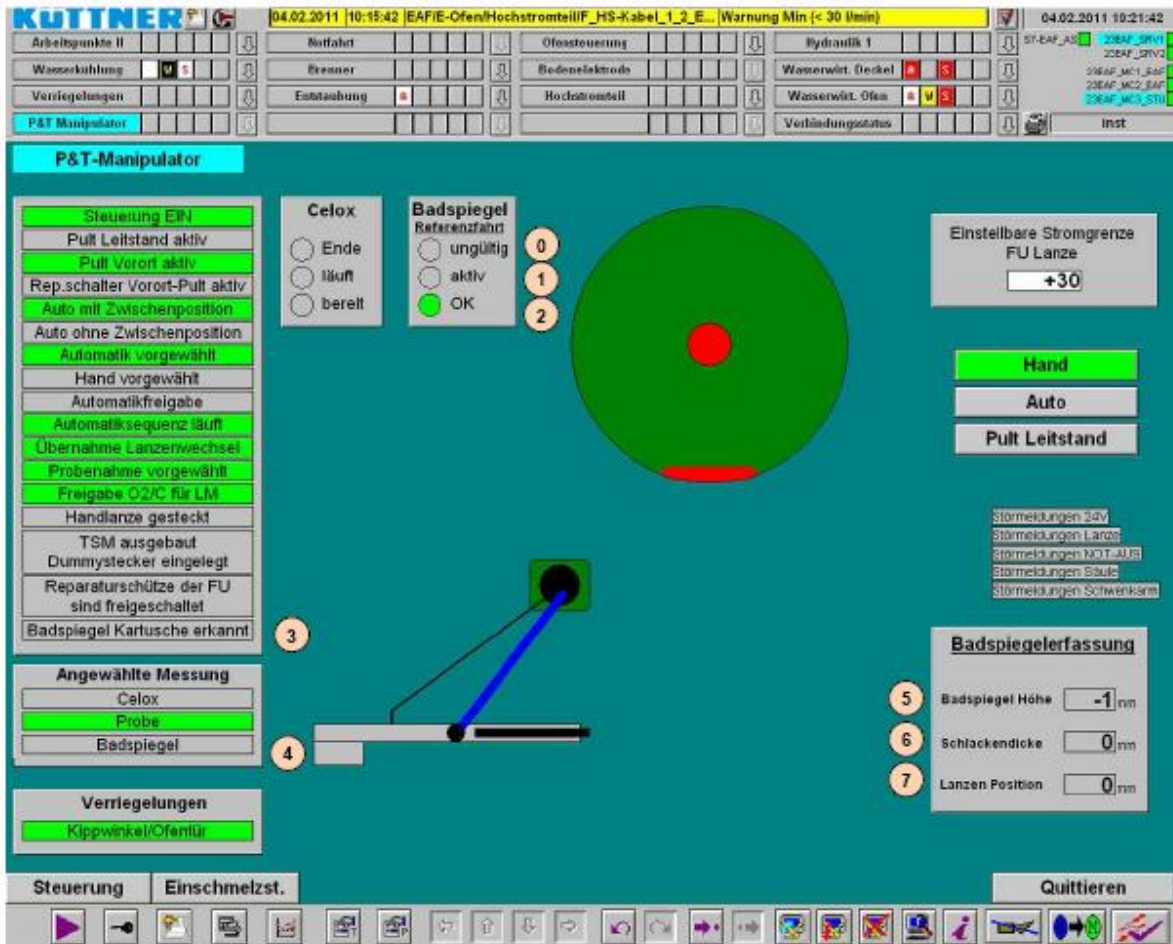


Figure 5: Operating screen for the lance manipulator at the GMH furnace

The whole measurement procedure with the Delta Dist sensor takes about one minute. To limit the resulting increase of the tap-to-tap time, the measurement is performed only for every third heat. This allows at least the tracking of the evolution of slag height and amount of the hot heel.

The Delta Dist sensor was calibrated and tested in several trial campaigns. Exemplarily measurement results for the steel bath level (blue bars) and the slag thickness (red bars) are shown for several consecutive heats in **Figure 6a**. Overall the measurement results are reasonable, only for few heats no measurement value for the slag thickness could be obtained. The steel bath level value is related to the level of the bottom anode after the installation of a new anode. The slag thickness value is an absolute value.

A dedicated measurement campaign was performed to check the repeatability and accuracy of the Delta Dist measurement. For this purpose, for one trial heat four consecutive measurements were performed in a short time period. The result of this campaign is shown in **Figure 6b**.

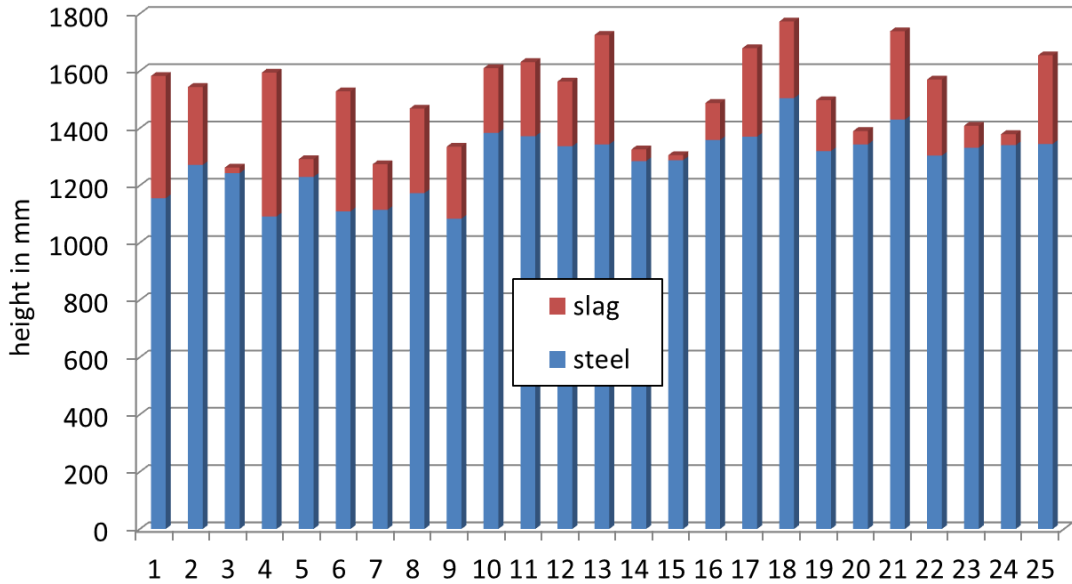


Figure 6a: Plant trials with Delta Dist measurement of steel bath (blue) and slag level (red) for consecutive GMH heats

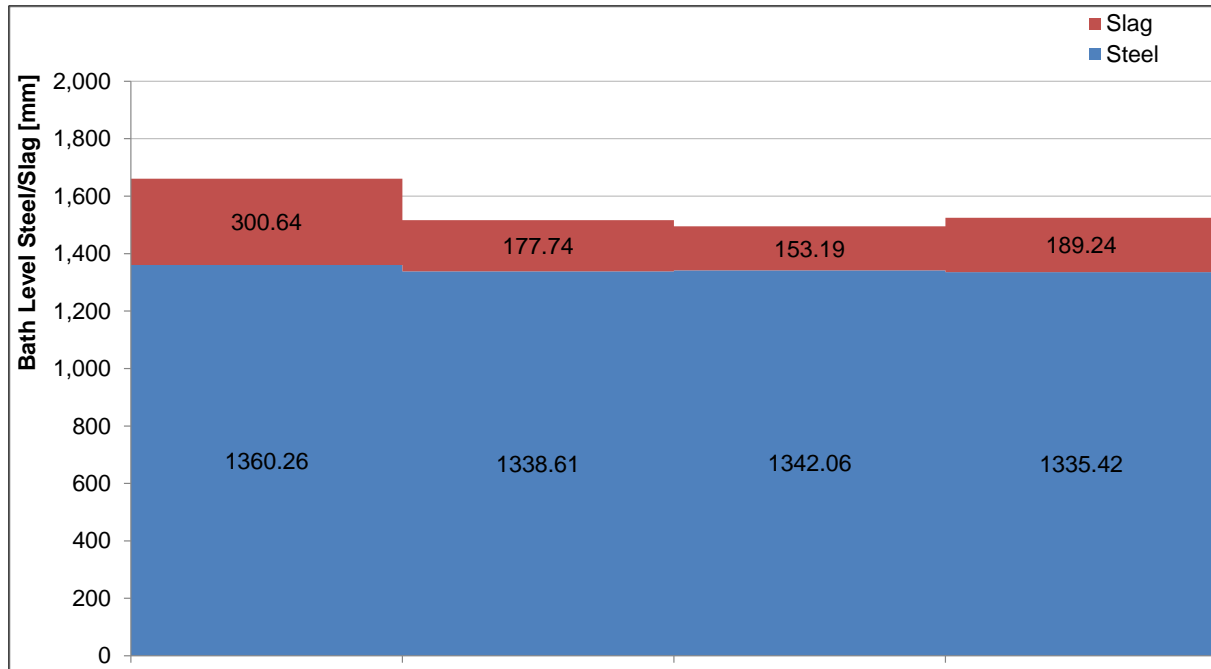


Figure 6b: Plant trial with 4 consecutive Delta Dist measurements of steel bath (blue) and slag level (red) for one GMH heat

The maximum difference of the steel bath level measurement is approximately 25 mm, and of the slag thickness about 150 mm. The standard deviation, which can be regarded as a value for the accuracy of the measurement, is 11 mm for the steel bath level (corresponding to a weight accuracy of 2.2 t), and 65 mm for the slag thickness (corresponding to a weight accuracy of 3.3 t).

Camera-based measurement system (BFI, GMH)

At the EAF of GMH an imaging system was applied to monitor the liquid bath level after tapping of the furnace. The requirements for the cameras to be used for monitoring the furnace with open roof from the top have been defined by BFI. GMH proposed the camera type to be used for this purpose, and BFI checked the properties of the camera. The camera was found to be appropriate as it fulfils the requirements. Thus, three cameras have been bought by GMH. They were installed

above the furnace at different positions to monitor the entire inner of the furnace from different angles of view. The positions of the cameras were chosen as illustrated in the schematic drawing of **Figure 7**.

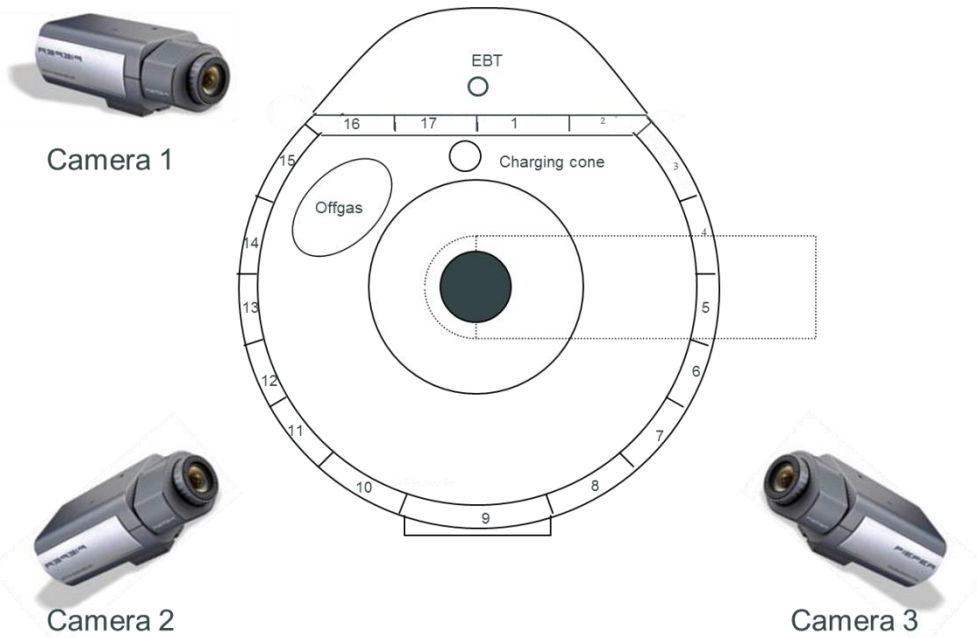


Figure 7: Schematic drawing of the EAF with the camera positions

A robust analogue 1/3" CCD camera with a high dynamic range was chosen. The resolution is up to 976 x 582 pixels and the shutter speed can be adapted between 1/60 up to 1/10.000 s. The cameras are covered in a protective housing to withstand the hot and dusty environmental conditions above the furnace (**Figure 8**).



Figure 8: Camera at position no. 3 installed above the EAF

The camera is connected via a BNC cable with the data acquisition unit to send continuously the video signal. The image acquisition system was set up using a frame grabber card which saves the images in mp4 data format. The furnace roof position is used as a trigger signal to start image acquisition when the roof of the furnace is opened. During first trials 276 short avi-videos were recorded. Visual inspection of the images showed that after tapping and before charging the first scrap basket the view is not obstructed by fume and smoke, and the hot heel can clearly be observed. **Figure 9** shows the view of all three cameras into the open and empty furnace. The hot heel can be seen at the bottom of the furnace.

For image analysis suitable grey value images were extracted from the image sequence (**Figure 10**). First an edge finding algorithm is used to fit an ellipse (green) to the upper contour of the furnace shell. The reference line for height measurement is defined as a horizontal tangent to the ellipse (blue line). The hot heel filling level can be interpreted as height of free board of the furnace. An algorithm was developed to find the transition between hot heel and refractory (red) within a predefined rectangular region of interest (green). The distance between hot heel surface and furnace contour is determined in the image in pixels. After correction for image projection, the height is converted in a length in meters. The results of the image analysis are given exemplarily for the images displayed in Figure 10. The free board of image a) was determined to be 3,13 m, for image b) 3,15 m, for image c) 3,51 m, and for image d) 3,60 m. The image analysis gives qualitatively plausible values for the hot heel level in all images as compared to visual inspection.

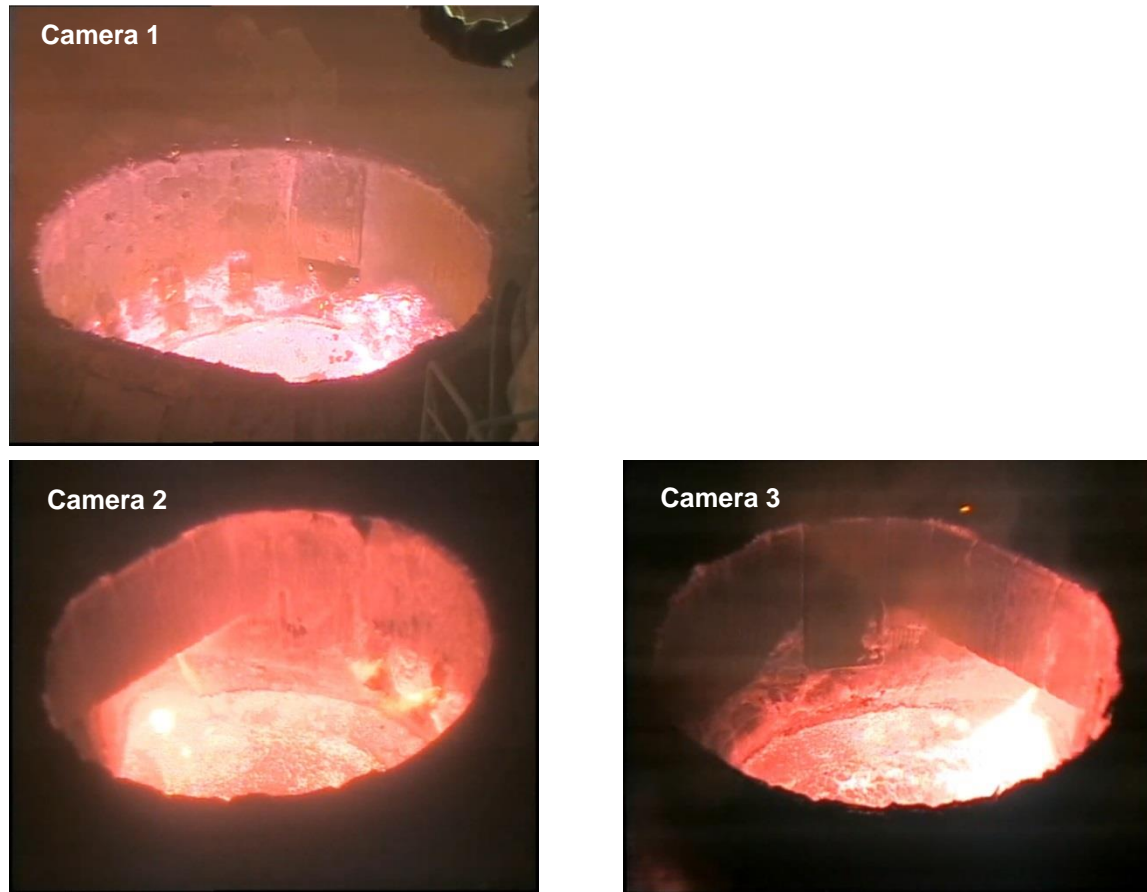


Figure 9: View into the open and empty furnace with hot heel by all three cameras.

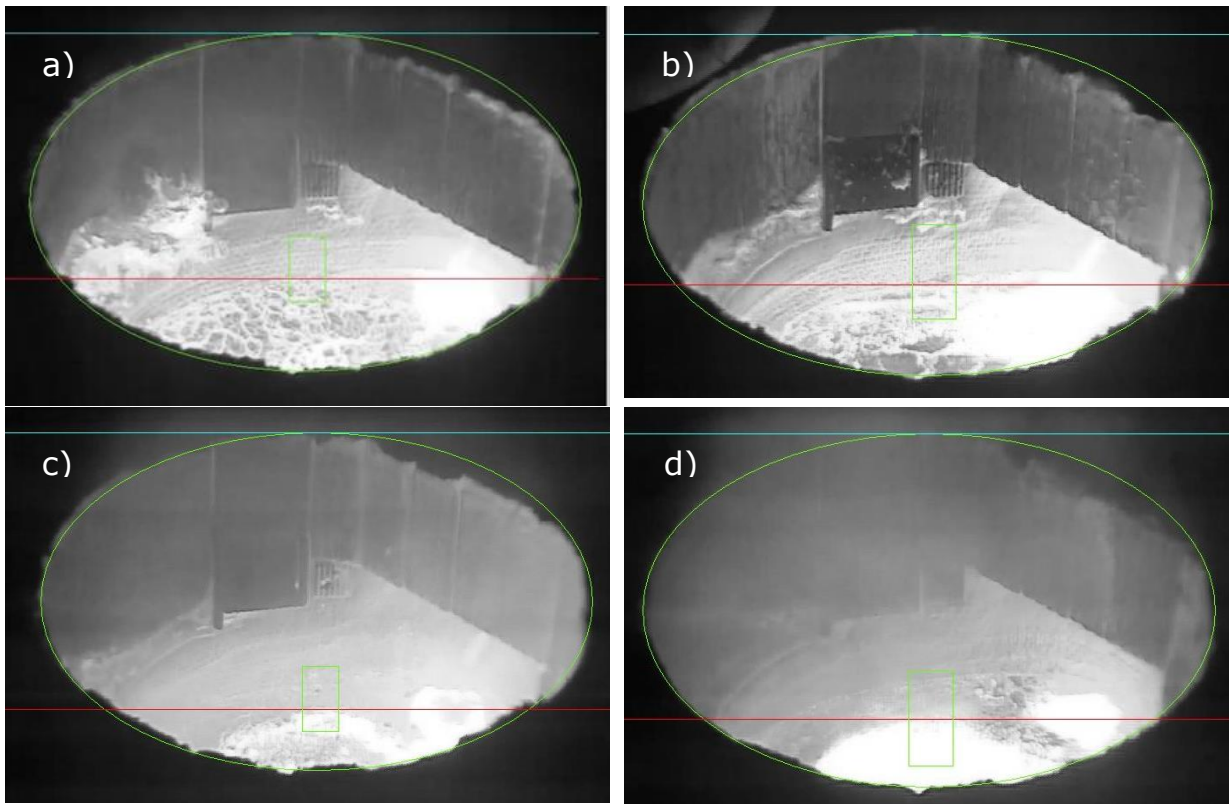


Figure 10: View from the position of camera no. 3 down to the furnace shell with hot heel. Colour lines from image analysis are superimposed

Images from the furnace interior were also recorded before and after charging of the second basket (**Figure 11**). However, the view is strongly obstructed from fumes and smoke which hampers the inspection of the scrap level inside the furnace.



Figure 11: View of camera no. 3 into the open furnace before and after charging of the second basket for two different heats.

Task 1.2: Application of deslagging monitoring and slag analysis to assess slag amount (BFI, GMH)

Deslagging monitoring with IR camera (BFI, GMH)

After the meltdown and refining phase slag has accumulated in the furnace. Already during the refining phase liquid slag is continuously running from the furnace via the slag door. Before tapping of liquid steel into the ladle, the furnace is tilted for deslagging. The slag is tapped through the slag door into a slag pot positioned below the furnace. At the GMH furnace, an infrared (IR) camera was installed to monitor this slag tapping and to detect when the slag is accompanied by steel. In a first approach, the camera was installed right opposite of the slag door with a straight view on the slag

stream. In the IR range liquid steel and slag at the same temperature can be distinguished as they have a different emissivity in the infrared. Thus, the emitted intensity from both phases at equal temperature differs, i.e. the slag is brighter. An imaging system was developed to detect the carry-over of liquid steel into the slag pot and to generate a control signal to finish deslagging by retilting the furnace. Avoiding the steel carry-over during deslagging should allow to minimize the steel loss and to increase the metallic yield.

In a first campaign deslagging was observed using the IR camera. IR images of the slag tapping process were recorded (**Figure 12 and 13**). An artificial colour code is used by the imaging system to display different intensities in the IR images. The colour code is chosen such that liquid hot steel is displayed in blue, whereas slag can be attributed to the yellow regions. In Figure 12 no big amount of steel was detected. In Figure 13 large blue areas are displayed indicating a significant amount of steel losses. In this case the software was able to automatically detect steel overflow, and a signal for stopping the slag tapping process by tilting back the furnace can be generated.

The success of automatic steel detection was evaluated by comparison with the actual standard procedure. The operator controls slag tapping by visual inspection. Bright sparks are indicating that steel is running together with slag into the slag pot. The correlation between both detection techniques was not as good as expected. The IR camera is not able to detect all events of steel overflow probably because the camera is looking from the front onto the deslagging stream while steel is hidden behind the slag. Since the density of slag is lower, slag is swimming on liquid steel.

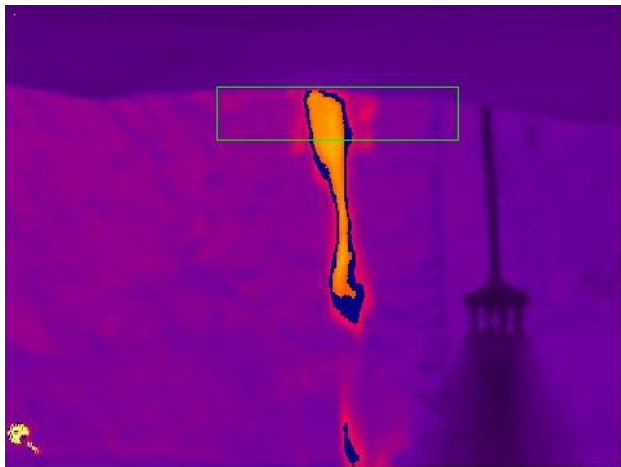


Figure 12: IR image during slag tapping without steel encountered

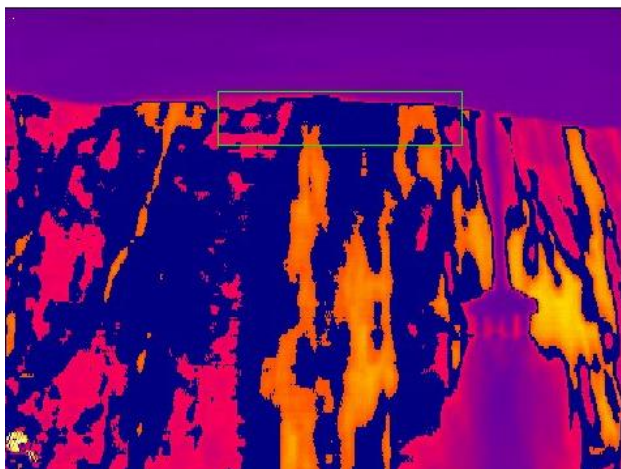


Figure 13: IR image during slag tapping with significant steel overflow

Thus, another installation site for the IR-camera below the furnace was chosen. Using a mobile IR camera further sequences of the deslagging process were acquired. The new position was about 5 m away from the slag door above the spray cooling device, giving sight on the slag stream from the side (**Figure 14**). The results of these trials from the new camera position were quite promising for a more reliable detection of steel overflow during slag tapping. Thus, the IR camera was permanently installed at the improved position at the side. The IR camera was running continuously, and the images were displayed in the control room.

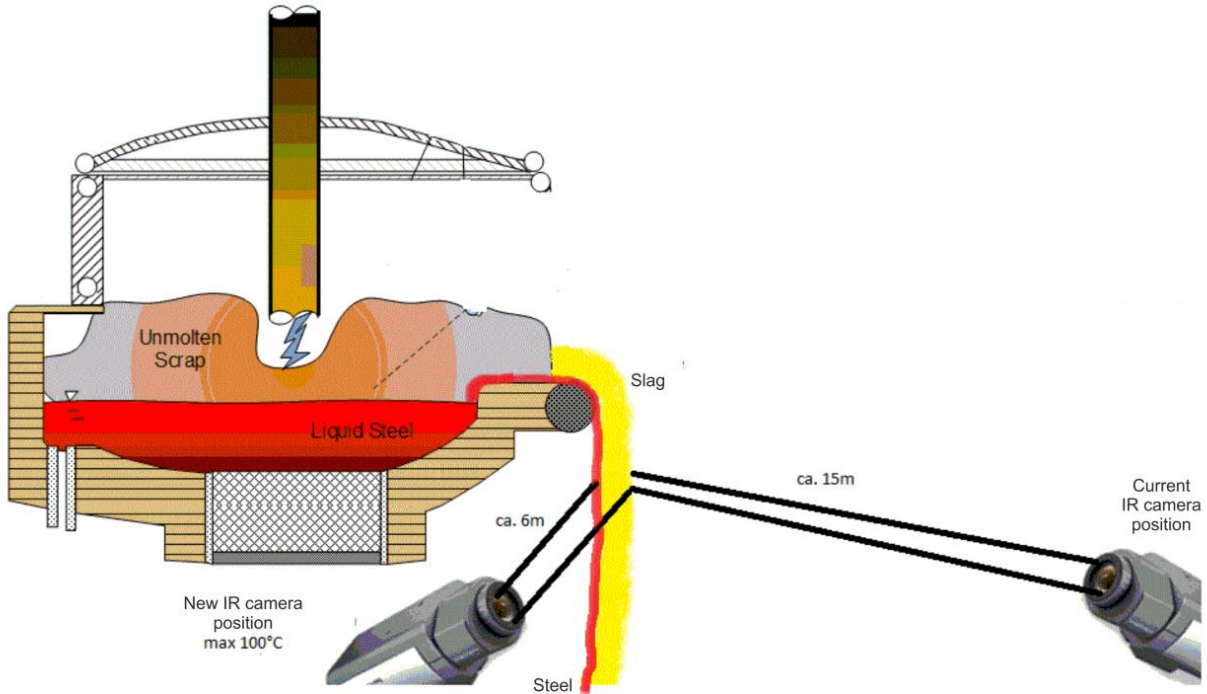


Figure 14: Previous position (from the front) and improved position (from the side) of IR camera for monitoring of steel running during slag tapping

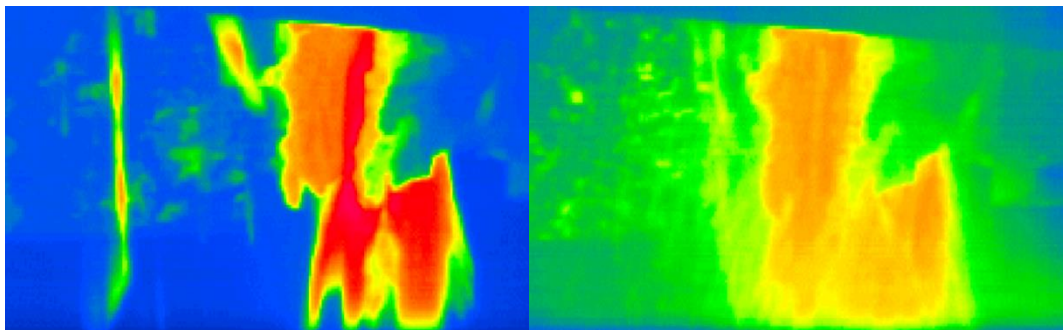


Figure 15: Images of IR camera during deslagging: only slag (left), slag accompanied by steel (right)

In a further trial campaign by IR imaging from the side installation position steel detection was analysed. To see clearly the different appearance between steel and slag, the furnace was deliberately tilted more than necessary for deslagging to allow some liquid steel to run into the slag pot. In **Figure 15** two images from the deslagging process are shown: during slag running (left) and when steel is accompanying the slag (right). In these images the colour code is chosen such that the slag is displayed in red/orange colours and the steel in yellow/green colours. Cold parts with low radiation are shown in blue colours.

In the right hand image of figure 15 steel carry-over can clearly be identified by the large green areas. However also in the left image the slag areas have a green contour. Thus, only large green

areas can be identified as metal flow, which limits the accuracy of the analysis of IR images for the purpose of steel running during deslagging. For this reason the task of detecting low radiating liquid metal within highly radiating slag was found to be much more difficult than detecting slag during metal tapping. Thus it was decided that the detection of metal losses in the slag stream during deslagging is not reliable enough to create a signal for automatic back-tilting of the furnace.

Acquisition of process data including slag analyses for a slag balance (BFI, GMH)

To follow the evolution of the slag analysis, at the GMH furnace for each heat at least one slag sample is taken at the end of the melting phase and analysed for all relevant slag components. GMH provided process data of about 500 heats produced in July 2014 to examine the evolution of the slag amount and analysis. This data set includes all relevant acyclic and also cyclic process data. The delivered process data set comprises:

- Electrical and chemical energy inputs
- Energy losses by cooling water
- Off-gas temperature, flow rate and analysis
- Input of blow carbon and dust
- All material inputs charged by baskets
- Temperature and Celox measurements
- Steel and slag analyses
- Measured tap weight and tapping additions

For all heats at least one steel and one slag analysis were performed. For 129 of these heats more than one steel analysis is available, and also 12 heats with 2 slag analyses are included in the data base. **Figure 16** shows the evolution of the EAF process for an example heat with two steel and slag samples. The first sample is taken when the charged scrap is molten down to approximately 80 %. The second sample is taken directly before tapping.

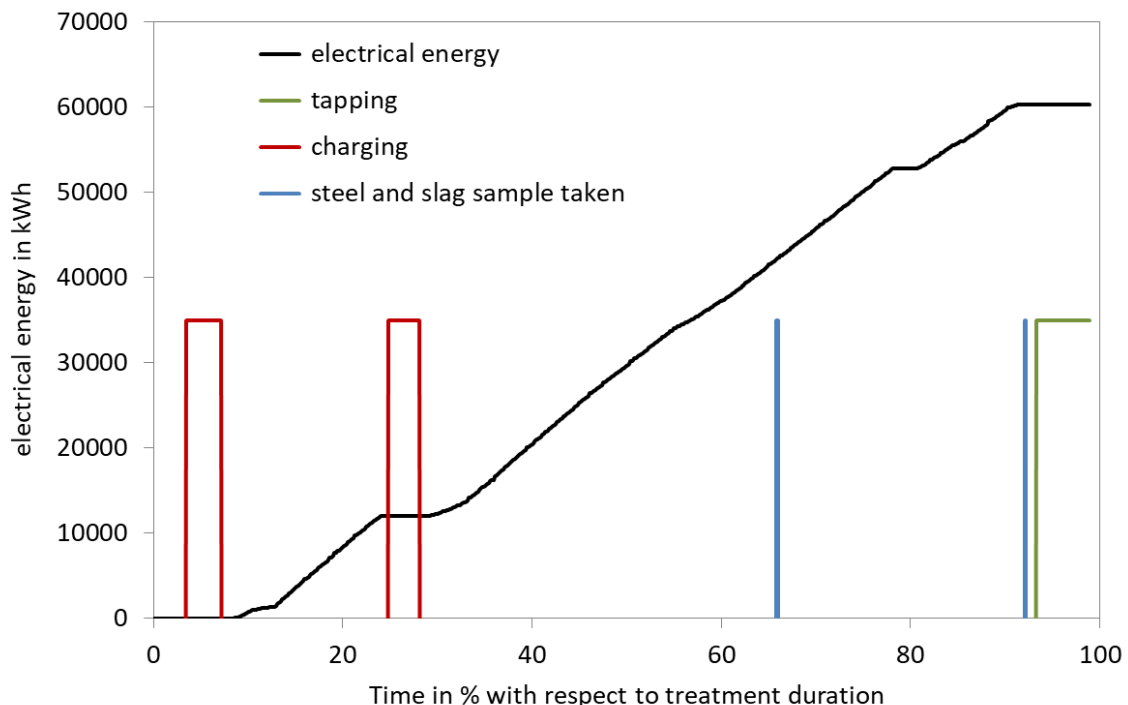


Figure 16: Timing of steel / slag sampling for a GMH example EAF heat

Furthermore the slag weight in the slag pot which is measured at GMH for every individual heat has been delivered by GMH. This data set has been used in Task 2.2 to set-up and validate an off-line slag balance calculation.

Task 1.3: Application of a monitoring system for scrap basket filling level before charging into EAF (GMH, BFI)

The filling level of each scrap basket should be assessed in the furnace hall just before charging of the basket into the EAF. For this purpose a laser-based line scanner and an imaging system were applied.

Application of a Line Scanner (GMH)

A line scanner was adapted to measure the filling level of the scrap basket. As a measurement system a bulk scanner laser volume flow meter of the company Sick was chosen. It uses the time-of-flight technology for non-contact measurement and is normally applied for measurement of volume flows on conveyor belts.

The scrap baskets are transported on an automated transfer vehicle from the scrap hall to the furnace hall. The laser scanner was fixed at the gate of the scrap hall at a height of 10 m above the railway. A scheme of the measurement setup and a photo of the installation position of the line scanner in the scrap hall of GMH are given in **Figure 17**. When the transfer vehicle passes through the measuring line of the scanner, the time-of-flight of the laser light is measured, giving the distance between the reflecting surface and the laser scanner (**Figure 18**). From this, the topology of the transfer vehicle with scrap basket is deduced.

The floor with the railway was used as a reference height. Deviations from the reference height due to the passing of the transport vehicle started the data evaluation. If a scrap basket was recognized by the edge detection, the measurement was started. Thus, also the filling level of empty baskets returning into the scrap hall can in principle be determined. From the difference of the filled and empty basket the scrap volume should be estimated in m^3 .

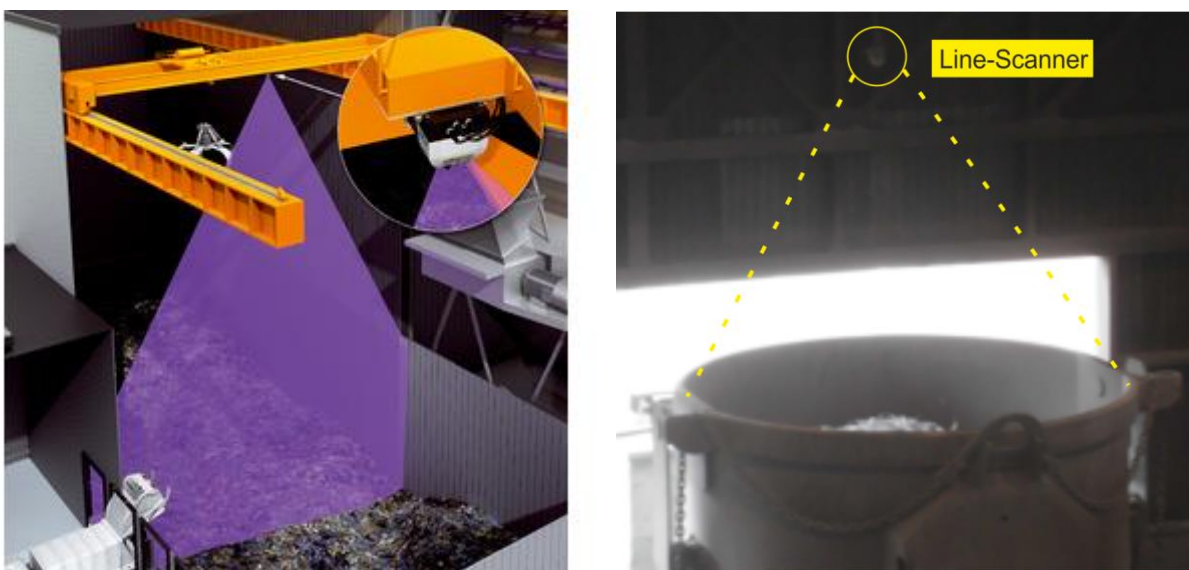


Figure 17: Functional principle of Bulkscan® Sensor [2] and installation in the scrap hall of GMH

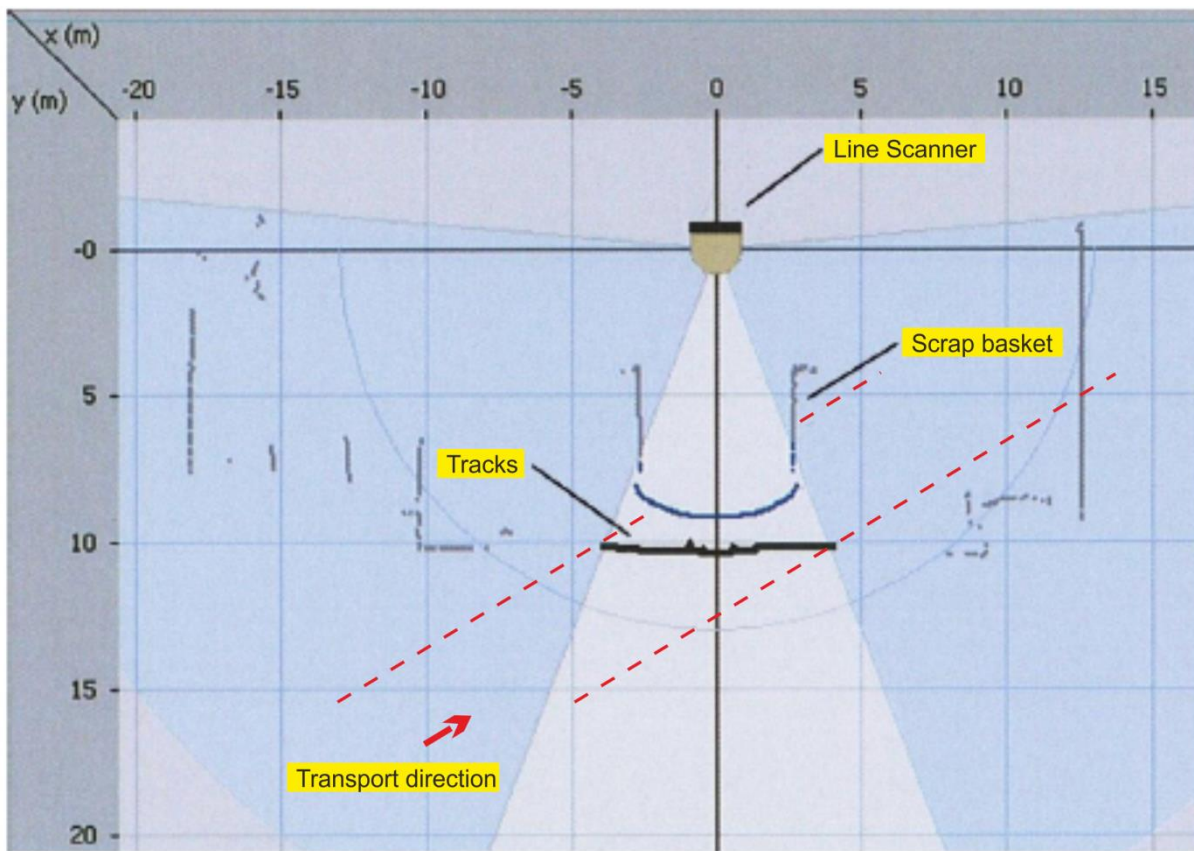


Figure 18: Schematic drawing of the scrap filling level measurement setup with line scanner

The industrial application of the laser scanner to determine the scrap basket filling level at GMH was found to be in principle a manageable task, but was experienced to be extremely difficult and time consuming. The filling level of the scrap baskets can vary between 50 and 100 %. To measure the filling level with the laser scanner, the height of the scrap in the basket and the surface of the empty basket on the transfer vehicle need to be measured. The difference is a measure of the filling level. Since the scrap basket has a height of more than 5 m, also the scrap height can vary by this amount. The maximum measurement distance of the line scanner is limited to 10 m. Due to these strong variations in the distance the measurement accuracy is very much limited. As the camera based filling level determination, which is described in detail below, is much easier and more robust, this technique was further applied to determine the scrap based filling level during further tasks. Instead the detection of the scrap basket filling degree by the line scanner was not further followed by GMH.

Development of an automated image analysis system to measure the scrap filling level (BFI, GMH)

An automated image analysis was developed to determine the filling level of scrap baskets. Images of the basket are acquired right before charging into the EAF using an existing camera in the furnace hall of GMH. The images are taken after the transfer vehicle has arrived at the end position in the furnace hall and before the basket is picked up by the charging crane. In a first development step, GMH recorded images of 14 scrap baskets with different filling levels at varying ambient conditions using a mobile image acquisition system provided by BFI (**Figure 19**). The image analysis had to cope with limited visibility of the basket due to fume c) and crane hooks b) in the image, and changing background illumination as sometimes the floor is illuminated by day light d), e), f). Software detection of the scrap basket position is necessary, since the position of the basket on the image vary for the first and second basket on the transfer.

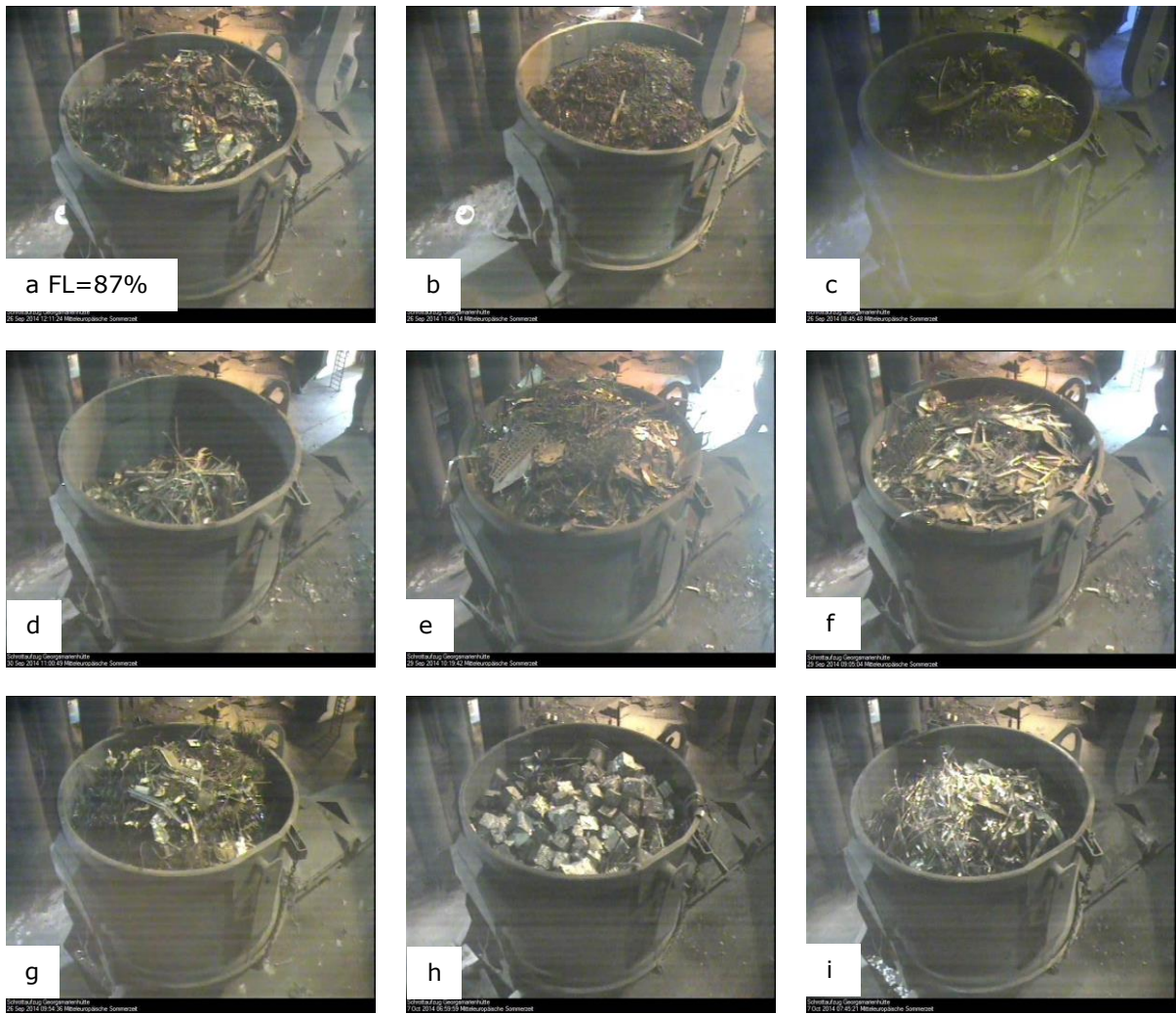


Figure 19: Image of a scrap basket on the transfer vehicle with loaded scrap

Thus, a correlation technique was used to identify the edge of the basket. A reference ellipse was manually adapted to the edge of the basket (**Figure 20 left**). Then a correlation of the reference ellipse with the image was calculated. The value of the correlation is displayed in the 3D plot (**Figure 20 right**). After optimization of the parameters and the line width of the ellipse, a distinct red peak is observed, indicating the centre of the basket edge. By this technique the basket edge can be reliably detected in most images.

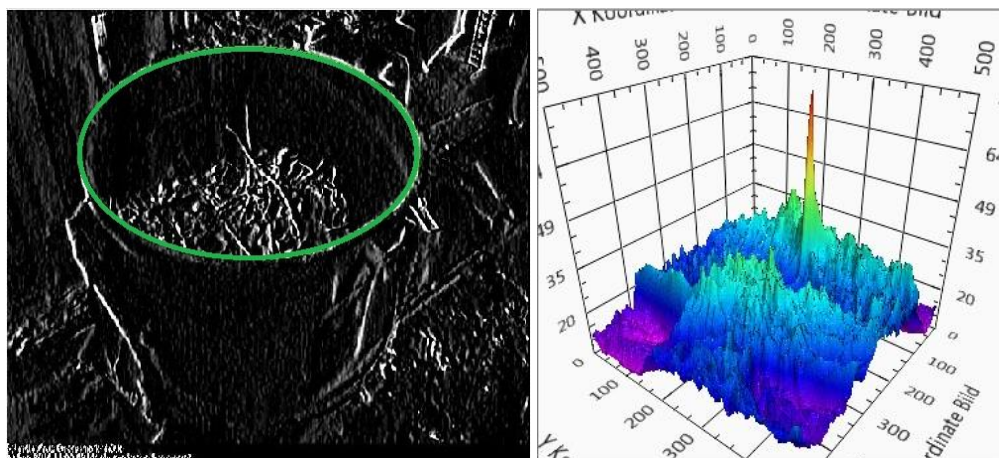


Figure 20: Manual adaption of an ellipse to the edge of a scrap basket (left) and 3D plot of the correlation between image and reference ellipse (right). The sharp and high peak in the plot denotes the centre of the basket which can be determined.



Figure 21: Images of the scrap basket with overlay for a cone shaped scrap pile.

Within the fitted reference ellipse the filling level of scrap in the basket was examined. The distance between reference ellipse and scrap was evaluated. Since the dimensions of the basket are known, the reproduction scale can be calculated. By this means the scrap basket filling level is determined. To take into account the cone of the scrap, the height of the scrap pile at the top (dark blue line) and at the base (bright blue line) of the cone are evaluated to account for different angles of re-pose (**Figure 21**).

To check the accuracy of the image analysis, in the table in **Figure 22** the filling level as determined by the image analysis is given for the images displayed in Figure 19. The image analysis gives good results at different ambient conditions and in a wide range of filling levels between 48% in image d) up to 94% in image e).

Image	Filling level (%)
a	87
b	-
c	-
d	48
e	94
f	84
g	90
h	80
i	76

Figure 22: Scrap basket filling level of images in Figure 19 by novel image analysis

For comparison, the results of the image analysis software and the results of operator estimations were correlated for 439 baskets (**Figure 23**). For a filling level of > 90 % the correlation is sharp since both techniques can identify a high filling level with good accuracy, while at medium filling levels the correlation is not as good for different reasons. The operator estimation is influenced by a different absolute scale of each person. Furthermore, it is difficult to reproducibly distinguish between different medium filling levels. In some cases the crane hook was in the field of view so that the image analysis wrongly detects it as scrap, which leads to an overestimated value especially at lower filling levels.

Scrap basket filling fraction

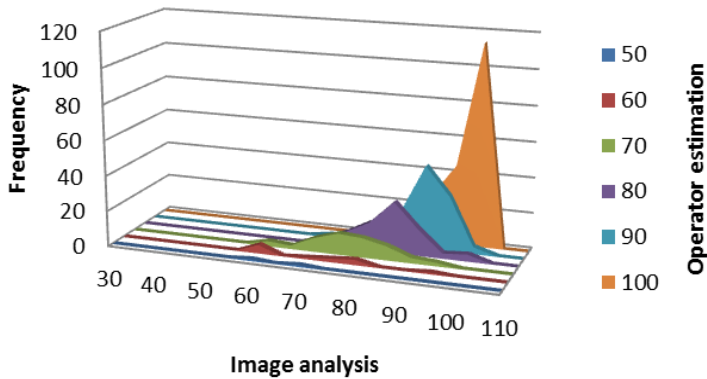


Figure 23: Comparison of image analysis results and operator estimations for the scrap basket filling level

Thus, the software is robust against changing conditions like illumination of the basket and day light in the background. Also the size, shape and colour of the scrap do not matter for the scrap detection, and the software gives a linear scale for different filling levels. The result of the image analysis on the filling level is transmitted via ODBC interface to a data base where it is stored for further calculations. The processed image and the evaluated filling level are displayed on a screen in the control room.

Based on the camera based determination of the scrap basket filling level together with the weight of the loaded scrap from the process data base, the mean scrap density was evaluated. This information is used to derive the average effective bulk density of each loaded scrap type by statistical analysis. The scrap basket has a filling volume of 110 m^3 . Using this information the relative filling level is converted into an absolute filled volume. The information on the weight of the loaded scrap types was accumulated. The mean scrap density is then calculated as the relation between accumulated weight and filled absolute volume. **Figure 24** shows the mean scrap density as a function of loaded total mass for a larger number of evaluated scrap baskets. For process reasons it is desired to charge most of the scrap and especially the heavy pieces with the first basket. This is reflected by the measurement results. The first basket is about 20 % heavier than the second basket and the mean density is higher by almost the same percentage.

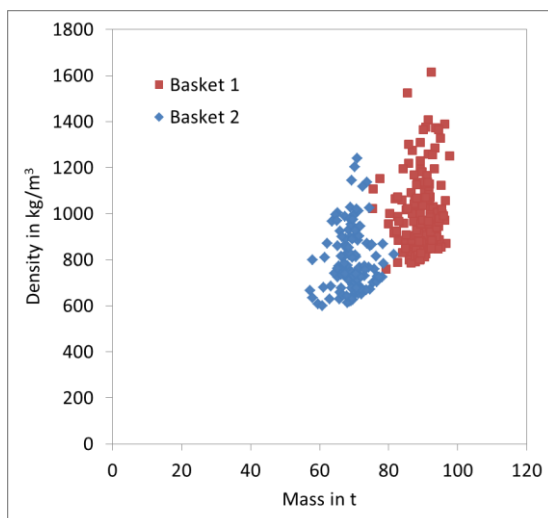


Figure 24: Mean density of the loaded scrap in the basket versus the loaded scrap mass for the first and the second basket

Based on the results of the mean scrap density and the knowledge of the loaded masses of the scrap types for individual baskets a statistical analysis was performed to evaluate the scrap density of the individual scrap types. Using the evaluated density and the loaded mass of individual scrap types the basket filling level was estimated. The results are plotted versus the basket filling level estimated by the operator during a trial campaign for about 500 baskets in **Figure 25**. The calculated filling level agrees with the measured filling level with an error standard deviation of 10.3 %.

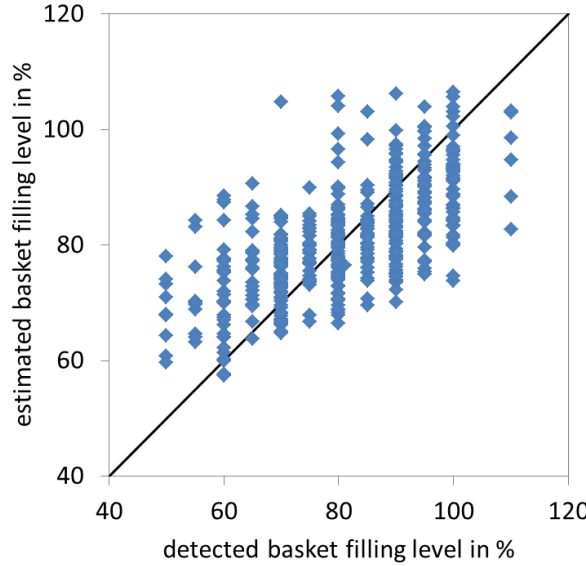


Figure 25: Estimated basket filling level based on the effective scrap density of the individual loaded scrap types versus the detected basket filling level

The calculated effective bulk density for some often used scrap types is listed in **Table 1**. These values were added to the material master data and used in the dynamic process model.

Table 1: Calculated effective bulk density for some often used scrap types

scrap type	calc. bulk density kg/m ³
E1	600
E2	1265
E3	1027
E40	1604
E8	658
E6	1257
E5M	1050
briquetted turnings	1321

Task 1.4: Installation of devices and development of analysis procedures to monitor scrap meltdown behaviour (HSU, GMH)

A vibration sensor system has previously been used at an AC furnace to detect and localize the disposition and level of foamy slag in the furnace vessel [3]. In this previous work, three vibration sensors were installed at the level of the water-cooled panels in a 120° angle, each one in line with one of the electrodes as shown in **Figure 26**.

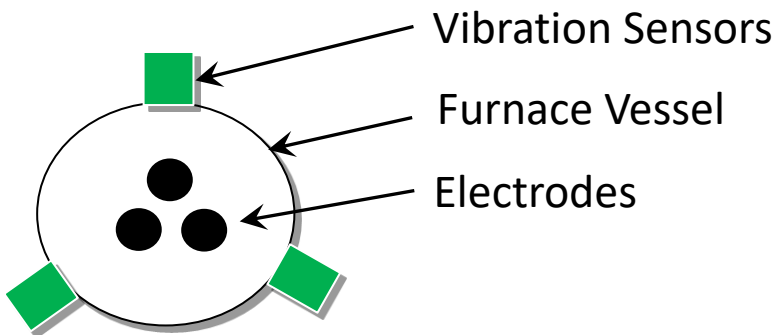


Figure 26: Vibration Sensor Configuration at an AC Furnace

In the underlying model to assess slag behaviour based on the vibration measurements, the electric arcs are considered to be the only vibration sources. The sensor signals are then compared with the effective power of the furnace and further process data. It is shown that due to the different vibration absorption behaviour of the different materials present between electric arc and respective sensor, most importantly steel, slag and gaseous phase, conclusions regarding disposition and level of foamy slag can be drawn. Further work in the current project was based on and extends this general approach, mainly by transferring these previously AC furnace specific findings to a DC furnace in the tasks defined in the outlined work programme.

One objective in this project was an on-line monitoring of the scrap meltdown behaviour by interpretation of vibration sensor signals. Especially a correlation between the vibration sensor signals and the level of unmolten scrap in the furnace was to be found. It was expected that the vibration spectrum changes during the meltdown process as observed in the above mentioned previous work. Thus it can be used to characterize the state of the process. The so-established assessment of the meltdown process by evaluating the sensor signals was then to be used for optimizing the point in time when the second scrap basket can be charged into the furnace.

The first step was to choose a suitable vibration sensor system and locations to place the sensors at the DC furnace of GMH. In previous experiments, vibration sensors had already been installed at this furnace at the main cooling water pipes, but the signals were last evaluated about seven years ago. So the general function of these sensors was uncertain. The exact installation locations of these sensors are shown in **Figure 27** and **Figure 28**. The existing sensors had been installed in three pairs with perpendicular directions of sensitivity at each green-circled position as illustrated in Figure 27. The functionality of these previously installed sensors has been re-evaluated but it was decided not to re-use them for the current project. Additionally, two vibration sensors had been installed on the fire-proof brickwork at the bottom of the furnace vessel before. However, these sensors had been destroyed after a short time due to excessive heat, as temperatures rise well above 250°C at this section of the furnace.

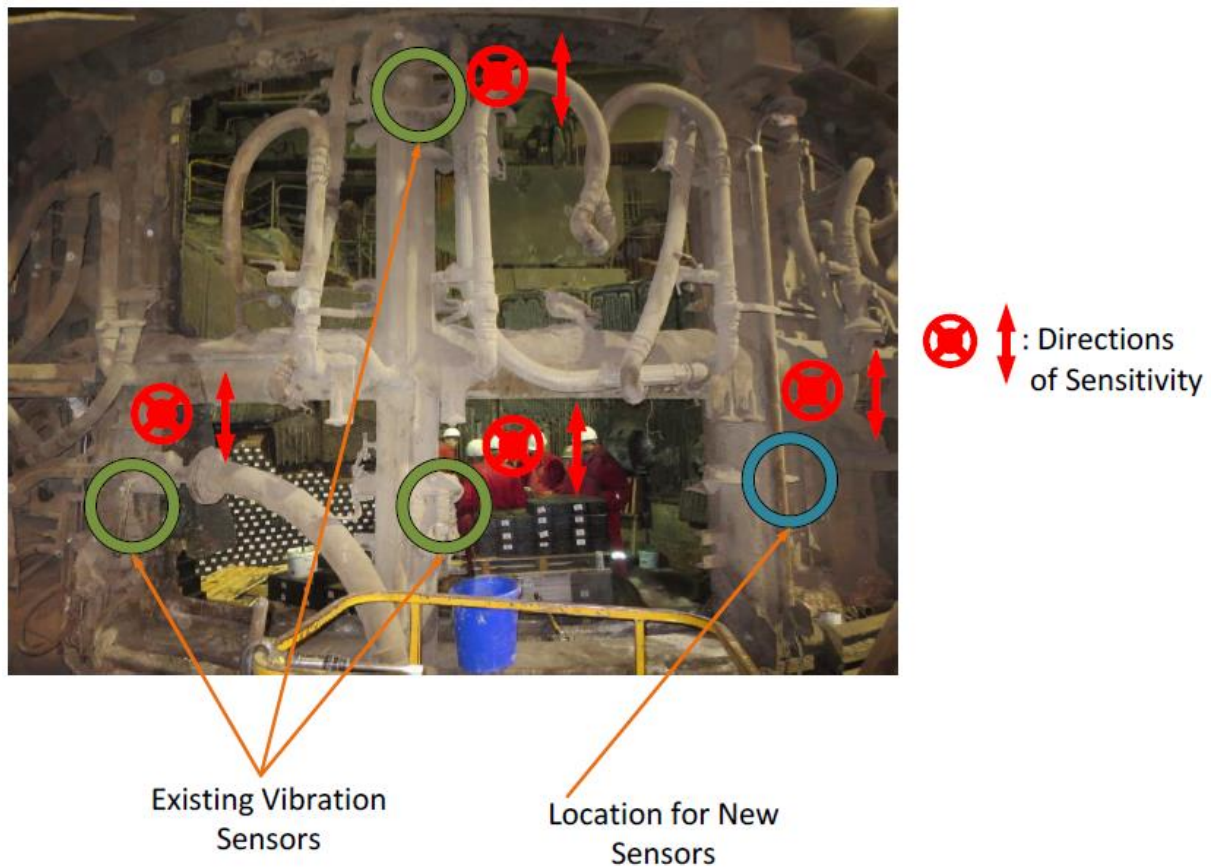


Figure 27: Vibration Sensor Installation Positions at the Main Cooling Water Pipes

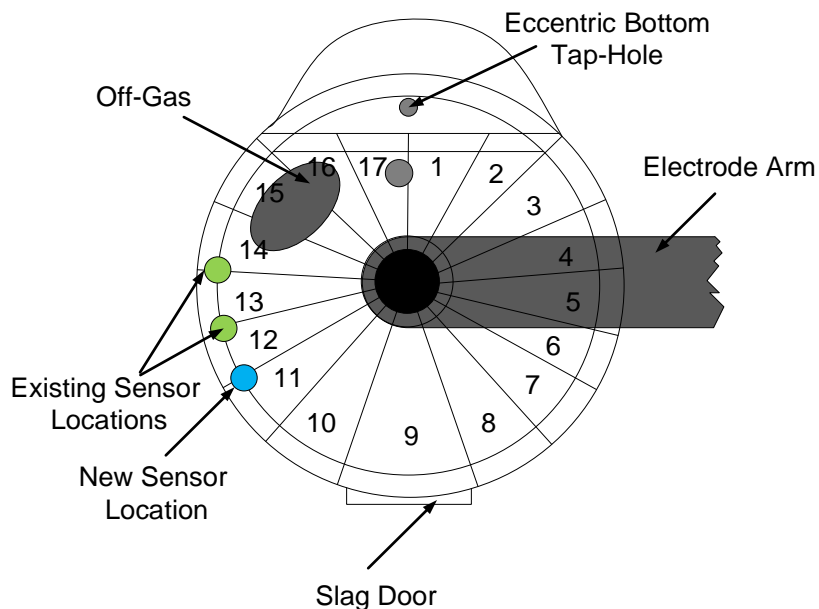


Figure 28: Schematic Top View of Vibration Sensor Positions at the GMH DC Furnace

Figure 29 shows several generally possible positions for the new sensors as well as their corresponding vibration transmission paths. Because of the negative experience of sensors overheating in the area of the fire-proof brickwork at the bottom, this area did not seem to be suitable for starting with vibration measurements in this project. The most sensible place to install the new sensors was considered to be at one of the main cooling water pipes, similar to the previously installed sensors. The exact position for the new sensors is also shown in Figure 27 and Figure 28. The advantage of this installation location is that generally these pipes will not be displaced during

maintenance work; hence long-term installation and operation at this location seem possible. Moreover, the expected temperature here is only about 60 °C and a good accessibility is given.

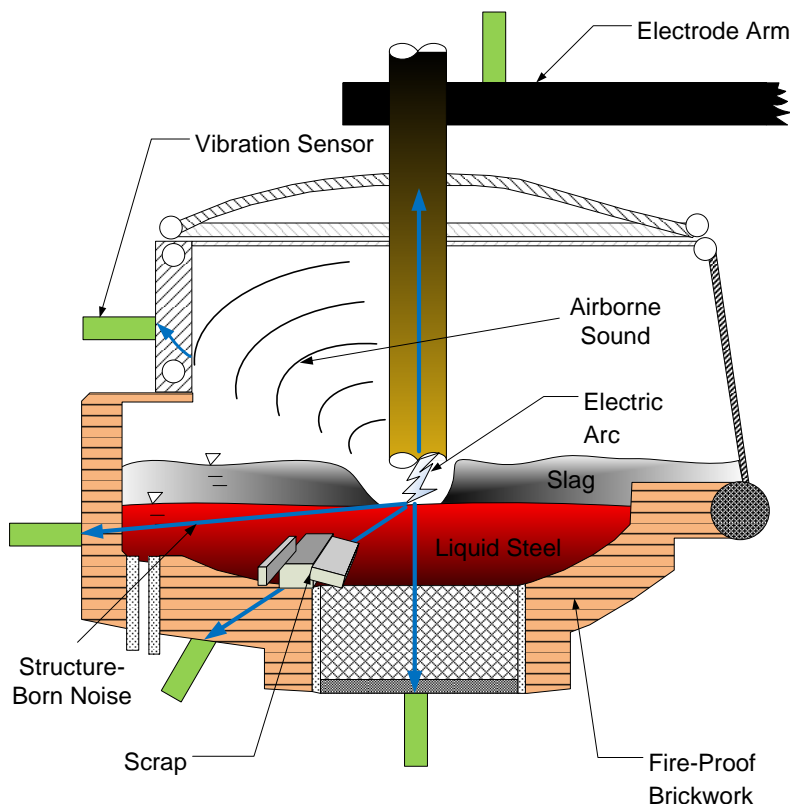


Figure 29: Generally Possible Positions for New Vibration Sensors

Concerning the sort of sensors to be used, a market research revealed many different functional principles and characteristics. However, most sensors are based on the same general concept. An electrical potential proportional to external vibrations is generated by a sensory element mounted between a moveable seismic mass and a fixed reference point. Sensory elements can be capacitive or based on the hall-effect. These types of sensors are characterized by a rugged design but they are highly susceptible to electromagnetic fields. Therefore, for industrial vibration measurements, sensors based on the piezoelectric effect are most commonly used.

There are several possibilities of piezoelectric sensor designs. In this project, a sensor with a state-of-the-art shear-design, as shown in **Figure 30**, was selected.

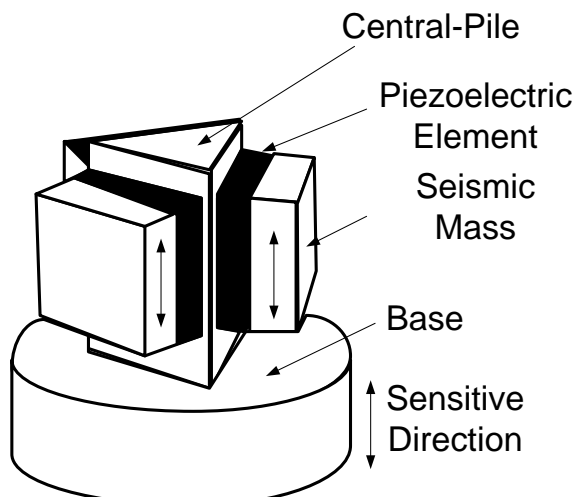


Figure 30: Design Principle of a Shear-Type Vibration Sensor

In this design, three piezoelectric elements, all polarized in the overall sensor's main sensitive direction, are arranged around a triangular central-pile. Three seismic masses are attached to the opposite faces of the piezoelectric elements. External vibrations along the sensitive sensor axis result in shearing strain in the piezoelectric elements; hence an electric charge signal proportional to the external vibration is generated. This assembly is suitable for vibration measurements in only one defined direction, whereas noise from the other directions cannot be detected.

The general advantages of piezoelectric sensors are a linear measurement range, a large frequency range and robust designs; they are mostly maintenance-free and built for durability. Therefore, it was decided to use this kind of sensor type in the project. It was assumed that these sensors are suitable to work in the rough environment around the electric arc furnace, as their heat resistance typically ranges up to 100 °C and they usually come hermetically sealed. However, piezoelectric sensors typically are uni-axial, so two identical devices were installed at the selected location in order to pick up vibrations in two independent directions. The specific sensors chosen for the project are furthermore equipped with integrated electronics for generating an output voltage signal proportional to the piezoelectric charge internally generated, hence it is possible to place the necessary amplifier more than 15 meters away from the sensors. In addition to the specified sensors, complimentary measurement equipment was selected and purchased, consisting of a four-channel measurement amplifier with a gain of 60 dB and integrated high-and low-pass filters, a calibrator, electromagnetically shielded cabling, mounting accessories and a PC for analysis. Furthermore an already existing one-channel portable measuring instrument was available for first measurement tests.

The next steps regarding vibration measurements were installing the sensors at the furnace vessel and establishing a connection to the amplifier, which was located 15 meters away from the planned sensor mounting position. The measurement setup is shown in **Figure 31a.) and b.).** First measurements were carried out by using a portable measuring instrument and magnetic mounting accessories.



a) Temporary installation of sensor and cabling b) Temporary installation of data recording-devices next to the EAF

Figure 31: Temporary Vibration Measurement Setup

In this way, further impressions of the characteristics of the vibration measurements were obtained.

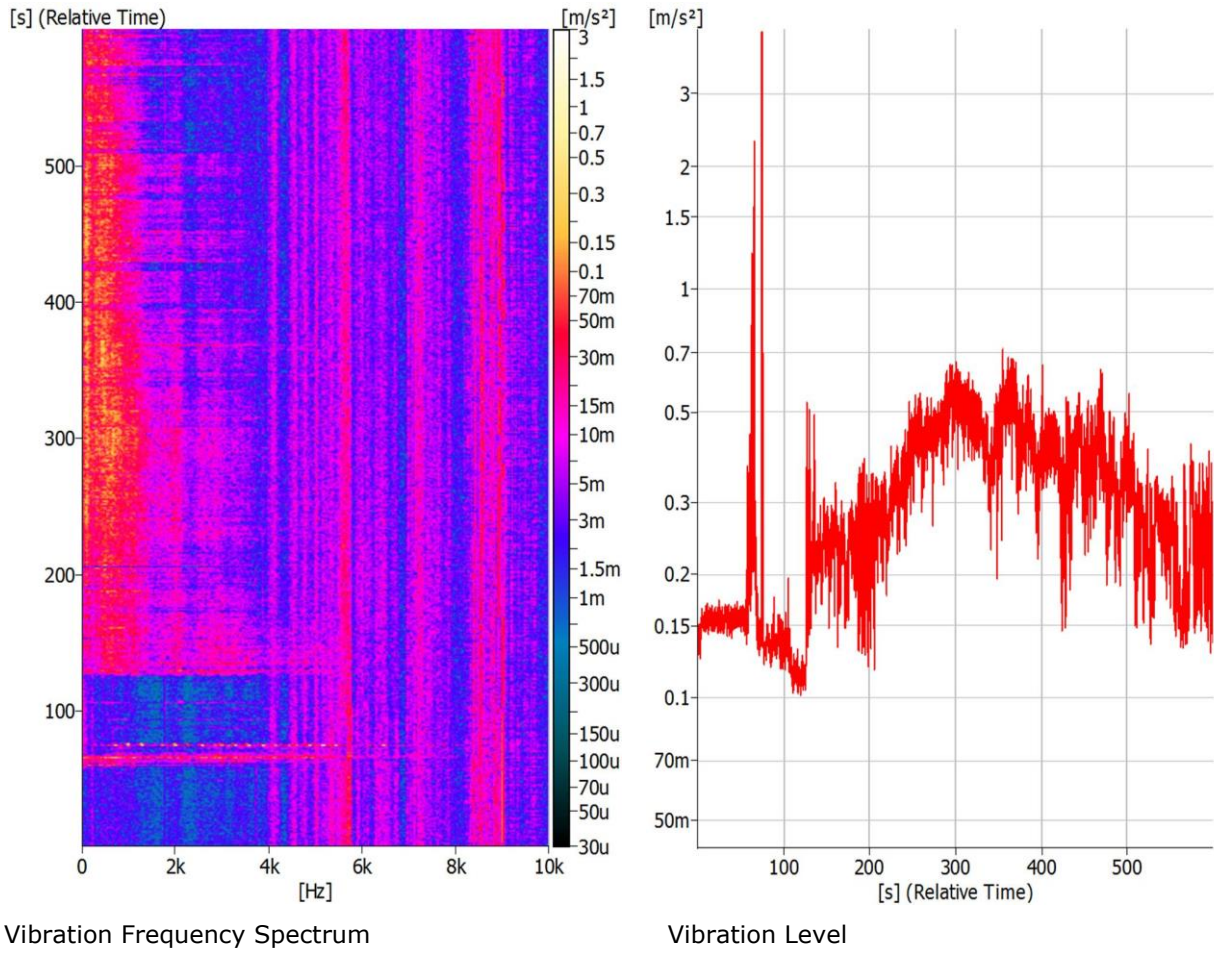


Figure 32: Vibration Measurement Signals of the First 10 Minutes into the Meltdown Process

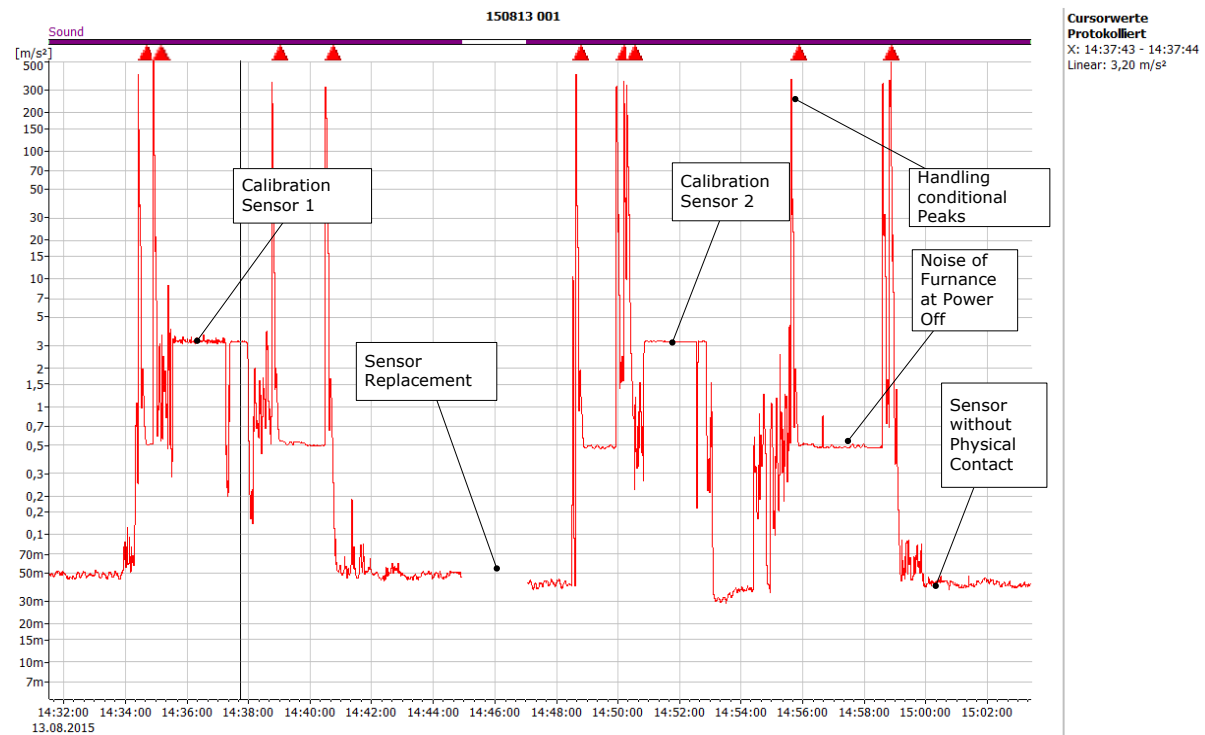
Figure 32 displays typical vibration measurement signals as gathered with the newly installed devices. The figure shows the frequency spectrum in a range between 1 Hz and 10 kHz (left part) as well as the resulting overall vibration level (right graph) during the first ten minutes of a meltdown process. A well-defined vibration peak due to scrap charging at 70 s is observable. At 120 s, electric energy input begins, resulting in a rise of the vibration sensor signals. Several series of similar measurements picked up at the predefined sensor positions and in the chosen orientation were recorded, confirming the suitability of the sensors' placement. Therefore the preliminary magnetic mounting of the vibration sensors was replaced by a long-term mounting at the selected placement as shown in **Figure 33**.



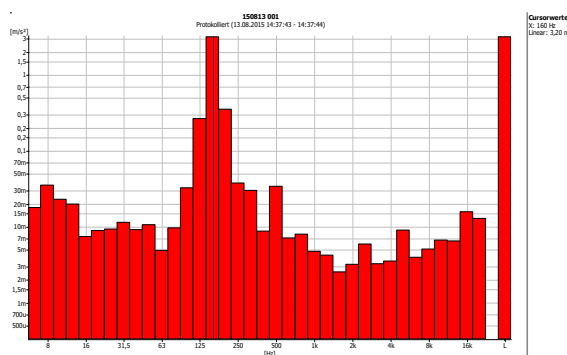
Figure 33: Long-Term Installation of the Vibration Sensors at the Furnace Vessel

Based on these initial results, the previously only roughly defined sensor positions were optimized, sensors were calibrated and the frequency range of interest was limited. In the time-dependent frequency spectra, nearly constant spectral components in the range from 4 kHz and upward were observed. These components are even present when the furnace is off, so they are obviously independent of the meltdown process and superimpose those signal components which do change as meltdown progresses. Therefore the frequency range of interest was narrowed down to a range from 1 Hz to 3.5 kHz by choosing a sampling rate of 7 kHz. Thus, constant spectral components with little information content were no longer taken into consideration. Furthermore, different methods of frequency analysis were tested for their suitability to derive conclusions about the scrap meltdown behaviour in the furnace from them.

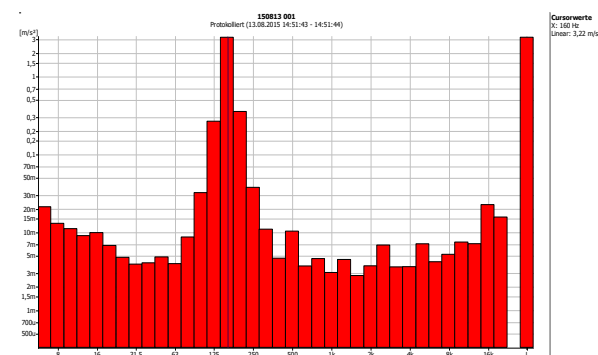
For long-term measurements, the sensors' wiring was extended and routed through to a separate measurement room about 150 meters of cable length away from the EAF. An already existing cable line could be used for this purpose and was successfully tested for suitability. For this test, the sensors were excited with a calibrator, which oscillates at a defined frequency of 159.2 Hz and amplitude of 3.16 m/s^2 . The corresponding vibration sensor signals were registered in the measuring room, exhibiting the expected level and frequency, as depicted in **Figure 34**.



Vibration Level during Calibration



Vibration Spectrum during calibration of sensor 1



Vibration Spectrum during calibration of sensor 2

Figure 34: Calibration of Vibration Sensors

Observations of the vibration sensor signals during furnace operation suggest that electromagnetic fields around the furnace do not seem to influence the signals. Whether the sensors are subject to long-term drift were evaluated in further re-calibration measurements.

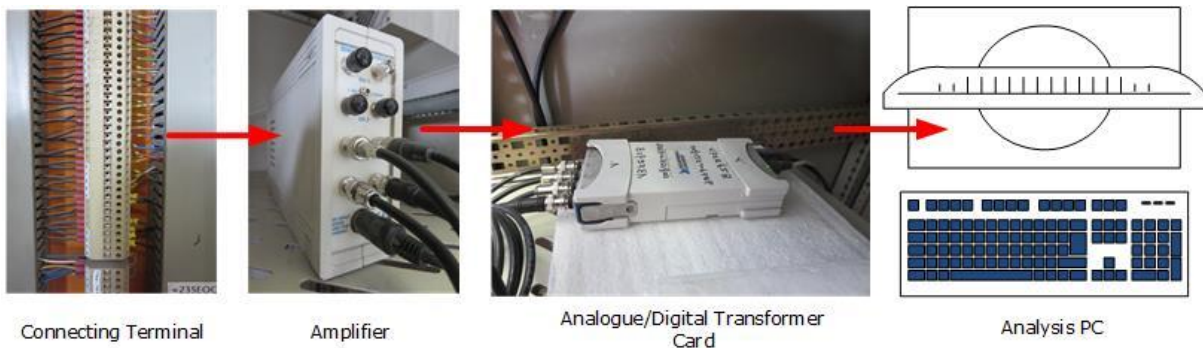


Figure 35: Signal Routing inside the Vibration Measurement Room

Figure 35 illustrates the signal flow within the measuring room. The vibration sensor signal wiring arrives at a connecting terminal in a bus bar. The signals are then fed into an amplifier with optional signal conditioning. Subsequently, the signals are digitized through a suitable analogue/digital transformer card in order to be recorded by the analysis PC. This computer is further connected to the central programmable logic control, facilitating the evaluation of the vibration sensor signals and their comparison with other process data.

In addition to the new vibration measurement system, a spectrometer system had previously been installed inside a water-cooled box, called BIO-Box, inside one cooling panel of the GMH DC furnace [4]. The set-up is drafted in **Figure 36**. This measurement system consisted of two spectrometers with different viewing angles and different ranges of detectable wavelengths. Two identical spectrometers were installed, but due to the considerable maintenance and repair effort caused by the spectrometer system, it was decided to unmount the devices so they were no longer available for the project. Nevertheless, first findings and results of the spectrometer system, gathered before it was removed are mentioned below, although they could not be used further for the project.

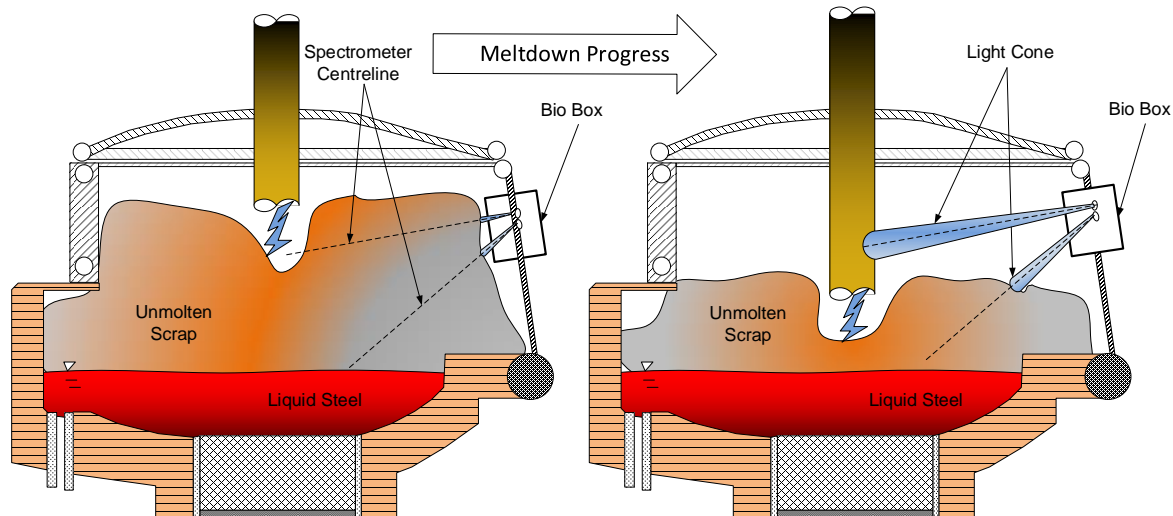


Figure 36: Observation of the Meltdown progress using a Spectrometer System

In this project, the spectrometer system was intended to be used to support the vibration measurement system by detecting scrap pile collapses and rendering additional information about the level of unmolten scrap or foamy slag in the furnace vessel. During the meltdown process, different

situations concerning the covering of the spectrometers' viewing ranges by the charged materials were expected as well as different distributions of the detected radiation. These meltdown-progress-dependent changes in the recorded spectra were analysed in order to derive a measure describing the meltdown behaviour.

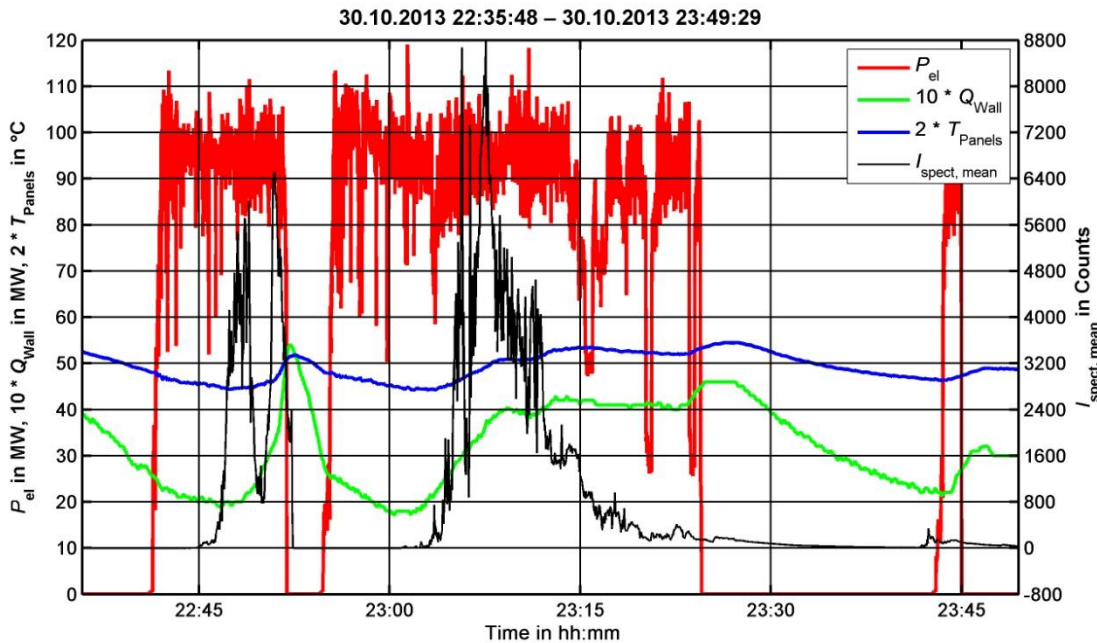


Figure 37: Process and Spectrometer Data during a Two-Basket Heat

Figure 37 and **38** show exemplary results from a previous project [4], in which the detection of a free-burning arc using the spectrometer measurements was the main objective. The assumed dependency of spectral data on the meltdown progress is emphasized by figure 37, where the run of the mean spectral intensity ($I_{\text{spect, mean}}$) over all detectable wavelengths of one spectrometer is plotted along the furnace's electric power (P_{el}) as well as the corresponding temperature (T_{Panels}) and thermal flow (Q_{Wall}) at the cooling panels. It can be seen that after charging a scrap basket (e. g. before 22:42 and between 22:52 and 22:55, when P_{el} is zero), a few minutes into the following scrap meltdown process, the mean spectral intensity rises. Reason being that scrap, as it melts down, slowly moves out of the corresponding spectrometer's viewing range, allowing the arc's radiation to directly pass through to the spectrometer. Later in the melting process, foamy slag is generated, again covering the spectrometer's viewing range and thus resulting in a declining mean spectral intensity curve towards the end of power-on-time. This general behaviour was analysed in more detail in this project, especially considering the additional information that can possibly be derived from the two different viewing angles or different wavelength ranges of the spectrometers. Instead of observing only the mean spectral intensity, the focus was on characteristic changes in observed spectral lines or the distribution of intensities in specific wavelength ranges.

Prerequisites for this new analysing approach are the following. First, the recorded spectra need to be reproducible in a short time frame (seconds) in order to allow deriving relatively stable indices from them. However second, on a larger scale (one to ten minutes), the spectra must exhibit changing characteristic features that can be correlated with the meltdown progress. In the recordings of the previous project, it could be shown that the installed spectrometer set-up fulfils both requirements.

In **Figure 38**, five spectra consecutively recorded by the high-resolution spectrometer installed in the upper position are plotted as intensity vs. wavelength graphs (3648 single, equally spaced

wavelengths from about 480 to 550 nm). Despite the variation in absolute intensity values, the overall shape of the spectra remains nearly unchanged, proving short-time reproducibility. Precedent analyses in the previous project have additionally shown that the example depicted here is representative for the majority of spectrometer readings.

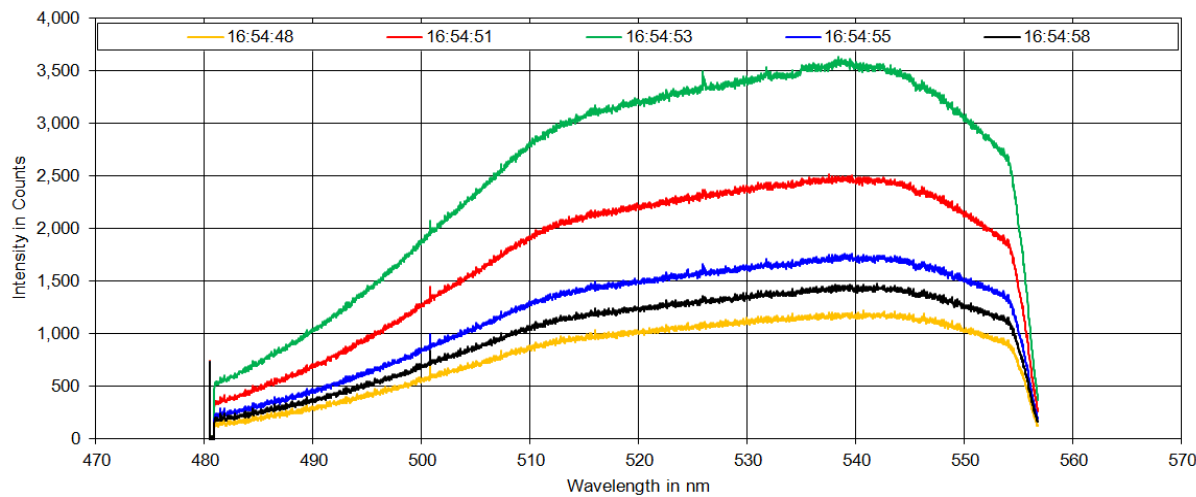


Figure 38: Spectra of a High Resolution Spectrometer, Installed in the Upper Position

Figure 39 and **Figure 40** show two similar sets of intensity vs. wavelength graphs, recorded by a broadband spectrometer (3648 wavelengths from about 200 to 1100 nm) installed in the lower position. Between these two sets, 10 minutes of the meltdown process have elapsed and a considerable change in the general shape of the spectra can be observed. For example, figure 39 exhibits a distinct absorption line at about 590 nm which is no longer present in figure 40. Moreover, the latter graph features two slight ridges at 590 nm and 760 nm that are absent in the first one. As most of the recorded spectra yield similar observations, the afore-demanded presence of meltdown-dependent characteristic spectral features is also generally confirmed. Consequently, it seemed possible to develop algorithms to automatically detect these features and correlate them with the meltdown process.

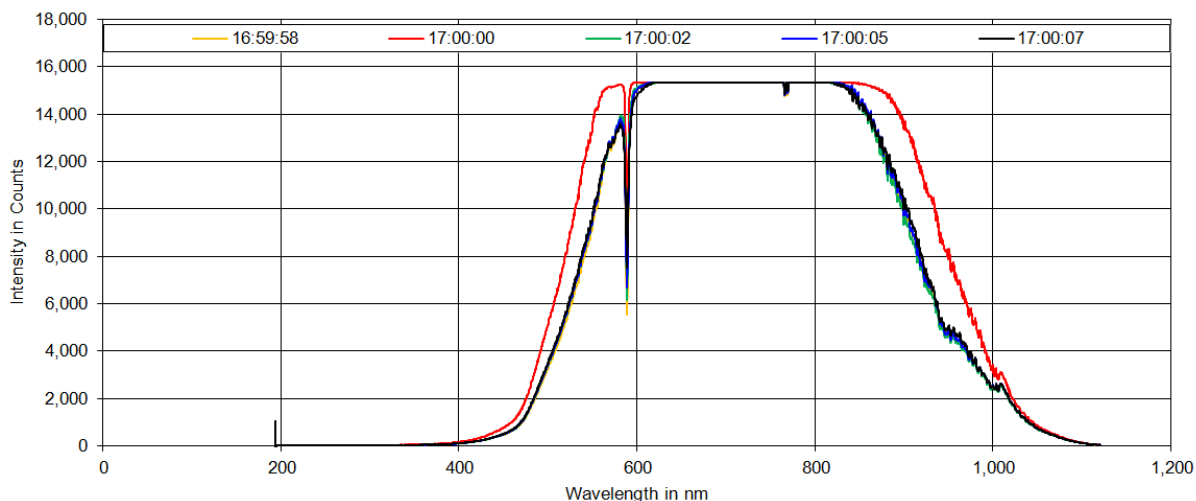


Figure 39: Spectra of a Broadband Spectrometer, Installed in the Lower Position (with Clipping Effect)

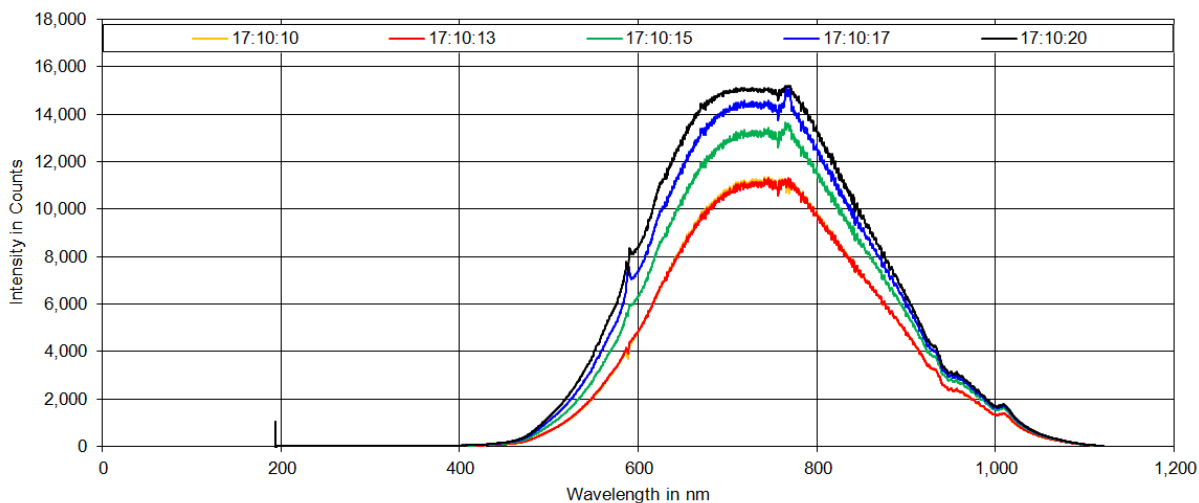


Figure 40: Spectra of a Broadband Spectrometer, Installed in the Lower Position

However, previous recordings also reveal that before any reliable conclusions may be drawn from the recorded spectral data, there is need for improvement at the data acquisition stage. Figure 39 illustrates a severe clipping effect occurring between 600 and 800 nm due to overexposure. This can possibly be counteracted by automatically adapting the spectrometer's exposure time to the actual radiation intensity conditions. This was considered in further developing the spectrometer system's software. The existing spectrometer analysis software was extended by new features including communication with the central programmable logic control in order to receive process data, e. g. furnace effective power or charging signal, and to send back the intended analysis results, for example the detected level of unmolten scrap in meters. The latest software revision allowed storing spectrometer and process data with the same time stamp, triggered by the beginning of a new melt. This established the basis for the following analyses of the meltdown behaviour and evaluation and optimizing of the underlying algorithms. The advantage of this set-up was that the analyses of spectral data are done in the spectrometer system's software which is directly connected to the spectrometer and therefore has access to the whole spectral information. In contrast to that, analyses carried out in devices connected to the central programmable logic control would be less precise because the data volume of the entire spectral information cannot be routed through or stored in this central system. Furthermore, the revised spectrometer system's software is equipped with error handling and diagnostic features, informing operators about the spectrometer working status, if it is covered by slag or if the lenses have to be changed.

The next steps regarding spectrometric measurements were installing the new software revision at GMH, testing the new features as well as evaluating and augmenting the algorithms, especially with the above-mentioned adaptive data-acquisition features. Additionally, the spectrometers were newly calibrated and their exact geometric conditions, e. g. position and viewing angle, were verified because these parameters need to be considered for optimizing the analyses algorithms.

After successful implementation of the new software, the spectrometers were totally damaged by water as a result of a leakage at the water supply of the spectrometer housing's cooling circuit. Consequently, new spectrometers were ordered, calibrated and installed as quickly as possible. In contrast to the previous project, where the requirements and objectives demanded two spectrometers with different wavelength ranges, two spectrometers with an identical wavelength range from about 200 to 1100 nm were installed. Reason being that for the objective of detecting different scrap levels by using the spectrometers as light barriers, directly comparable measurement signals from identical spectrometers seemed more helpful.

Another problem which was detected while evaluating the new software revision after the installation of new devices were several cable breaches. The data cable connecting the spectrometers and the corresponding analysis PC runs about 200 meters, so troubleshooting, failure localization and repair turned out to be rather time-consuming.

In parallel with the above mentioned repair work, further development was carried out regarding the technical challenge of permanently providing an unobstructed view into the furnace through the spectrometer lenses. Especially during the melting process, sputtering slag is prone to hit the view hole and to thereby constantly block it. Furthermore, the atmosphere around the furnace is generally loaded with fine dust, which is bound to form obstructing deposits along the light channel. Therefore, in order to generate reliable and robust online spectrometer signals for the industrial application considered here, alternative designs of spectrometer lens adapters have been developed and tested. The resulting geometries are illustrated in **Figure 41** and **Figure 42**.

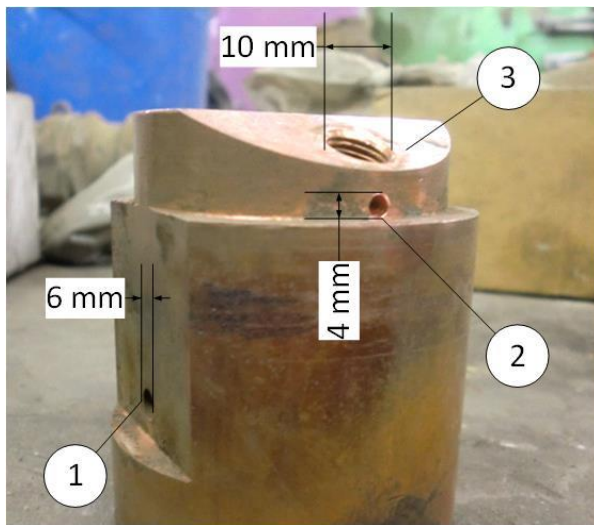


Figure 41: Original Design of a Lens Adapter

Figure 41 shows the first design of a lens adapter as used in the previous project. Pos. 1 marks the nitrogen inlet allowing a slag-rinsing gas flow from the inside of the pressurized water-cooled box along the light channel and into the furnace. An additional nitrogen inlet is situated at Pos. 2, directly in front of the lens, in order to prevent fine dust from accumulating. This drill hole was added during this project and proved effective. The lens itself can be attached to the thread at Pos. 3.

Newly developed designs especially addressing the necessity to prevent slag from getting stuck in front of the view hole are depicted in Figure 42.



a.) Isometric view with direct drilling fluid supply and passive flush of surrounding area

b.) Sectional view with direct drilling fluid supply and passive flush of surrounding area

Figure 42: Geometric models of lens adapters for use of spectrometers at the GMH EAF

Figure 42a.) and b.) show the final lens adapter design which was installed in the upper spectrometer view hole at the furnace. The functional principle is based upon a special arrangement of drill holes which direct the nitrogen flow into a circulatory movement, drilling the light channel free from slag deposits. These drill holes may be directly fed with nitrogen using an extra supply or otherwise nitrogen will flow through the holes due to the overpressure inside the water-cooled box. Additionally, six secondary nitrogen conductors through the lens adapter are situated around the central light channel. These conductors are also supplied through nitrogen overpressure and flush the surrounding area of central light channel.

In comparison with the very first adapter design, every new design extends slightly further into the furnace wall. As a result, the face of the adapter pointing towards the furnace centre is aligned with the interior furnace wall. In the previous design, an undercut formed in the wall surface due to the shorter adapter, which facilitated slag deposition. First measurements verified a significant increase in availability of reliable spectrometer signals with this new adapter design.

Considering the spectrometer signals gathered, it can be noted that they generally seemed suitable for aiding the detection of unmolten scrap in the furnace. However, signal interpretation needs to be carried out carefully, as ambiguous signal conditions are bound to arise due to the underlying light barrier principle. In this setup, it can only be detected whether there is an obstacle present between the electric arc and the spectrometer view hole or not, whereas the nature of such an obstacle cannot directly be determined. For example there is no difference between the online spectrometer signals that result from scrap covering or from slag covering the view hole. In both cases, a low signal level will be observed, as the light originating from the electric arc cannot directly arrive at the spectrometer. A distinction can only be made by including additional measurements and process data or by further observation of the signal level development. In case of scrap covering being the reason for the low signal level, a rise is due to occur as the scrap level declines during the meltdown process. If slag covering causes a low signal level, the lens adapter is either blocked and no subsequent signal level increase will be observed, or there is foamy slag in the furnace as is typical during the refining phase. In the latter case, the spectrometer signal will only rise again when the foamy slag level decreases towards the end of the overheating phase, shortly before tapping.

Ultimately, the meltdown behaviour and progress of each charged scrap basket therefore was intended to be derived from a combined analysis of the vibration sensor signals, the spectrometer recordings and further process data. Appropriate indices were defined which characterize the meltdown behaviour of the different scrap mixes.

2.2.2 WP 2: Industrial campaigns to derive additional process information from new measurement devices

Task 2.1: Determination of liquid steel and hot heel amount (BFI, GMH)

To determine the current liquid steel and hot heel amount with the help of the measurement devices installed in Task 1.1, the information of the furnace volume of the GMH DC furnace is needed. As the furnace volume depends on the refractory wear, a simple model has been developed for its determination. For this approach the furnace vessel has been divided into two parts as shown in **Figure 43**, a bottom part where the vessel shape is running diagonally to the anode and an upper cylindrical part.

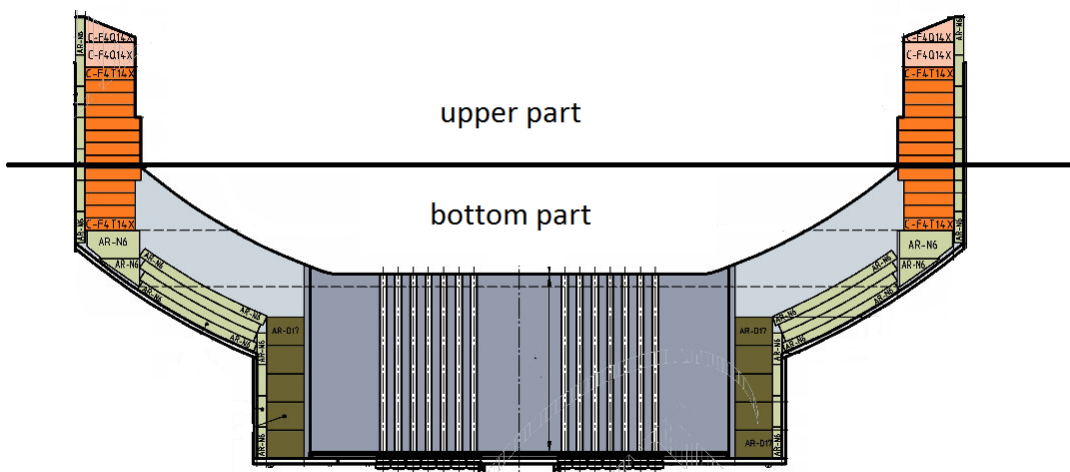


Figure 43: Subdivision of the vessel volume of the GMH furnace into an upper and bottom part

The delta dist sensor measurements are performed just before tapping, when the bath level is in the upper part of the furnace, which means that the bottom part is totally filled with liquid steel. The liquid steel amount can be estimated by the sum of the bottom volume and the filled volume of the upper part which can be derived from the measured level.

The refractory wear of the bottom part has been estimated with the help of the anode wear which is captured after each revamp. A furnace campaign covers about 2000 heats and the mean loss of thickness in the anode area is about 30 cm which means a capacity increase of about 50 t of liquid steel over one furnace campaign. Furthermore the volume of the upper part increases according to the refractory wear at the slag line. Due to the progress of the furnace campaign the diameter increases by about 15 cm which means a further capacity increase of the furnace volume. However, the slag line is the part with the largest wear and the regular maintenance causes further inaccuracies in the estimation of the diameter.

Based on the measured steel bath level and the information of the vessel volume, the amount of liquid steel just before tapping has been determined for a trial campaign of about 100 heats. For this campaign the bath surface was estimated to 28.5 m^3 . Assuming a liquid steel density of about 7 t/m^3 the increase of steel weight in the upper part of the furnace can be estimated by 2 t per cm. The amount of liquid steel in a height of 1200 mm, which covers the whole bottom part of the vessel, was estimated to 147 t. During this campaign the level measurement with the Delta Dist sensor was performed for 34 heats whereby 30 reliable values were acquired.

Figure 44 shows on the left hand side the histogram of the measured steel bath levels for this trial campaign. The average measured value for the bath level just before tapping is 1370 mm. On the right hand-side of Figure 44 the histogram of the estimated liquid steel derived from the measured steel bath level is shown. The average liquid steel weight is about 181 t with a wide scattering.

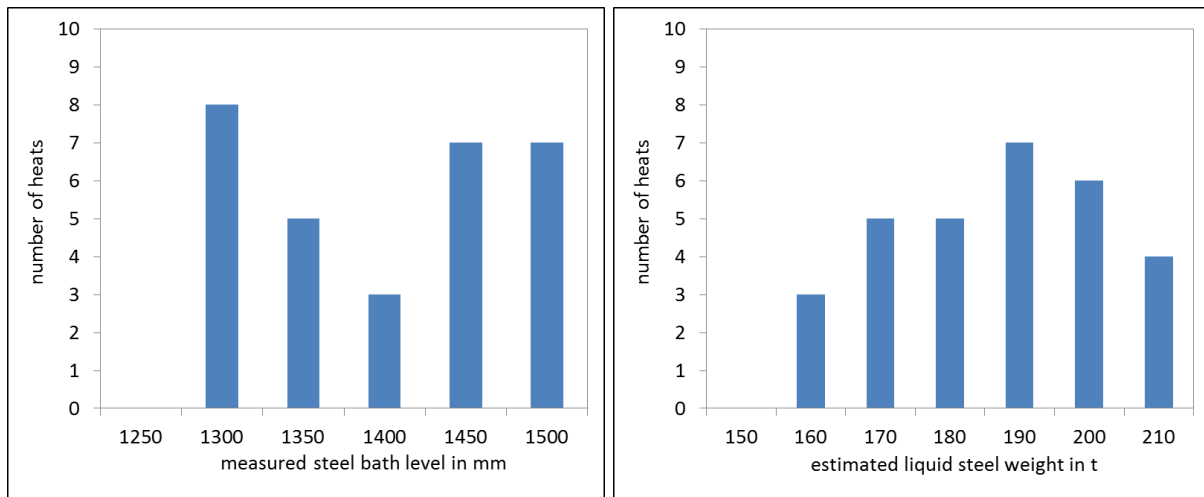


Figure 44: Histogram of measured steel bath level (left) and estimated liquid steel weight (right)

On the basis of the estimated steel weight before tapping, a follow-up of the liquid steel and hot heel amount has been set up. **Figure 45** shows the evolution of both amounts. The values coming from the level measurements are indicated by dots. As the Delta Dist sensor measurements were not performed for each heat, for heats without measurements the follow-up of the amounts was performed according to the expected metallic yield from the charged materials.

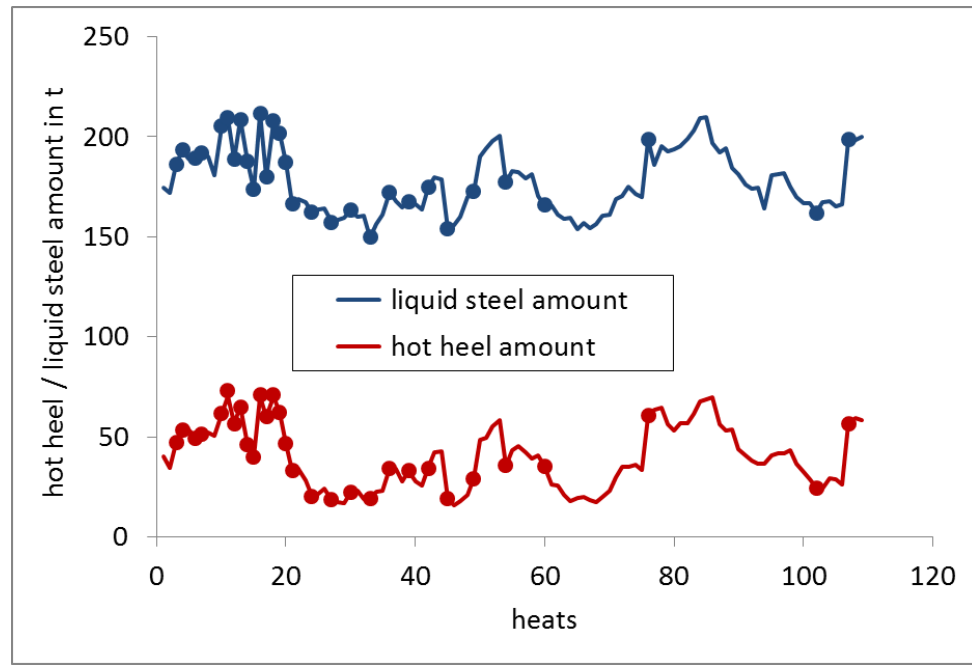


Figure 45: Follow-up of liquid steel and hot heel amount for one trial campaign at GMH

The evolution of the liquid steel and the hot heel shows significant variations which demonstrate the importance of their determination. The application of the Delta dist sensor in regular intervals has been decided by GMH. However, the measurement is not performed for each heat as it causes a delay of about 1 minute. The estimation of the hot heel amount was used in Tasks 3.2 and 5.4 to improve the determination of the scrap-individual metallic yield by a statistical analysis.

In addition to the calculations based on the dip sensor measurements of the steel bath level before EAF tapping, the hot heel amount was also assessed by monitoring the hot heel level after EAF tapping by an imaging system. As described in Task 1.1, three cameras in a protective housing were installed above the EAF to image the entire furnace interior from different angles of view. Image acquisition is triggered when the furnace roof is opened and before the scrap of the first basket is charged. Two images from different cameras are displayed in **Figure 46** exemplarily. For image analysis suitable grey value images were extracted from the image sequence. An algorithm was developed to find within the region of interest (green box) the slag line which is the transition between hot heel and refractory (red line). The hot heel filling level is given with respect to the upper edge of the furnace hearth (blue line) as the height of free board of the furnace. The number of pixels in the image between slag line and furnace contour was then converted into a real space length using the reproduction scale and translated into vertical height information by trigonometry.

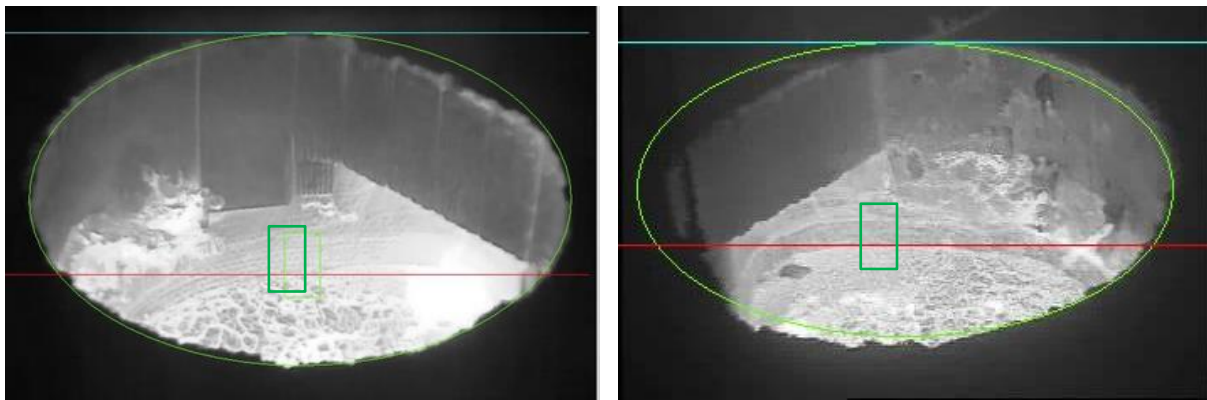


Figure 46: Images of camera 1 and 2 of the inner furnace with results of image analysis

According to the determined free board height and the furnace dimensions together with the refractory wear, the hot heel amount after tapping can be estimated.

To reference the results of the filling level by image analysis, their values were compared to Delta Dist sensor measurements for individual heats (**Figure 47**). The dip sensor measures the height of steel and the thickness of the slag from the furnace bottom before EAF tapping (left part of the sketch). So based on the dip sensor measurements the height of the bath surface after tapping was calculated, taking into account the weight of the tapped liquid steel and the steel density, assuming a surface area of 30m^2 .

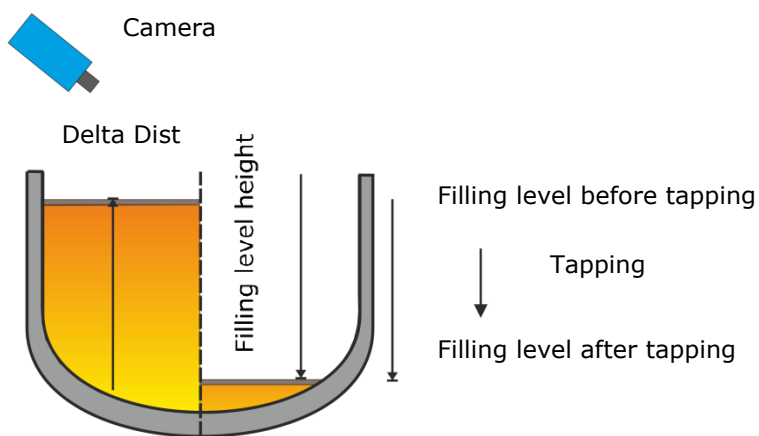


Figure 47: Schematic drawing of the electric arc furnace illustrating the height as measured by the Delta Dist sensor before tapping (left) and the filling level as determined by image analysis after tapping (right)

In **Figure 48a** the results of the dip sensor measurements of the analysed heats are shown. Within this campaign the measured slag height of more than 600 mm for heat no. 5 and no. 9 seems unrealistic, probably as the slag thickness was measured when the slag was still foamy which causes some uncertainty. Thus, these values were eliminated from further analysis. In **Figure 48b** the hot heel level derived from the dip sensor measurements before tapping were compared to the results of image analysis of the hot heel level after tapping. The values based on dip sensor measurements are in a range from 3.9 m to 4.3 m, whereas the results of the image analysis are in a range from 4.1 to 4.3 m. The comparison only showed a weak correlation of both measurement techniques. The dip sensor measurements are taken shortly after heating and oxygen blowing, when the slag might still be a bit foamy. So the result depends on the slag condition. Furthermore it needs to be corrected by the tapping weight which imposes a further uncertainty on the measurement results. On the other hand the image analysis has an accuracy of about 5 pixels which corresponds to about 10 cm in height. Nevertheless, this accuracy should be sufficient to control the hot heel at a constant level. The resolution can in principle be further improved by increasing the reproduction scale choosing an objective with a higher focal length or by increasing the resolution of the camera.

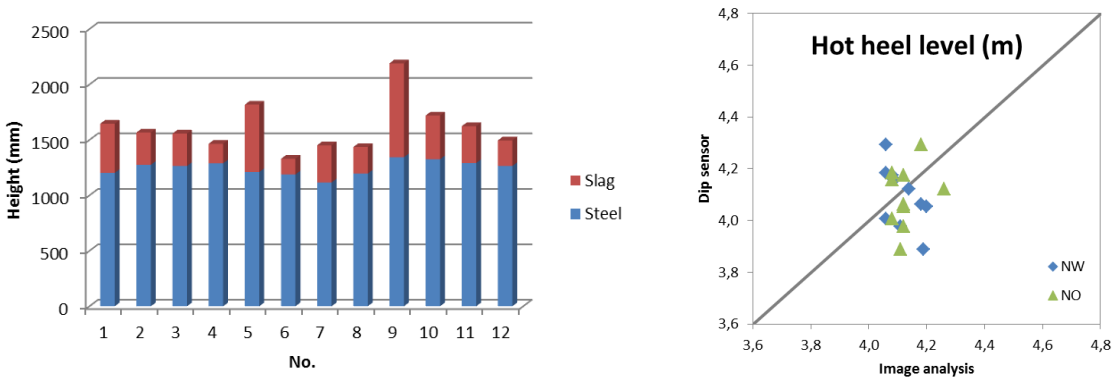


Figure 48: a) Dip sensor measurements for selected heats and b) comparison of hot heel level based on dip sensor measurements and image analysis from two different cameras (NO, NW)

From the hot heel level, the hot heel amount was derived using a simple model for the furnace hearth volume based on a linear wear model of the furnace, which has already been described above. The information on the amount of hot heel is used as an input value for mass and energy balance modelling of the next heat. Together with the filling level of the scrap baskets, the hot heel level which corresponds to the free furnace volume at the beginning of a new treatment is also one input parameter for model calculations to optimise the time for charging the second basket.

Task 2.2: Determination of the slag amount (GMH, BFI)

The slag amount, which accumulates during the meltdown process in the EAF, was estimated with the help of the collected process data described under Task 1.2. For this purpose an off-line slag balance has been set up to determine the heat-individual slag amount. The calculation bases on a CaO balance with known amounts and compositions of added slag formers.

At GMH 24 different material groups are charged into the EAF. These groups consist of 21 scrap groups, 2 different kinds of slag formers and coke. Beside the two different slag formers, a significant amount of CaO is also introduced by the scrap types pig iron skulls and pig iron. By knowing the charged amount of CaO, the slag amount can be estimated with the help of the analysed CaO content in the slag. For the investigated heats a slag sample was always taken together with a

steel sample, after all slag formers have been added and shortly before the whole scrap was molten down, and analysed in the laboratory.

Figure 49 shows the histogram of the calculated slag amounts for about 500 heats. The mean value of the calculated slag weight is 17.2 t. These are the estimated slag weights at the time when the slag samples were taken. For this calculation the weight and composition of the slag at the beginning of a heat, which is remaining in the furnace after deslagging, has been assumed to be constant.

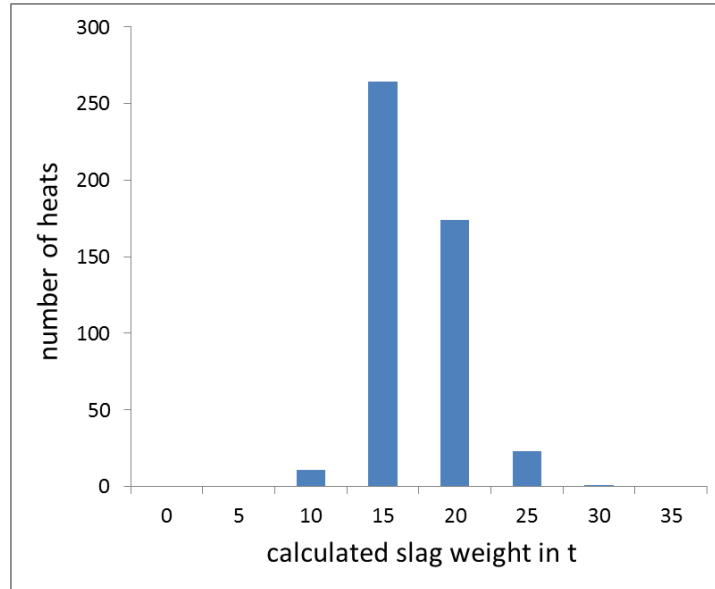


Figure 49: Histogram of the calculated slag weight for the examined heats at GMH

As described under Task 1.2, GMH provided also the measured deslagging weights. At the GMH furnace for each heat the weight of the slag in the slag pot is recorded just before departure by a scale in the hydraulic system of the slag pot carrier. **Figure 50** shows the measured deslagging weight in a histogram for the examined heats.

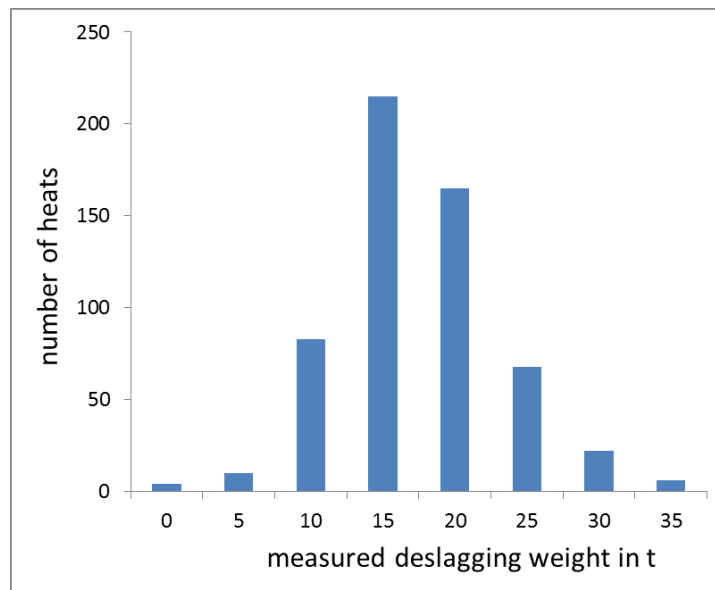


Figure 50: Histogram of the measured slag weight for the examined heats at GMH

The mean weight of 17.4 t is very close to the estimated mean value coming from the CaO balance. The main difference between both histograms is the wider scattering of the measured values.

The heat-individual change in the slag amount is displayed in a further histogram (**Figure 51**). For the largest number of heats the value zero is found, which means that the slag amount does not change from one heat to the next one.

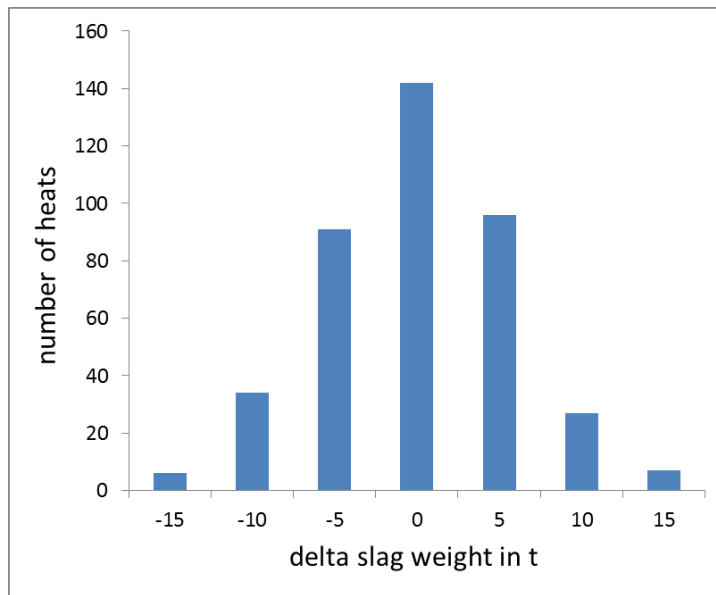


Figure 51: Histogram of the variation in the slag amount for the examined heats at GMH

In **Figure 52** the evolution of the slag weight for a consecutive sequence of 30 heats is displayed. The calculation starts with a default slag amount of 20 t. The changes in the slag weight coming from the difference between calculated and measured slag weight from the following heats were added to this value. The remaining slag amount varies from heat to heat with a maximum value of 15 t.

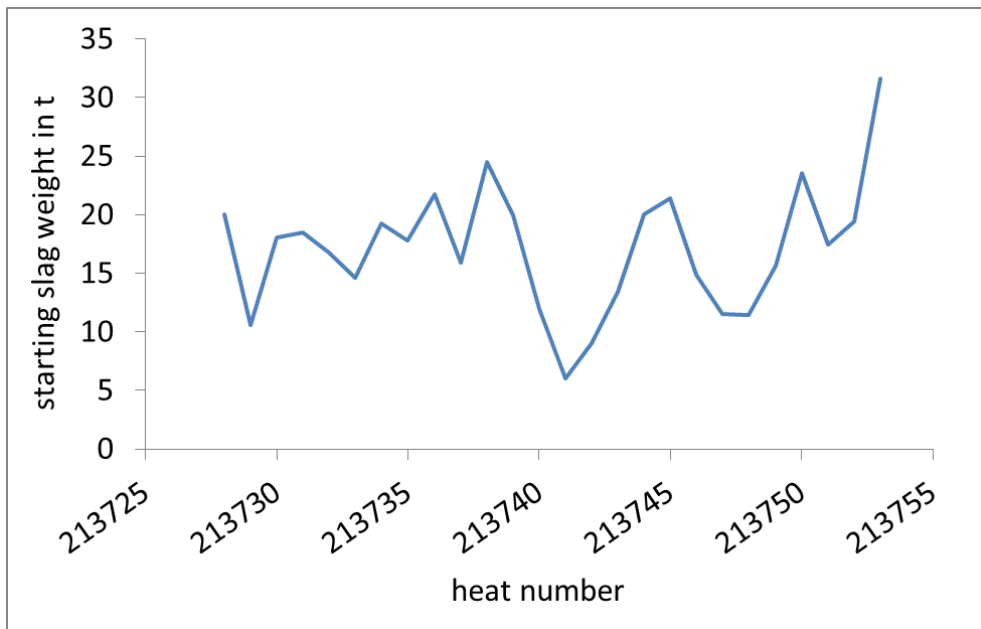


Figure 52: Evolution of the remaining slag in the furnace for a consecutive sequence of 30 heats

Furthermore the calculation of the slag weight remaining in the furnace after deslagging has been performed with the help of the dip sensor measurements described in Task 1.1. During the trial campaign described in Task 2.1 also the slag height was measured by the dip sensor. The slag weight per cm was set to 0.5 t which corresponds to a slag density of about 1.75 t/m^3 . In this stage of the process the slag is still agitated because of the foamy slag creation during refining.

Figure 53 shows the evolution of the estimated slag weight together with the measured values pointed out by dots.

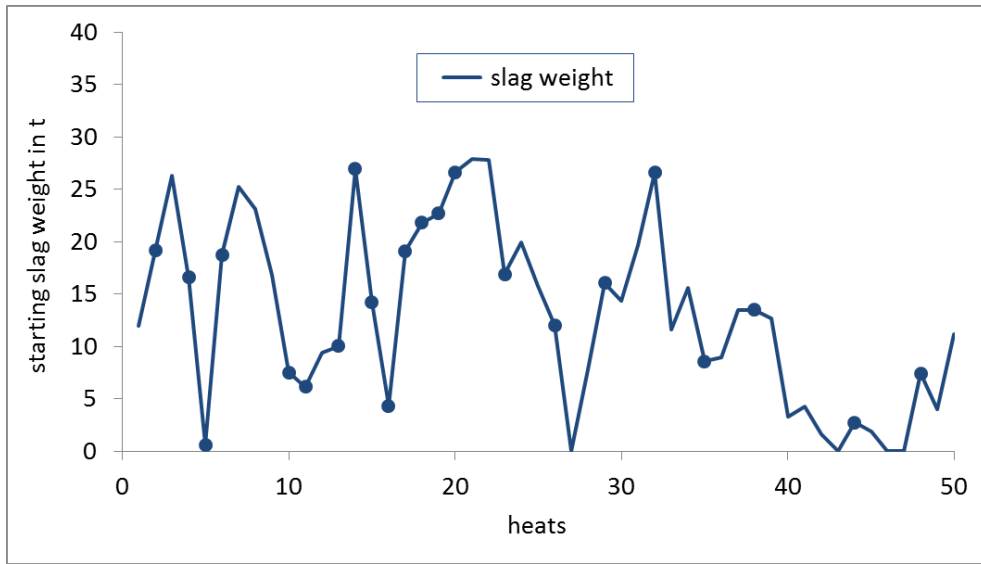


Figure 53: Evolution of the remaining slag in the furnace for a trial campaign

For the heats without dip sensor measurements the remaining slag weight has been calculated on the basis of the CaO balance and the measured slag weight in the slag pot as described before. The trend of the slag weight shows significant variations whereby the estimated weights derived from the slag height measurements are in a range between 0 and 30 t.

Task 2.3 Monitoring of the melting behaviour of the different charged scrap types and mixes (BFI, GMH, HSU)

The monitoring of the scrap melting behaviour was performed via the vibration sensors, via the off-gas analysis based on a mass spectrometer, which is permanently installed at the GMH furnace and – in the first phase of the project – by the spectrometer system. In the course of the project, the approach of supporting scrap meltdown monitoring by an additional spectrometer system has proven impracticable for GMH during long-term measurements, mainly due to extensive maintenance and repair demand. Frequently occurring data cabling breaks between spectrometer system at the furnace and Analysis-PC caused lots of maintenance and repair effort which did not seem to be justified by the expected benefits. For this reason the spectrometer system was removed from the installation site at the GMH furnace in May 2016 and has not been available for the remaining time of the project. Therefore, first findings and ideas obtained while the spectrometers were up and running will be shortly mentioned but have not been used for the final results. The same applies for the modeling described under Task 3.3, where the supporting signal gathered from the spectrometer system was replaced by the electrode path after ignition as an auxiliary signal for analysis and modelling.

Vibration sensor signal

Figure 54 exemplarily shows the overall vibration RMS signals of the two installed sensors during one complete melt. The RMS vibration level measured at position 1 represents the vessel vibrations in the direction across the longitudinal axis of the electrode, whereas at position 2 the vibration along the electrode axis is registered. The scrap basket charging process is characterized by narrow but significantly high peaks in the vibration level signals (designated as Charge Basket 1 and 2 in the graph). During bore down and main meltdown phases, levels quickly rise when active power is switched on. After that, the vibration levels slowly decline along the progress of meltdown. During the liquid bath and overheating phases, shortly before tapping, almost constant low levels are observed.

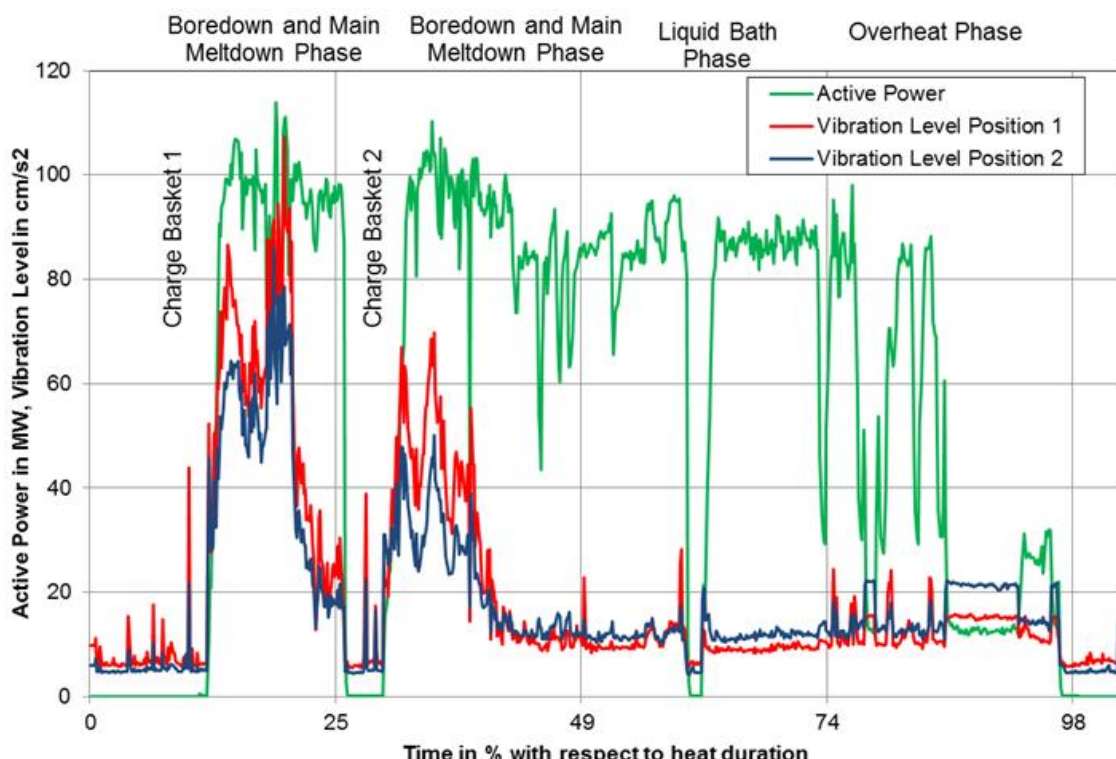


Figure 54: Vibration Levels and Active Electric Power during a Melt

This general behaviour was observed in all recorded melts. Comparing the vibration signals picked up across and along the electrode axis, it becomes apparent that signal levels across the electrode are usually higher than those along the electrode during the bore down and meltdown phases. During the liquid bath and overheating phases however, higher vibration levels in the direction along the electrode are observed. An explanation may be that as long as there is solid scrap present in the furnace, the foot of the electric arc stochastically moves across the scrap heap's surface, imposing shearing forces upon the electrode and the whole furnace construction. Furthermore, scrap pile collapses frequently occur during these phases, adding to the lateral mechanical load upon the furnace vessel. Both effects may account for the higher vibration levels across the electrode during the bore down and main melting phases. In contrast to that, during the liquid bath and overheating phases, mechanical load on the furnace vessel is mainly caused by bath movement in the form of surface waves, which primarily seem to exert longitudinal forces on the vessel.

However, both vibration signals generally exhibit quite similar behaviour during the course of a melt, which is apparent in figure 54. The strong correlation between these signals is confirmed in **Figure 55**, where they are plotted against each other and a high correlation coefficient results. Therefore, for a robust scrap level estimation model, a geometric combination of the two signals is one possibility. Another reasonable possibility which was mainly applied in this project is just using one of the two signals (direction across electrode) for modelling. In this way, the second signal can be used to check the function of the sensor relevant to model calculations by signal correlation and as a reserve signal for model calculations in case of a detected malfunction.

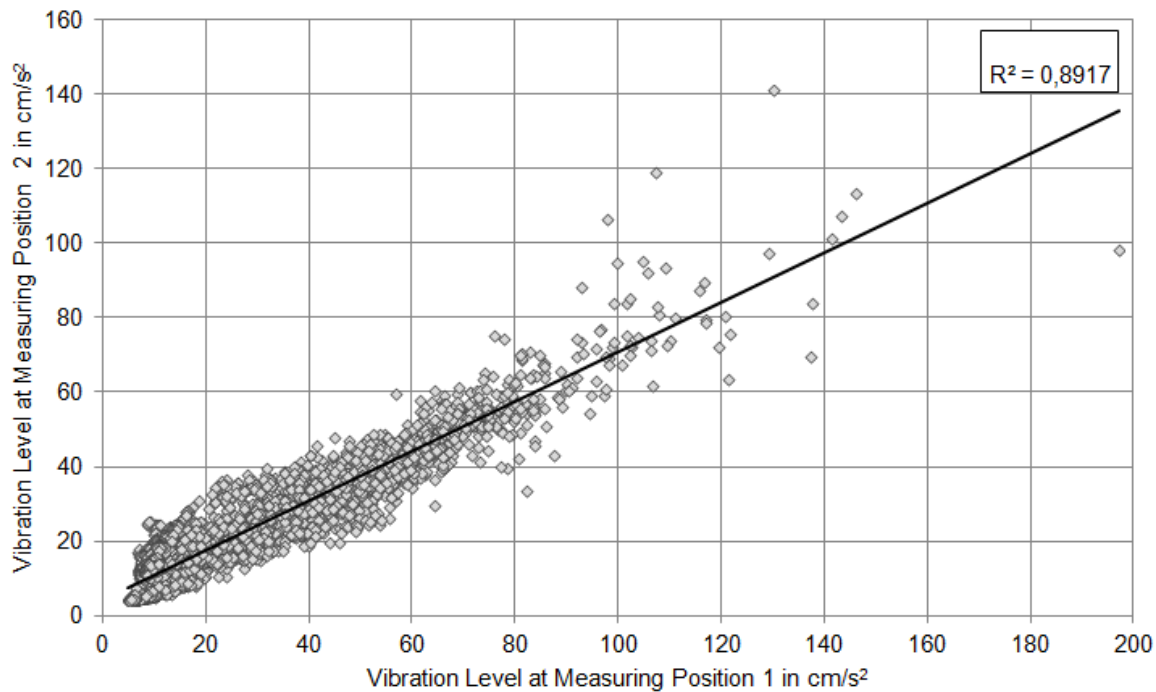


Figure 55: Correlation of the Vibration Level Signals picked up in different directions of Sensitivity

Focusing on the meltdown behaviour during the second basket, a typical signal trend of the vibration levels over an entire melt is presented in **Figure 56**. It can be seen that vibration signals significantly decrease when fine coal injection is started at minute 28. This corresponds to the acoustic observation that furnace operating noise abates with fine coal injection and foamy slag formation.

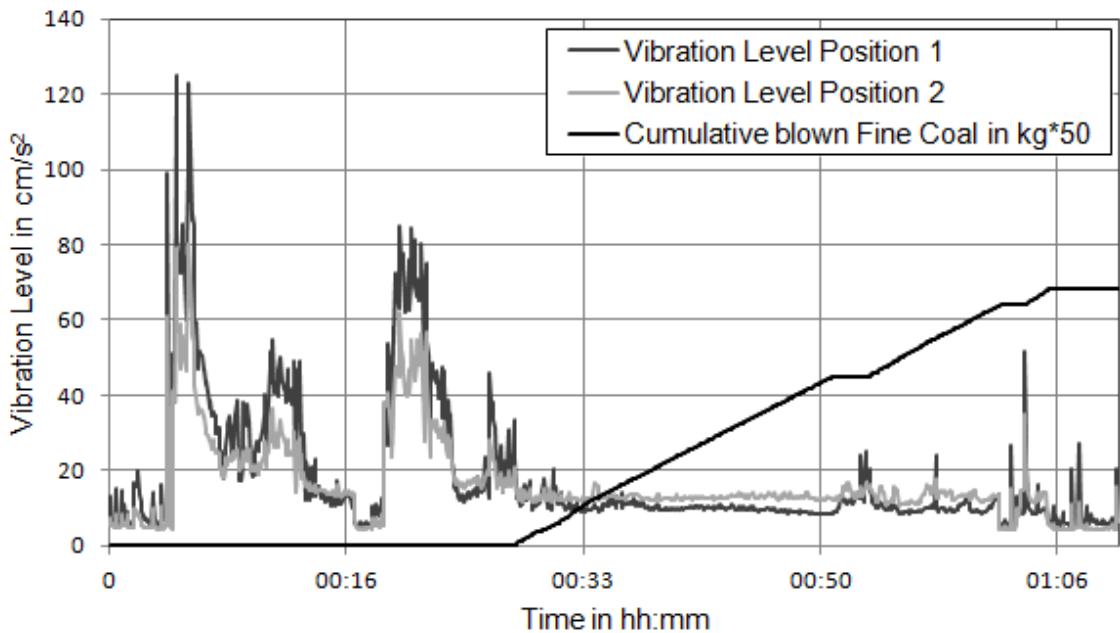


Figure 56: Vibration Level Trend goes along with Fine Coal Injection

A disadvantage of the pure examination of the RMS signals is the relatively big difference between the biggest and smallest measured amplitudes, especially for a graphical representation and for modeling. Therefore a dimensionless characteristic vibration number corresponding to

$$L_a = 20 \log \frac{\tilde{a}}{a_0} \text{ dB} \quad (1)$$

was established where \tilde{a} is the RMS vibration level. The reference vibration level a_0 is defined as

$$a_0 = 10^{-5} \frac{m}{s^2}. \quad (2)$$

In **Figure 57**, the characteristics of the logarithmical vibration level signals are presented. It exemplarily shows the typical vibration level during one complete heat. It is observable that both sensors deliver almost the same signal. The meltdown process of basket 1 finishes at about 25 % of heat duration, recognizable by the sudden decline in the vibration level.

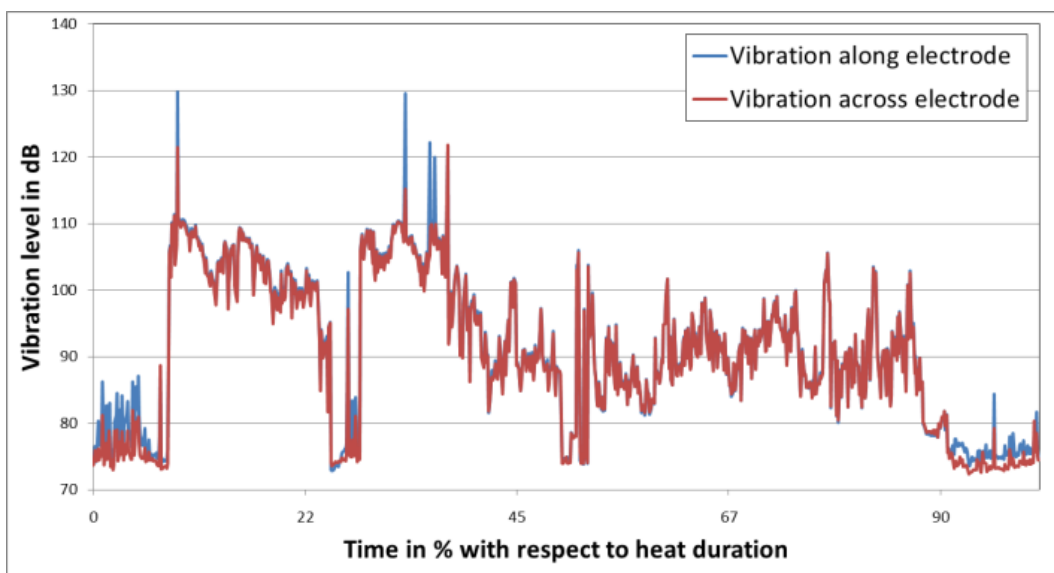


Figure 57: Vibration level during one complete heat

Figure 58 shows the statistical distribution of the vibration levels at the beginning and at the end of the first basket's meltdown process. Thus, a general reduction in vibration level during this pro-

cess is identifiable. On this basis, the objective was to generate a signal which can be used to indicate the completion of the meltdown phase of the first scrap basket and thus the optimal point of time for charging of the second scrap basket.

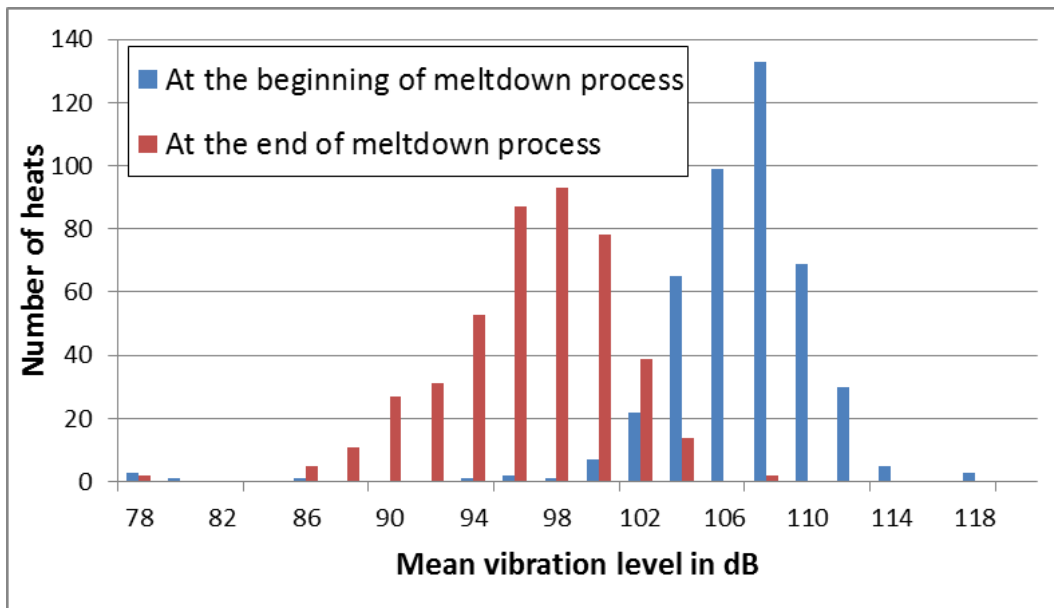


Figure 58: Distribution of mean vibration level during first basket meltdown process

Spectrometer sensor signal

Figure 59 exemplarily shows the relationship between the combined vibration level and the detected irradiance of the upper spectrometer. At very close examination it can be recognized that at the beginning of the recording, a very low, but greater-than-zero irradiance level is measured. This low-level signal is caused by hot heel radiation. Scrap charging occurs at about 2 minutes and a characteristic peak in the vibration signal curve results. After that, the hot heel is covered by solid scrap and the spectrometer signal approaches zero. This is due to the fact that the scrap now covers the radiation sources inside the EAF from the viewpoint of the spectrometers. At arc ignition (4 minutes), the vibration signal suddenly rises and then slowly decreases by trend as meltdown progresses, according to the above mentioned observations. Towards the end of the first basket's meltdown phase, the spectrometer signal starts to rise. This indicates that the solid scrap has collapsed as far as to allow electric arc radiation to arrive at the spectrometer lens. The same general signal behaviours repeat during the meltdown of the second basket from 22 minutes until the end of this particular melt. Despite these promising and plausible results, the spectrometer system had to be removed from the furnace and could no longer be used for this project, as explained earlier.

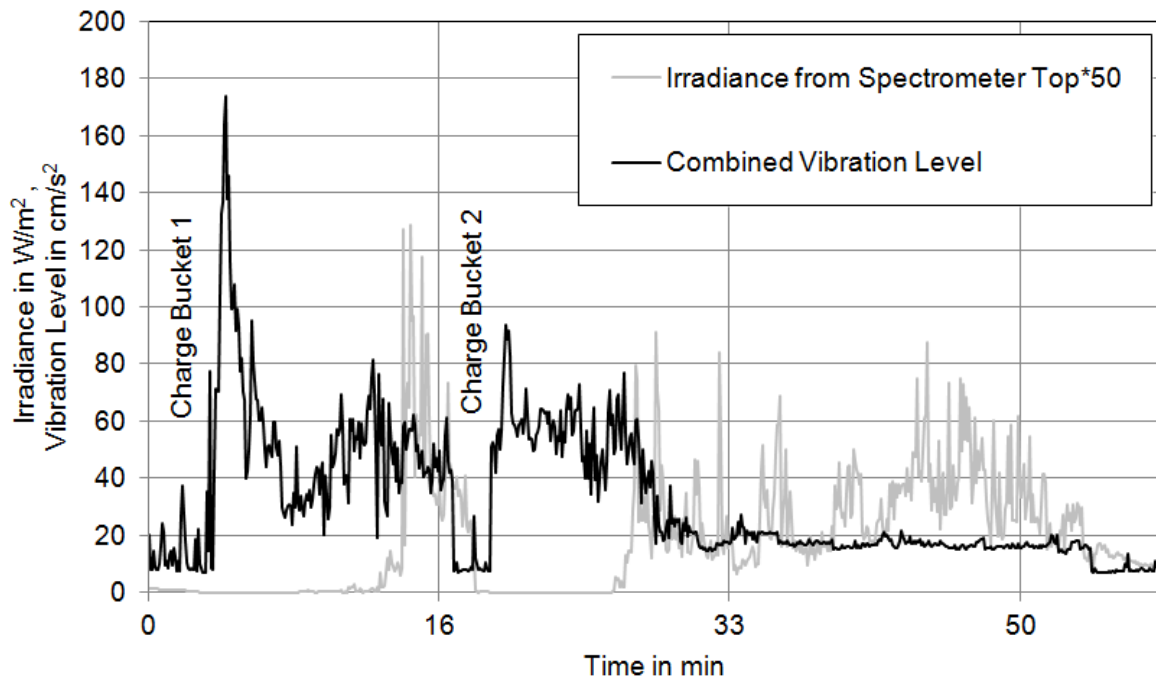


Figure 59: Typical Vibration and Irradiance Level during one complete Meltdown-Cycle

Electrode path signal after ignition

Instead of the spectrometer system signals the electrode path after ignition was analysed. The relative electrode position is measured by a distance measurement system which is installed at the electrode arm. By using additional information of the electrical current flow, the electrode path after ignition is a defined positive value, measured by the distance measurement system and starting with zero as soon as an electrical current flow is detected. The trend of the electrode path signal after ignition as well as the corresponding vibration level signal are exemplarily shown in **Figure 60**.

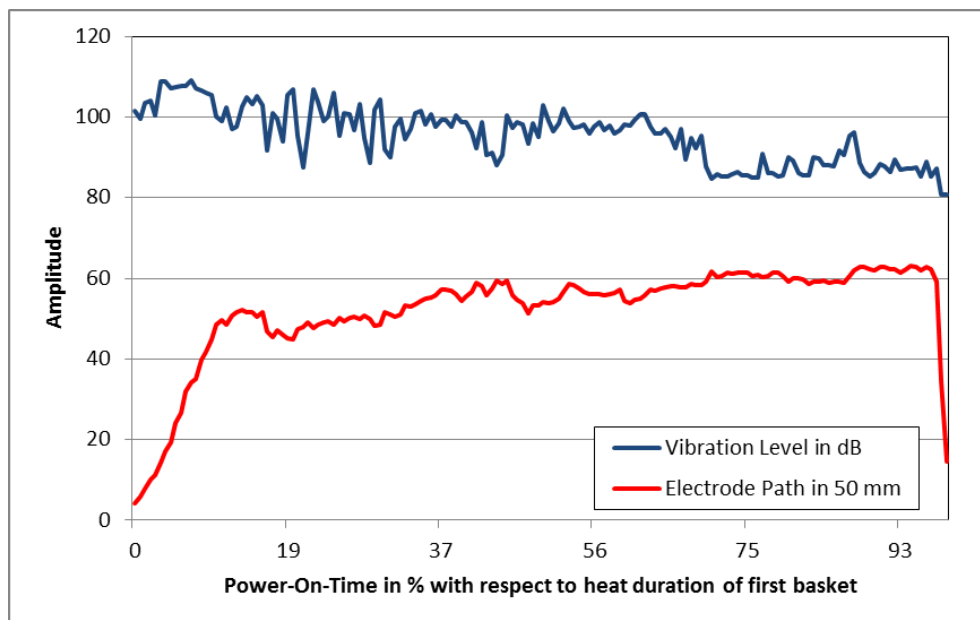


Figure 60: Vibration Level and Electrode Path during First Basket Meltdown Process

The correlation of both signals, vibration level and electrode path, is represented in **Figure 61**. As the electrode travels further down into the scrap pile, lower vibration levels result, because of the potential arc shielding by the solid scrap surrounding the electrode. Contrarily, a comparatively

high vibration level indicates a bad arc shielding and therefore a low scrap level surrounding the electrode. This characteristic was used for the furnace filling level estimation specified in Task 3.3.

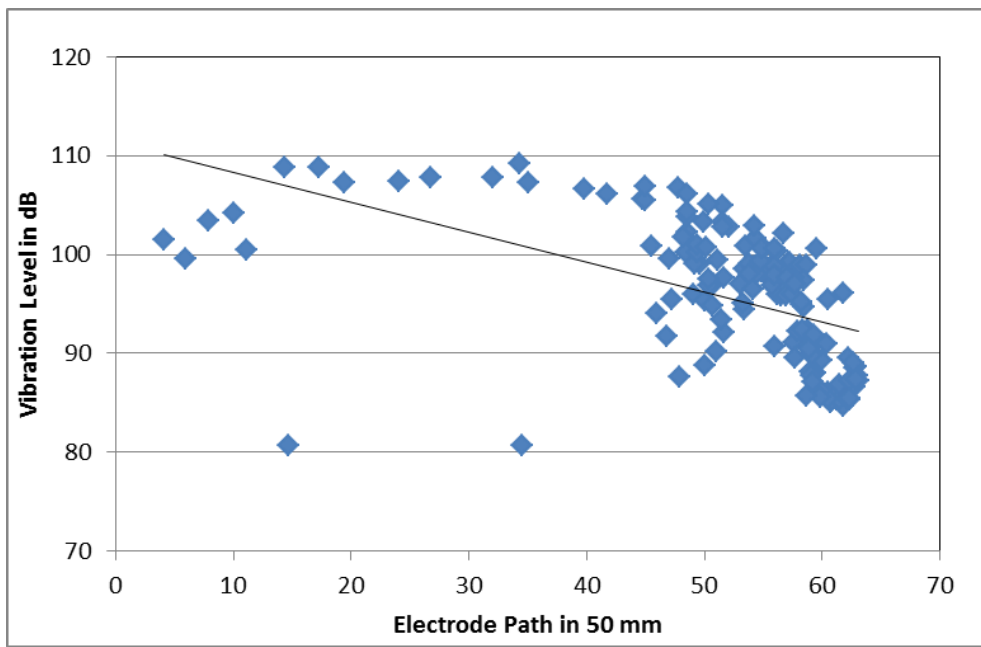


Figure 61: Correlation of vibration level vs. electrode path

Off-gas composition depending on the scrap mix

The scrap-individual requirements and the effectiveness of the chemical energy inputs have been investigated with the help of measured off-gas values acquired via a mass spectrometer which is permanently installed at the GMH furnace [5].

BFI investigated the off-gas amount and composition during the meltdown process of the first scrap basket. For this investigation the first 8 minutes of power on have been considered. The correlation between the weights of charged scrap types and the off-gas amounts of CO and H₂ has been examined by using a multi-linear regression model. The aim was to determine the scrap types with the most significant influence on the off-gas composition. **Figure 62** shows the calculated off-gas volume of CO and H₂, resulting from the regression model which considers the charged scrap types and amounts, against the measured values. Both off-gas components show a high variation which obviously strongly depends on the charged scrap mix.

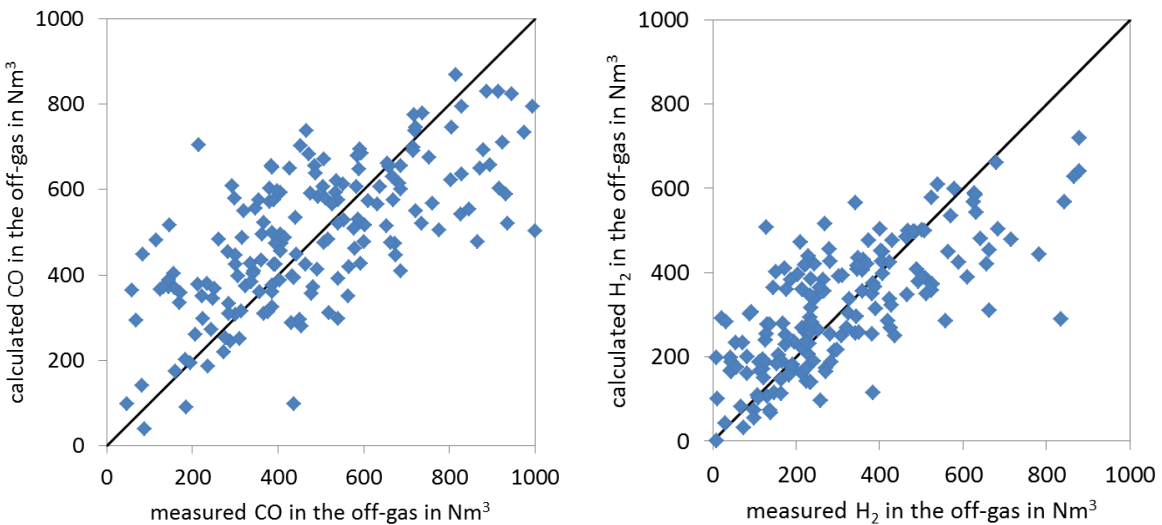


Figure 62: Calculated volume of CO (left diagram) and H₂ (right diagram) against measured one during the meltdown process of the first scrap basket

The regression calculation shows that the scrap types have different impact on the off-gas amount and composition. The most relevant influence on the off-gas components CO and H₂ is coming from the charged coke, pig iron skulls and turnings. Scrap mixes including these materials should be treated with an increased oxygen input for post-combustion for CO and H₂, to increase the efficiency in using the reaction energy for scrap meltdown. **Figure 63** shows in addition the correlation between the amounts of CO and H₂ in the off-gas. Both values are strongly correlated which is due to the water-shift reaction. The contents of CO₂ and H₂ are in equilibrium to CO and H₂O.

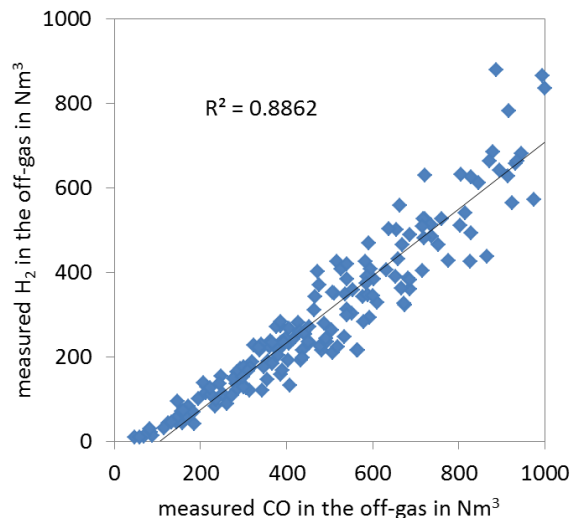


Figure 63: Correlation between amounts of CO and H₂ in the off-gas during the meltdown process of the first scrap basket

2.2.3 WP 3: Enhancement of existing process models by using information from newly applied measurement systems

Task 3.1 Incorporation of additional process information in EAF process data base for modelling and validation purposes.

In order to correlate the new sensor data with other process data and to make them available for process control, the corresponding PCs collecting and pre-processing the new sensor data were attached to the data handling and storing system already available at GMH. The data of the novel sensors together with the already available process data are stored in a SQL data base which feeds data analysis as well as process modelling and control. Thus, a data interchange network was implemented. **Figure 64** gives an overview of the information flow within this data exchange network.

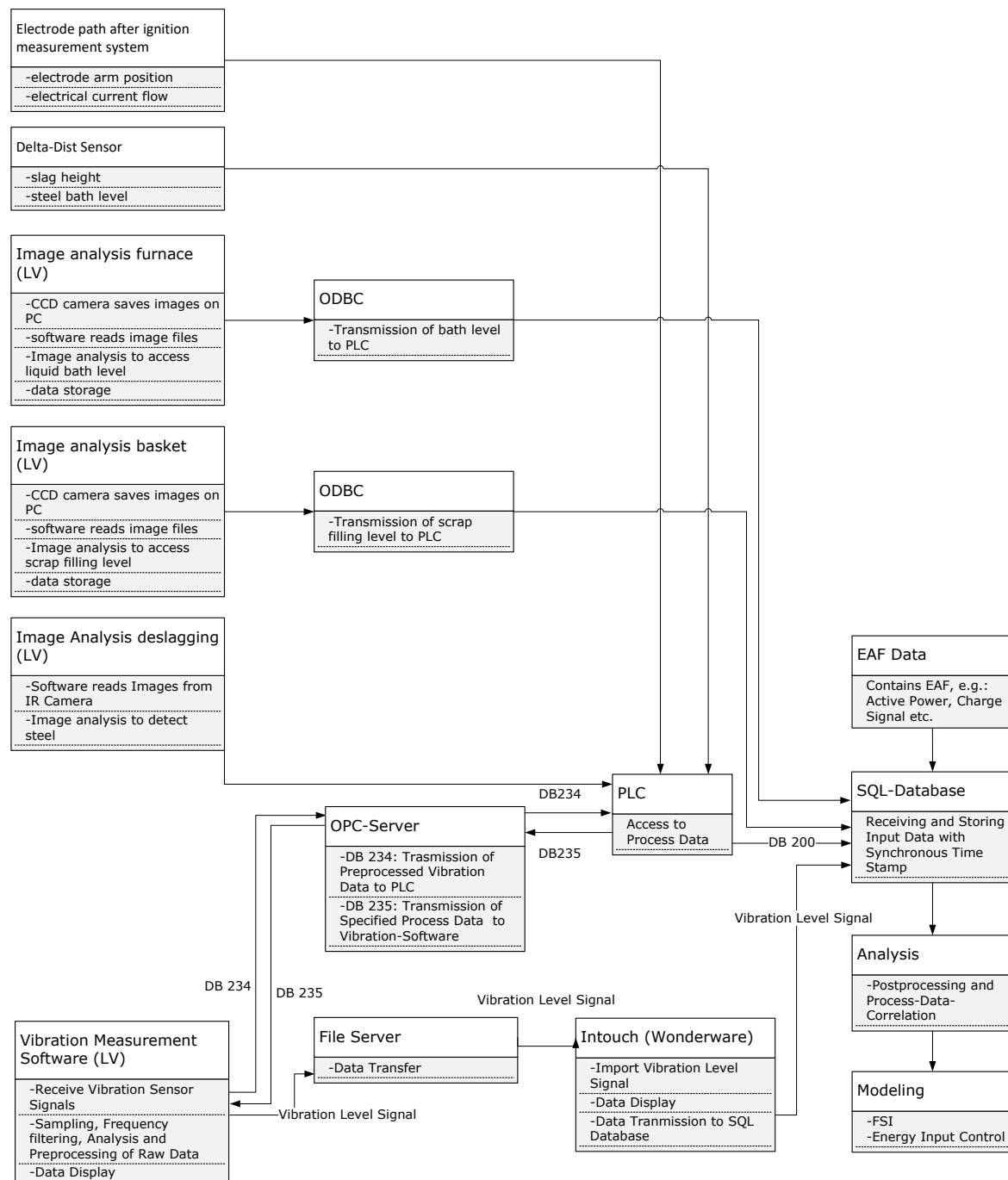


Figure 64: Data exchange network at GMH

The Delta-Dist sensor evaluates slag height and steel bath level. Cameras are used to monitor the liquid bath level in the EAF, the deslagging process of the EAF and the scrap basket filling degree before charging into the EAF. LabView (LV) based image analysis routines running on PCs are used to determine the liquid bath level in the furnace and the basket filling level. The PCs are equipped with network interface cards allowing an Ethernet connection to the PLC (central programmable logic control). An OPC (open platform communications) server and an ODBC (open database connectivity) server are installed on the PCs, which provide the results for the PLC and for the SQL data base, respectively. For vibration measurements, incoming sensor raw signals are digitized and pre-processed on a dedicated PC by using specially developed and configured software modules. These software modules include several features, e. g. analysing and display functions. The vibration analysis software is additionally equipped with a function for direct communication with the PLC data exchange system via an OPC server. Therefore it allows an on-line correlation with other process data. The electrode after ignition measurement system uses the electrode arm position and the electrical current flow signals to derive a signal for the electrode path after ignition on the PLC. The result is also stored on the SQL data base.

As the spectrometer system was removed from the furnace during the project for reasons described above, the concerning software and signals are no longer part of the data exchange network which was finally established in this project.

All software modules are expandable and can be modified to meet future requirements that might come up in further developments. Details of all sensors and the specific communication are listed in the corresponding boxes on the left side of Figure 64.

Regarding an all-encompassing EAF process data base as needed for the modelling and validation purposes in this project, the previously existing SQL data base of GMH was the obvious choice. Therefore, the signal collection and pre-processing PCs route their corresponding measurement signals through to suitable server combinations managing the subsequent data transfer to this central SQL data base. Arriving there, the newly acquired process information is simultaneously stored with all other available process data. Thus, a consistent data base with synchronous time stamps is established. For data interpretation purposes, suitable excerpts containing selected signals recorded in a given time frame can easily be drawn from this data base by using already existing access tools.

Task 3.2 Use of additional process information within statistical and dynamic models to improve the assessment of the scrap melting yield and composition (BFI)

Scrap characterisation

For analysis of the scrap properties (yield as well as residual and alloy element concentration) the following process data were collected for about 500 heats at GMH:

- Weights of each charged scrap type
- Weight and composition of each charged slag former
- Measured EAF tap weight
- Lab analysis of simultaneously taken steel and slag samples

At GMH in normal operation one slag sample is analysed for every heat. **Figure 65** displays the BFI tool for determination of the metallic yield, which has been developed within the previous RFCS project Flexcharge [6], applied for the 17 different scrap types used at GMH. The selection of heats to be considered can be done in a pop-up menu. Under "No. of occurrence" the number of heats

with utilisation of each scrap type and their mean percentage in the scrap mix is given. These values give an indication for the reliability of the respective calculated yield value. The accuracy of the calculation is figured in the diagram with an error standard deviation of 6.4 t, by comparing the calculated with the measured tap weight. Outliers can be explained by a strong variation of the hot heel amount, which was set to a constant value for this evaluation.

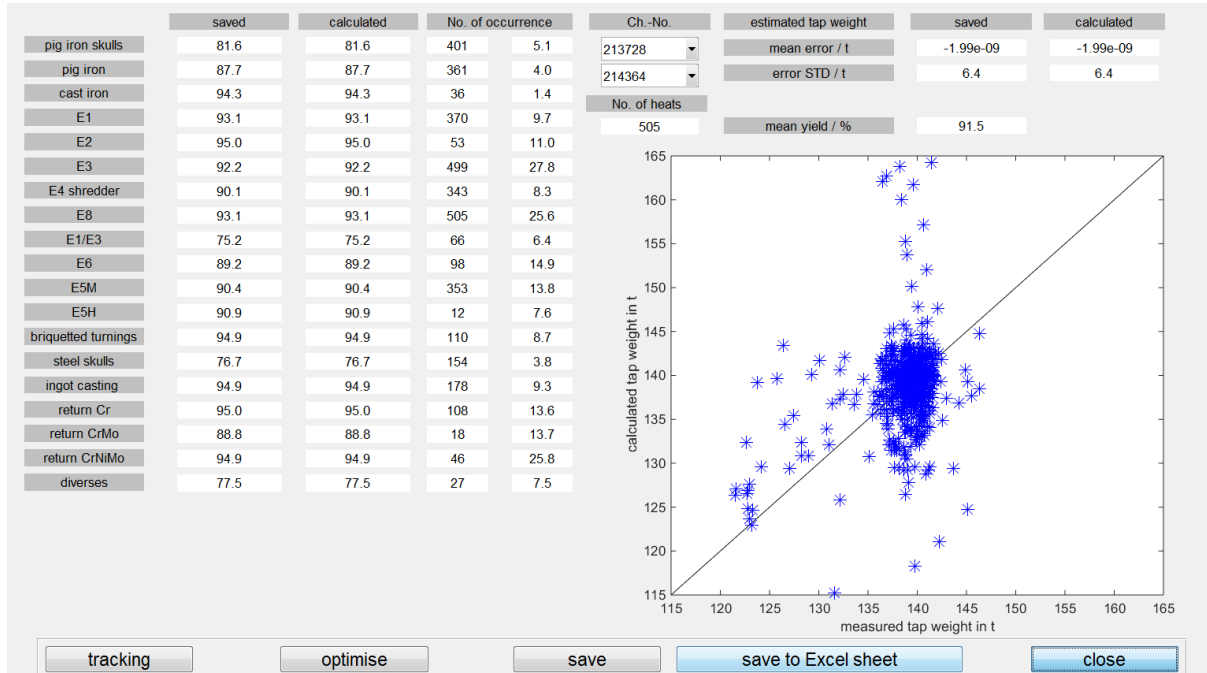


Figure 65: Determination of the scrap-individual metallic yield at GMH

The calculated yield values consider the oxidation of metallic components during furnace operation. The average metallic furnace yield of the scrap charge is 91.5 %. A low metallic furnace yield of a scrap type can be caused by a low metallic content, but also by an unfavourable meltdown behaviour which supports metallic oxidation. The metallic furnace yield is an important parameter for scrap mix optimisation to consider the quality of each scrap type.

For determination of the element-wise yield for tramp and alloy elements the analyses of steel samples taken before EAF tapping have to be provided for each produced heat. To improve this calculation the influence of the previous heat is considered by its analysis and the hot heel amount.

Figure 66 shows the mask for calculating the element-wise yield factors for each scrap type and each analysed element, exemplarily for Cu. The calculated element-wise yields are shown for each scrap type. The diagram compares the calculated to the analysed Cu content for the tapped steel. The error standard deviation of the estimation is 0.03 %.

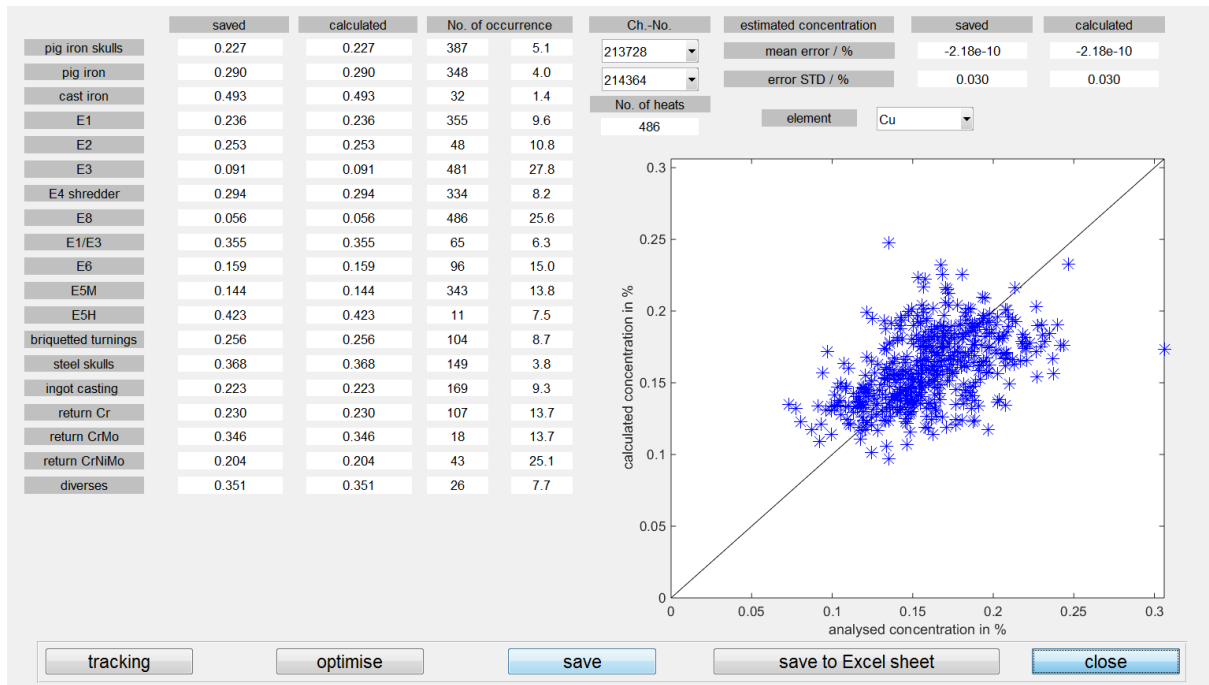


Figure 66: Determination of the scrap-individual yield parameters for the Cu content at GMH

The calculated parameters are also furnace yields for the respective elements. For non-oxidisable elements like Cu and Sn its value matches with the actual scrap type content. For oxidisable elements like Si, Mn and Cr further information from lab analyses of slag samples taken in the furnace has to be taken into account to gain the element content for each scrap type. **Figure 67** shows exemplarily the determination of the scrap-individual Chromium content for a data set with provided slag analysis. A high accuracy with an error standard deviation of 0.074 % can be achieved. For the oxidisable elements the actual content of the scrap types is higher than the element-wise furnace yield. About 58 % of Chromium charged by the scrap is oxidised until the beginning of refining when the steel and slag samples are taken.

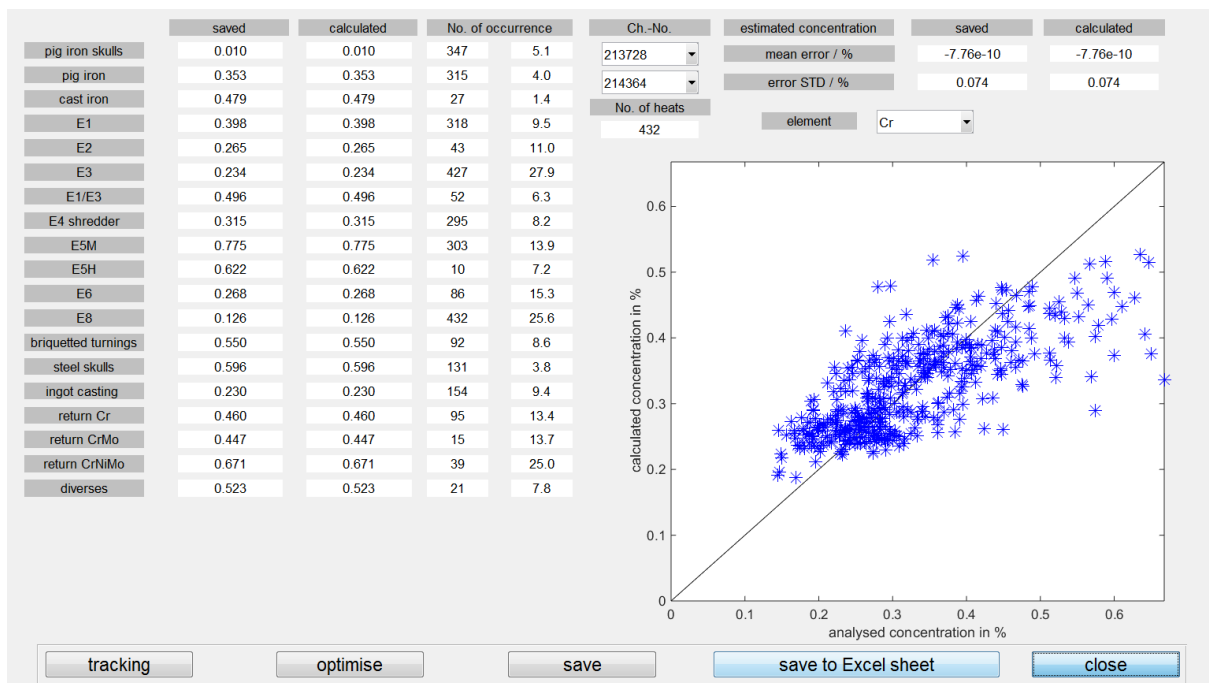


Figure 67: Determination of the scrap-individual Cr content at GMH

BFI has also analysed the variation in the composition of different scrap types over time for the GMH site. On the basis of a large data set (about 500 heats) the evolution of scrap type characteristics has been investigated with the help of the regression analysis. Variations in the metallic yield and element composition of different scrap types over time are caused by different suppliers and deliveries.

For this purpose the regression analysis has been performed for short consecutive sections. The section window moves over the whole data set and the determined properties figure the development over time. The length of each section was set to 100 heats. The reliability of the calculated values is pointed out by the number of inserts of the selected scrap type per heat batch.

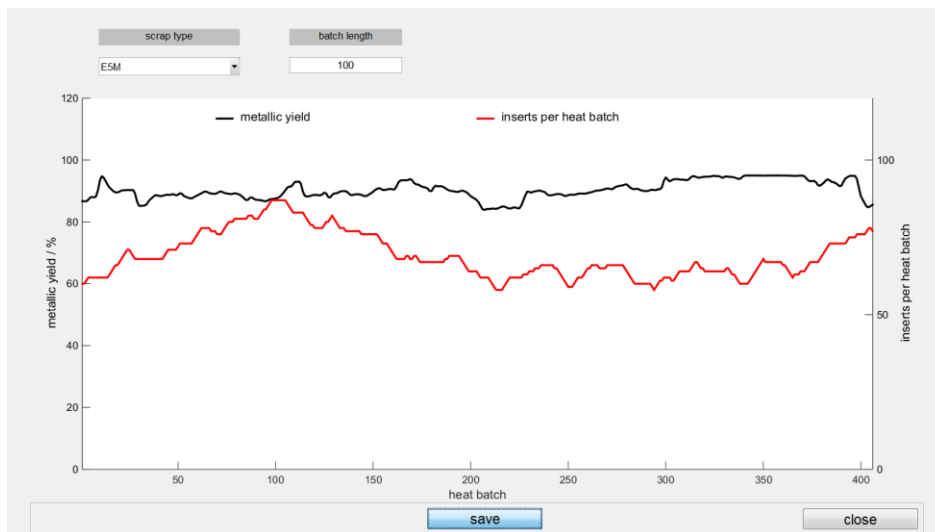


Figure 68: Evolution of the metallic yield over time for scrap type E5M

Figure 68 displays the development of the metallic yield over a production period of about one month for the scrap type E5M, calculated with a batch length of 100. The number of inserts per heat batch (red line) indicates the frequency of usage which varies between 50 and 90 for this scrap type. The adequate usage of this scrap type demonstrates the reliability of the achieved results. **Figure 69** displays the development of the Cu content for the scrap type E5M. The chart shows strong fluctuations over time which makes it necessary to repeat the determination of the scrap-individual parameters. The maximum allowed copper content of this scrap type is defined with 0.4 %. The chart shows that this limit value is not exceeded for this time period.

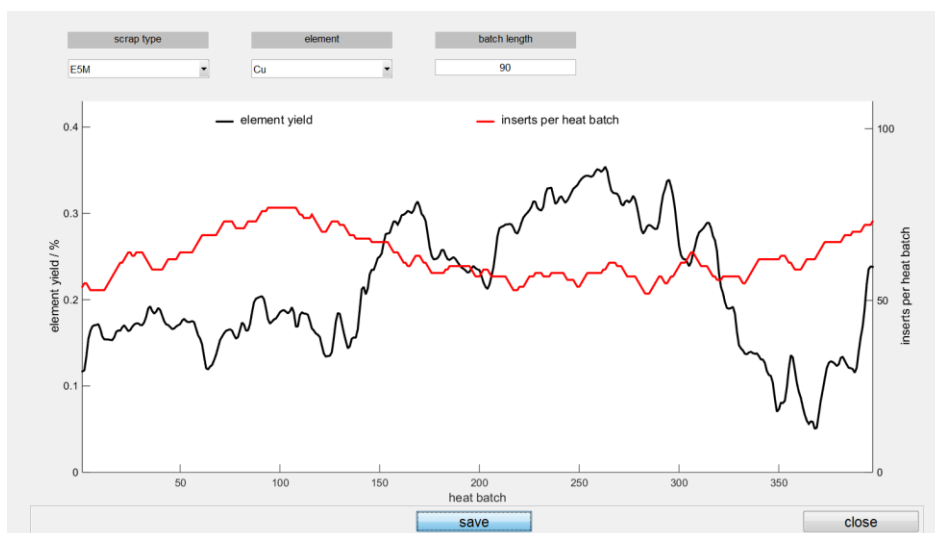


Figure 69: Evolution of the Cu content over time for scrap type E5M

Extension of dynamic process model

The dynamic EAF process model of BFI, which was initially developed in the scope of an ECSC [7] and a RFCS project [8], describes the energetic status of the melt by dynamic mass and energy balance calculations. **Figure 70** shows the structure of the process model with the main function blocks and the most important input values.

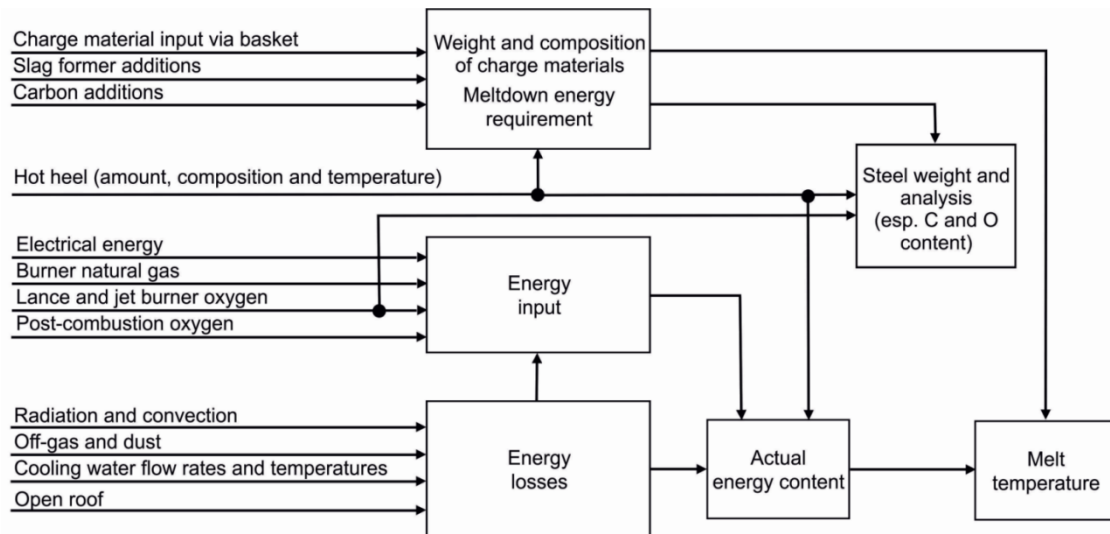


Figure 70: Structure of the BFI dynamic process model for the EAF

The block 'Weight of charge materials and meltdown energy requirement' calculates the total weight and composition (steel and slag) of the melt from the metallic materials charged with the scrap basket, carbon and slag former (like lime and dolomite) additions, as well as carbon and lime injection via shell injectors. From the specific meltdown energy of each material, the totally required energy is calculated. Additionally the amount of the hot heel in the furnace has to be considered in this calculation.

The 'Energy input' comprises the electrical and the chemical energy input. The latter one consists of the energy input by burner gas, by oxygen input through door lances and shell injectors, and by oxygen input for post-combustion. The 'Energy losses' consist of losses by off-gas, water cooling and overall radiation losses. The off-gas losses can be determined with the help of a mass spectrometer installed at GMH. The thermal losses by water-cooled panels and roof are calculated from the cooling water flow rates and the difference between inlet and outlet temperatures. Radiation losses are taken into account by model parameters for the different process phases like charging, meltdown and refining, considering also the effect of an open roof. The difference between energy inputs and losses gives the actual energy content of the melt. The actual energy content is related to the materials meltdown energy requirement to calculate the current melt temperature.

For validation of the model, GMH provided acyclic and cyclic process data of about 500 heats consisting of:

- Inputs of all materials (weights of scrap, slag formers and carbon)
- Cyclic data of electrical and chemical energy inputs
- Energy losses by cooling water and off-gas
- Analyses of simultaneously taken steel and slag samples with timestamps
- Temperature measurements
- Celox measurements (temperature and oxygen content)

The result of the dynamic energy balance calculation is shown for one example heat of GMH in **Figure 71** where the evolution of the calculated melt temperature is displayed. The times when the two baskets are charged are clearly indicated by the temperature drop. To verify the dynamic process model, the calculated temperature is compared to the temperature measurements before tapping. For this heat the correspondence between calculated and measured temperature is very good. The adaption to plausible temperature measurements increases the accuracy of the model for the further treatment.

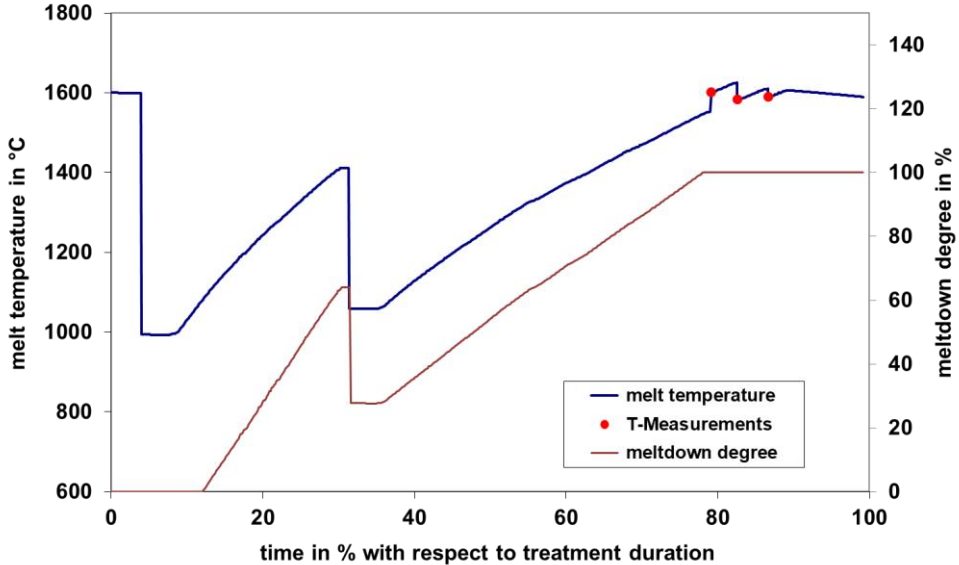


Figure 71: Calculated melt temperature and comparison with measurements for one example heat of GMH

The accuracy of the model calculation for the melt temperature was evaluated for all GMH heats with plausible temperature measurements. In **Figure 72** the calculated temperature is plotted against the first measured one on the left, and after adaption of the model calculation to this measured value for all further temperature measurements on the right. A modelling error standard deviation of about 20 K after adaption was achieved. With respect to the total energy input of around 690 kWh/t, this is a relative error of the energy balance of less than 1 %, which is a very good accuracy.

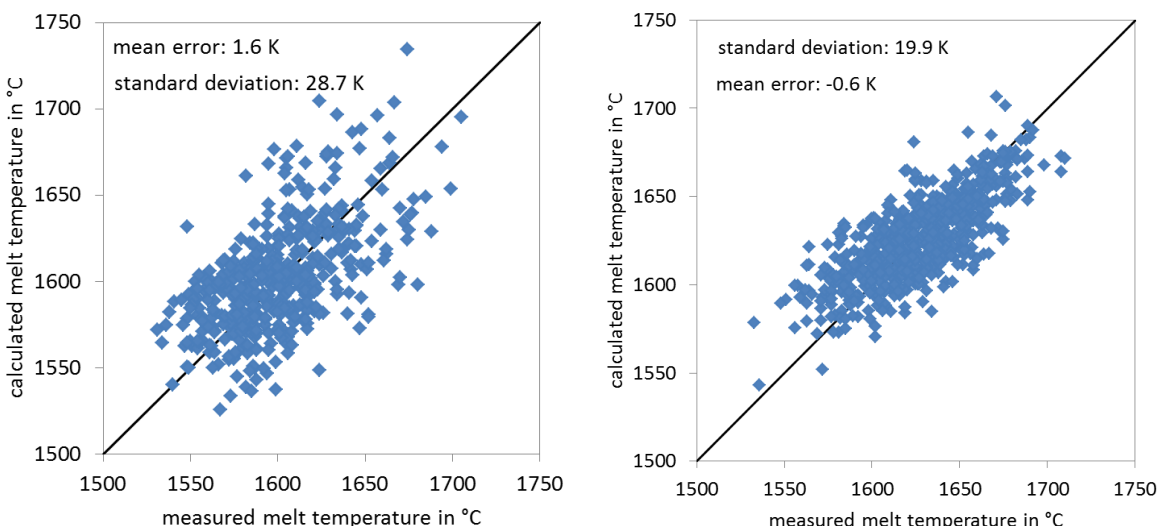


Figure 72: Model accuracy of melt temperature calculation for GMH (Left: First measurement; Right: Further measurements after adaption to first one)

The dynamic process model of BFI also comprises a detailed carbon and oxygen balance calculation. To determine the current carbon content and the oxidation status of the steel melt it considers the carbon input by the different charged scrap types and the charge carbon. Furthermore carbon is injected into the bath via 3 carbon lances in parallel to the injection of oxygen, to create a foamy slag. This oxygen input also leads to a slagging of iron and other metallic elements.

The validation of this carbon balance model was performed via the analysed carbon content from the steel samples taken at the end of the melt down phase. The oxygen model was validated with the help of Celox measurements. **Figure 73** shows the evolution of the calculated carbon and oxygen content for one example heat, together with the analysed carbon and the measured oxygen content of in total 3 Celox measurements.

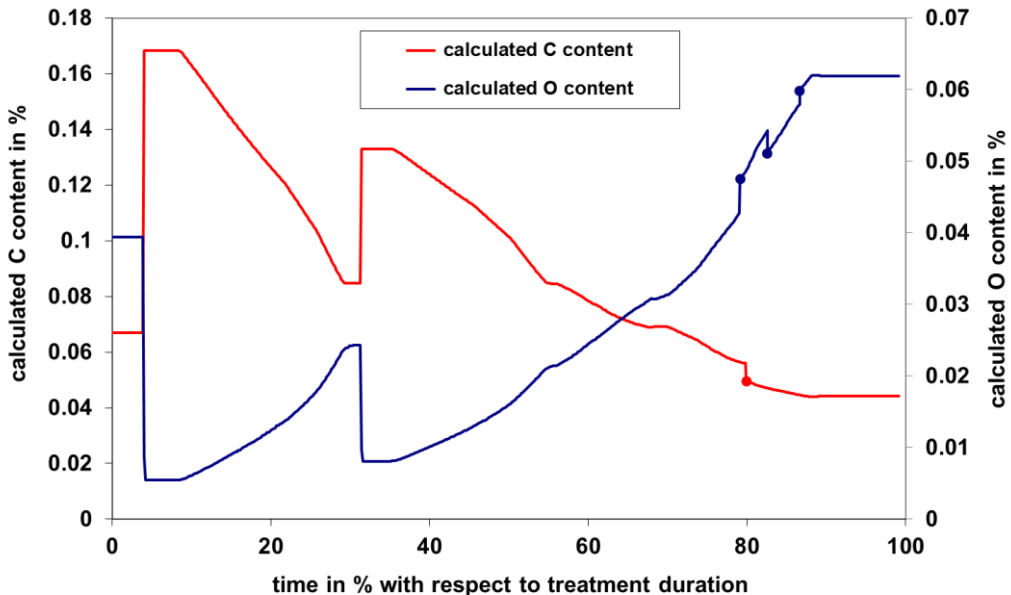


Figure 73: Calculated carbon and oxygen content evolution for one example heat of GMH

The figure clearly shows the carbon input from the two baskets and the decarburisation via lance and jet oxygen. A steel sample is taken in minute 43 and the model adapts to the analysed value. The measured values of three CELOX measurements are met by the model calculations with a quite good accuracy.

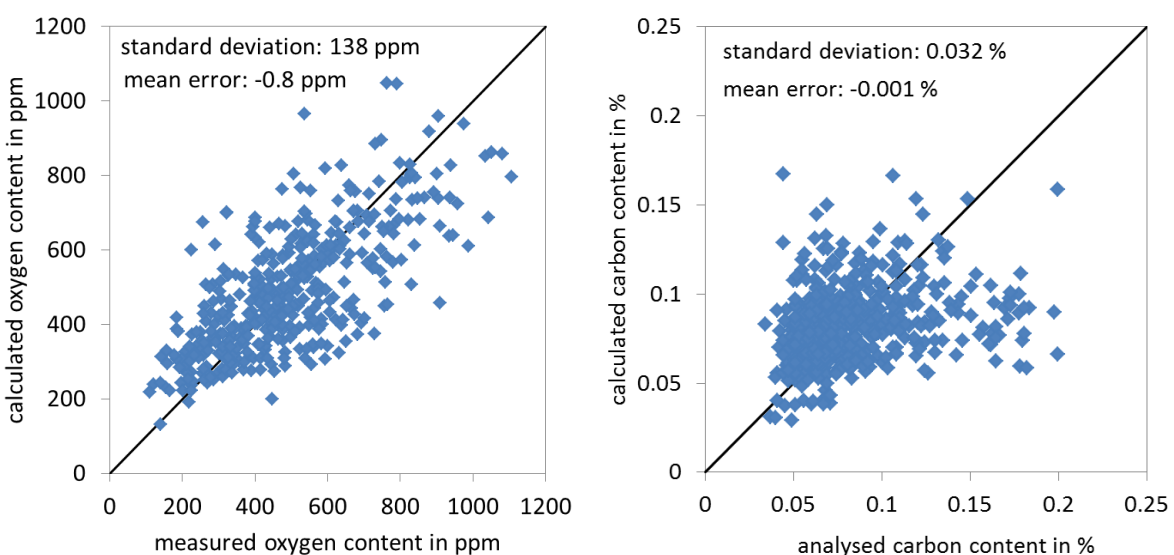


Figure 74: Model accuracy of steel oxygen (left-hand side) and carbon content (right-hand side)

The achieved model accuracy is shown in **Figure 74** for all investigated heats. For the carbon content the model error standard deviation is 0.032 %, which is satisfactory considering the numerous influencing parameters which are partly difficult to assess. For the oxygen content a model error standard deviation of about 140 ppm was achieved.

The dynamic process model was further extended by an oxidation as well as a steel and slag interaction model, to calculate the oxidation of all relevant elements like Si, Mn, Cr etc. according to the oxygen inputs by lances and injectors. The reduction of slag oxides by the injection of blow carbon is considered in the model too. On the basis of these oxidised components, actual slag weight and composition are calculated.

Figure 75 shows the calculated slag and steel weight for one example heat. For this heat a Delta-Dist measurement was performed shortly before tapping and the model calculations were adapted to the values.

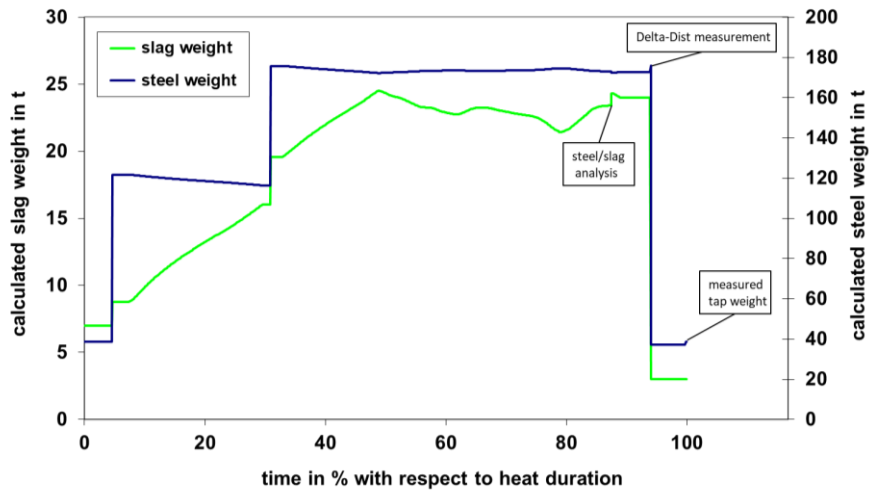


Figure 75: Calculated slag and steel weight evolution for one example heat of GMH

Figure 76 shows the evolution of the calculated slag components CaO and FeO for one example heat, together with the analysed contents from a slag sample. CaO is only coming from the charged slag formers and the pig iron skulls. As both scrap baskets include lime, the CaO content increases after each charging. The decrease during meltdown and refining is caused by oxidation of especially Fe, which is reflected by an increasing FeO content. On the other hand the FeO content also decreases due to the reduction by carbon injection.

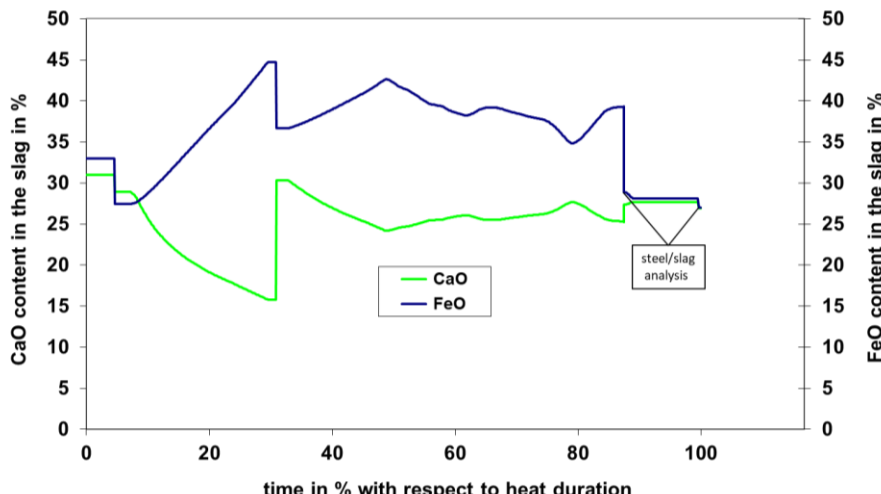


Figure 76: Calculated CaO and FeO content evolution for one example heat of GMH

Figure 77 shows the model accuracy regarding both slag components. For CaO a mean error standard deviation of 4.3 % and for FeO of about 6.3 %. was achieved.

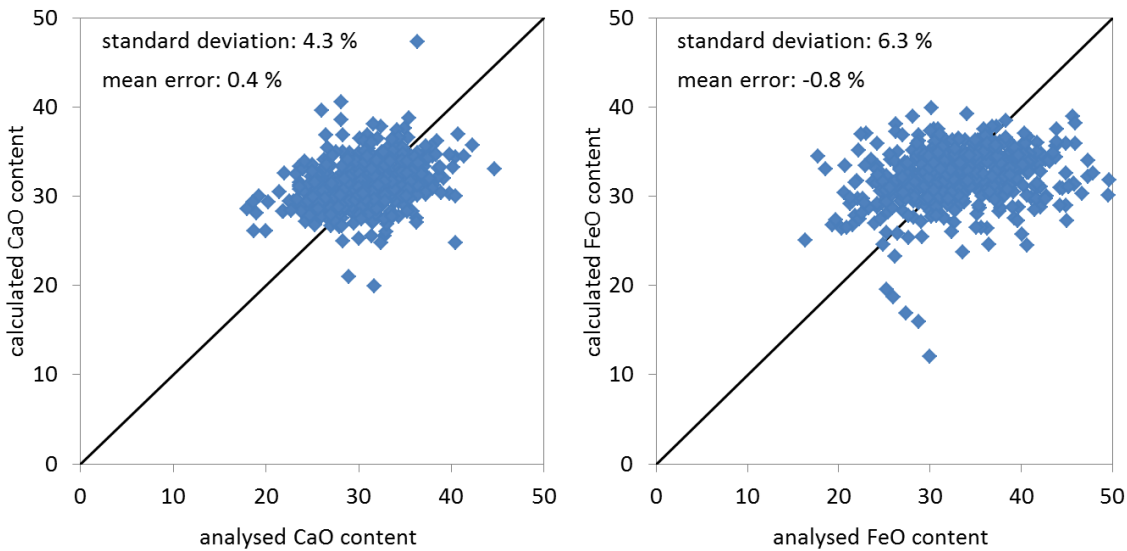


Figure 77: Model accuracy of slag CaO (left-hand side) and FeO content (right-hand side)

For the calculation of the Cr content the scrap-individual properties regarding oxidisable elements are needed which have been determined as described above.

Figure 78 shows the evolution of the calculated Cr content in steel and Cr_2O_3 content in the slag for one example heat, together with the analysed content from simultaneously taken steel and slag samples. After charging the first scrap basket the Cr content decreases due to oxygen injection, and it increases again with charging of the second scrap basket. During the refining phase the Cr content further decreases by oxygen inputs. The content of Cr_2O_3 in the slag proceeds contrary to the steel Cr content.

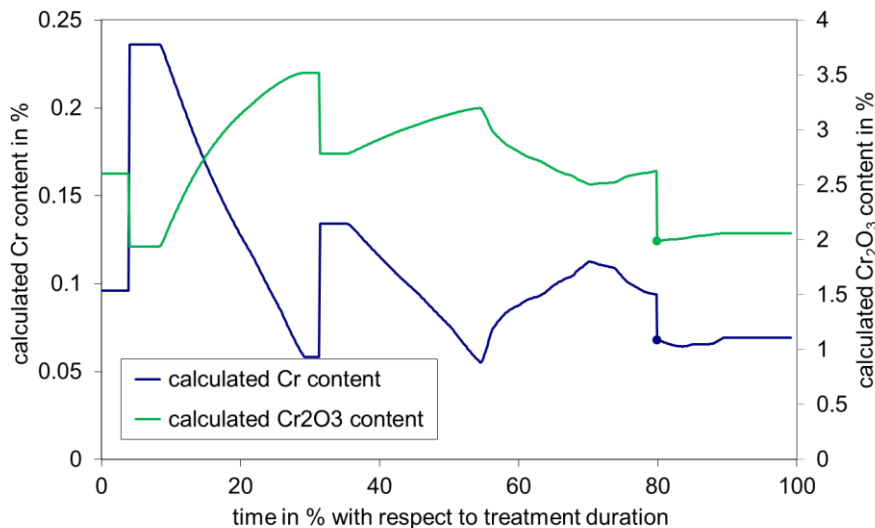


Figure 78: Calculated Cr and Cr_2O_3 content evolution for one example heat of GMH

Figure 79 shows the model accuracy regarding Cr calculations for all evaluated GMH heats.

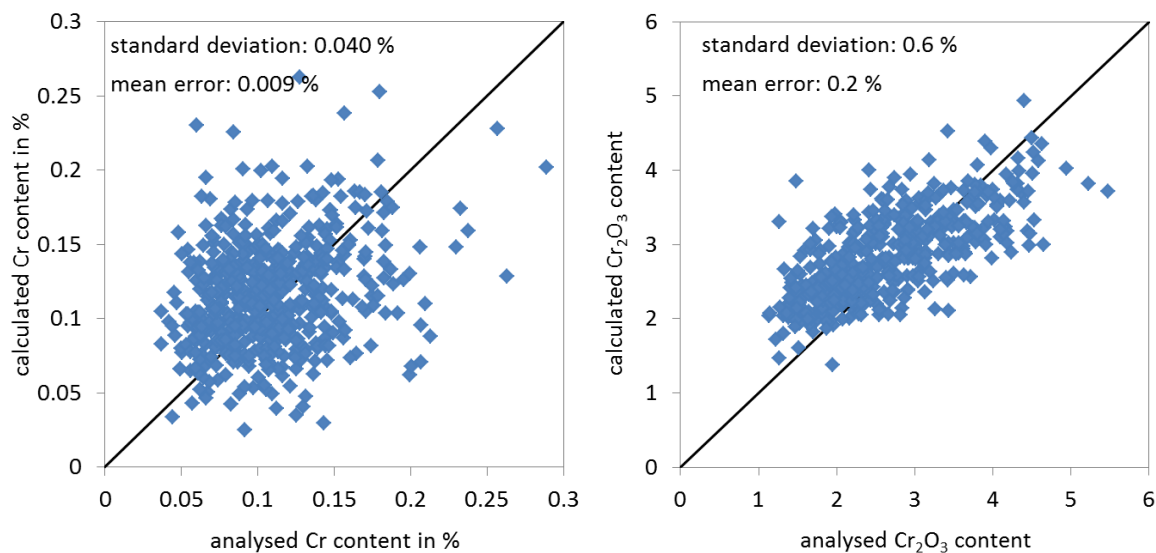


Figure 79: Model accuracy of Cr content in the steel (left-hand side) and Cr₂O₃ content in the slag (right-hand side)

The steel Cr content can be calculated with an error standard deviation of about 0.04 %, for the slag Cr₂O₃ content a model accuracy of about 0.6 % was achieved. **Table 2** shows the model accuracy for all analysed slag components. The information about the slag composition can be used to estimate the viscosity which is important for foamy slag building, the knowledge about the MgO saturation helps to avoid excessive refractory wear.

Table 2: Model accuracy regarding slag components

	CaO	SiO ₂	FeO	Al ₂ O ₃	MnO	MgO	Cr ₂ O ₃	P ₂ O ₅
mean content	30.8	11.0	33.0	5.6	7.0	7.3	2.6	0.5
mean error	0.4	0.5	-0.8	0.0	0.1	0.0	0.2	0.1
standard dev.	4.3	1.8	6.3	1.2	0.8	1.8	0.6	0.1

The advantages of the hot heel follow-up on the quality and accuracy of the dynamic and statistical model results have been investigated. However, at least for the dynamic process model no significant improvements in the accuracy of the energy and mass balance have been found. This might be caused by the fact, that for the evaluated heats most of the estimated hot heel amounts are close to the mean value which has so far been used in the model calculations.

Figure 80 shows the evolution of the hot heel amount starting after a maintenance shift where the furnace was nearly emptied. With the first heat the hot heel is build up to nearly 60 t. In the following course the amount varies with only few exceptions in the range between 30 and 60 t, whereby all measured weights are in this range. These variations seem to be too weak to have significant influence on the dynamic model calculations.

On the other hand one aim of this project is to operate with a fixed steel bath level to guarantee optimal energy efficiency, and a nearly stable hot heel amount is an indication for it.

The evaluation of the impact of new process information on model accuracy was continued with the process data of the plant trial period performed in WP 5.

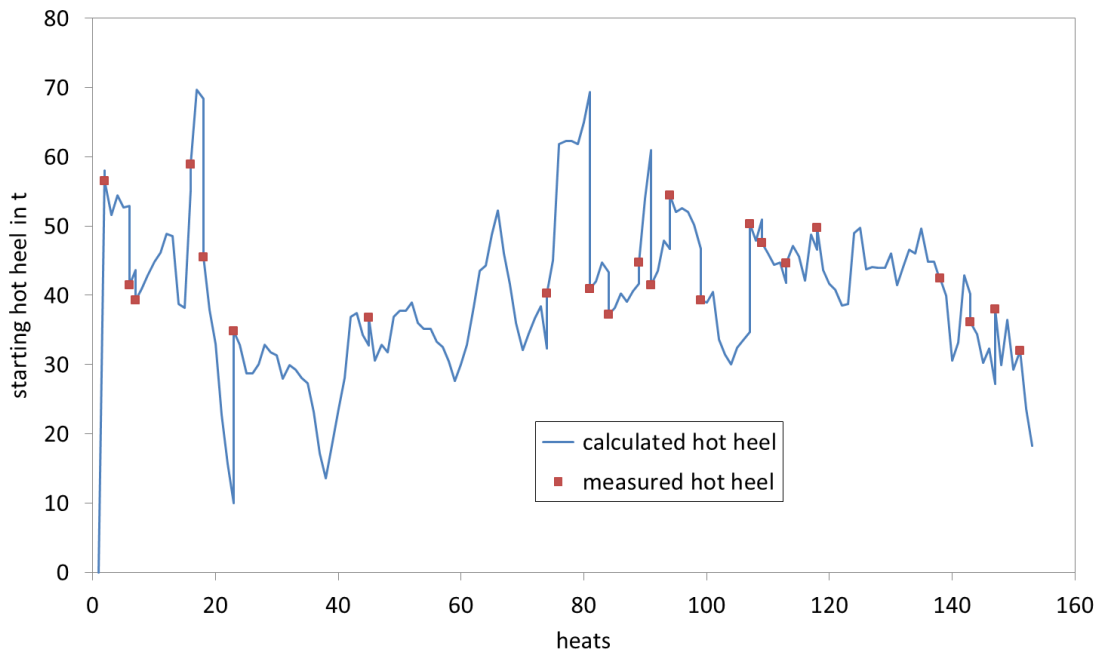


Figure 80: Follow-up of the hot heel amount and measured weights derived from Dip sensor measurements for a longer time period

In the frame of the RFCS project Flexcharge [6], also a scrap mix optimization tool was developed which includes a statistical analysis to determine scrap properties regarding metallic and element-wise yield. For oxidisable elements like Si, Mn, Cr etc. within this tool, so far only effective yields were determined, as the share of the charged element which is oxidised and remains in slag was not captured. To enhance the determination of scrap characteristics the BFI approach has been improved to estimate also the content of oxidisable elements in the different scrap types with the help of the determined slag weights described under task 2.2.

Task 3.3 Use of additional process information and dynamic models to assess the energetic melting behaviour for optimal energy input control depending on the charged scrap mix (BFI, HSU)

To determine the characteristics of the different scrap mixes regarding the efficiency of the different chemical energy inputs, the scrap load of the baskets was investigated for the first and the second load separately, and grouped by similarity with the help of cluster analyses.

Cluster analysis of first scrap basket

The scrap weights of the first basket were investigated for about 3800 heats. In normal operation the load is limited to about 90 t because of the limited crane performance. The scrap loads of the first baskets were divided into 5 groups with similar distribution by means of a cluster analysis using the standard metric.

Table 3 shows the result of the cluster analysis. The five clusters are differently-sized, for example the largest group (cluster 2) covers nearly half of the whole data, whereby other group sizes are below 10 % of the data (cluster 1 and cluster 3).

Table 3: Cluster analysis of the scrap load for the first basket

	# heats	RE Bären	RE Masseln	E1	E2	E3	BatRec	E40 Schredder	E5M	E5H
All	3833	1.3	1.3	3.7	3.6	28.1	0.1	2.1	9.8	0.1
Cluster 1	287	1.7	1.3	3.6	0.5	22.1	0.1	0.6	1.2	0.0
Cluster 2	1801	1.6	1.3	3.3	0.9	32.8	0.0	3.1	10.1	0.0
Cluster 3	627	1.3	1.3	3.2	1.1	24.4	0.1	0.7	12.6	0.0
Cluster 4	887	0.5	1.2	4.0	12.5	25.7	0.1	2.1	10.0	0.0
Cluster 5	231	1.2	1.0	6.9	0.7	18.7	0.1	0.4	11.0	1.0

	E6	E8	Spänebriketts	Stahlbären	WW Schrott	Rück Cr	Rück CrMo	Rück CrNiMo	Gussbruch	Restblöcke
All	2.2	19.6	1.8	2.0	4.5	3.2	1.6	1.8	0.0	0.3
Cluster 1	14.2	36.2	0.3	1.6	0.4	0.2	0.2	1.4	0.0	0.1
Cluster 2	1.8	19.5	2.1	1.9	8.6	0.2	0.1	0.0	0.0	0.2
Cluster 3	0.5	16.6	2.1	3.1	0.5	18.2	0.7	0.2	0.1	0.5
Cluster 4	1.0	17.4	1.4	2.3	1.5	0.5	6.2	0.2	0.1	0.3
Cluster 5	0.0	16.1	1.9	0.1	0.1	0.1	0.1	26.2	0.0	1.0

To characterise the efficiency of the different chemical energy inputs, the off-gas composition regarding unburnt chemical energy sources was investigated. With the help of the off-gas analysis and the results of Task 2.3, the average amounts of CO and H₂ in the off-gas during meltdown were determined. **Table 4** shows the average amounts together with the post-combustion degree, defined by the ratio between CO₂ and CO₂ + CO, for those heats where off-gas data were available.

Table 4: Mean amounts of CO and H₂ in the off-gas for clustered scrap load of the first basket

	# heats	H ₂ / Nm ³	CO / Nm ³	PC-degree / %
All	2870	597	746	51
Cluster 1	224	451	595	58
Cluster 2	1426	628	769	50
Cluster 3	465	618	779	48
Cluster 4	633	552	711	52
Cluster 5	122	652	825	47

Cluster 3 und 5 show the largest amounts of the unburnt chemical energy sources CO and H₂ in the off-gas. For these two clusters also the PC-degree is lower than for the other clusters, pointed out by values below 50 %. Cluster 1 contains the lowest amounts of CO and H₂ together with the largest PC-degree. One reason for this is the lowest amount of turnings (E5M and E5H) in the scrap load. The regression analysis in Task 2.3 has shown that the turnings are one of the most important sources of carbon and hydrogen, due to their high content of oil and grease.

It was also examined if there is a correlation between the charged scrap mixes and the vibration signals. Therefore the different scrap types and mixes have been clustered into five groups and correlated with the mean vibration level of the first six minutes of power on during the first basket's meltdown process. The period of analysis was limited to the beginning of the meltdown process after charging of the first scrap basket with the expectation of detecting more significant differences between the different scrap mix clusters while the arc burns on cold and solid scrap. If instead the whole meltdown phase is evaluated, a progressive homogenization of the scrap mix is to be expected, minimizing possible differences between scrap mixes. The result of 275 analysed heats is shown in **Table 5**.

Table 5: Analysis of mean vibration level and charged scrap cluster

Cluster	Number of heats	Mean vibration level during first six minutes in dB	Standard deviation
2	219	105.73	4.35
3	7	106.03	5.37
4	49	105.70	4.33
All	275	105.73	4.35

Within the evaluation period, three of the five scrap clusters have been used. However, on the basis of these data no significant differences between scrap mix and mean vibration level could be observed.

Additionally, an examination of the relationship between the mean vibration level at the end of the first basket's meltdown process and the corresponding basket filling level was undertaken. For this consideration, the point in time when to observe the vibration level was chosen to be at the end of the meltdown process. The reason for this choice is the general assumption that the arc burns on the liquid fraction of the then molten scrap at almost the same level by the end of the first basket's meltdown process. The basket filling level was estimated by the operator with ten per cent accuracy before charging. The result is shown in **Figure 81**. A slight tendency of falling vibration levels with rising basket filling levels can be observed. This behaviour can be explained by the hypothesis that superior arc shielding occurs with light (less dense) scrap in comparison to heavy (more dense) scrap. As the charged scrap mass is nearly constant in each charge, the basket filling level is mainly determined by the density of the scrap.

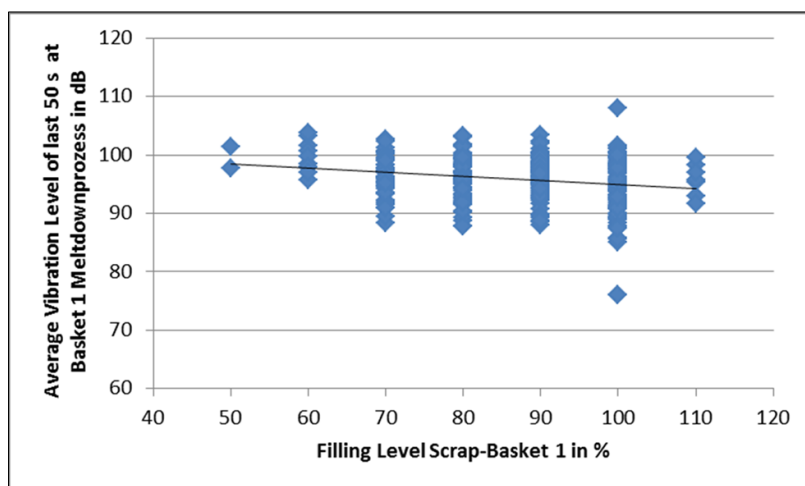


Figure 81: Mean vibration levels at the end of first basket meltdown process vs. first basket filling level

Cluster analysis of second scrap basket

The same investigations have been performed for the scrap load of the second basket. **Table 6** shows the mean scrap load of the 5 groups resulting from cluster analysis of about 3800 baskets. For the second basket the sizes of the different groups differ significantly, too. The largest group (cluster 3) covers about one third of all data, whereby the number of baskets assigned to cluster 1 is below 10 %.

Table 6: Cluster analysis of the scrap load for the second basket

	# heats	RE Bären	RE Masseln	E1	E2	E3	Müllsep	E40 Schredder	E5M	E5H
All	3807	0.4	3.4	5.9	0.7	19.1	0.8	6.9	6.3	0.0
Cluster 1	295	0.4	2.6	2.1	1.5	13.1	0.7	5.1	0.7	0.0
Cluster 2	949	0.3	3.8	3.3	0.3	21.8	0.8	10.8	0.1	0.0
Cluster 3	1250	0.4	3.5	8.7	1.6	12.1	0.8	6.3	12.3	0.1
Cluster 4	866	0.5	3.2	6.8	0.1	22.5	0.8	7.4	9.6	0.0
Cluster 5	447	0.3	3.4	4.1	0.1	30.5	0.7	0.3	0.2	0.0

	E6	E8	Spänebriketts	Stahlbären	WW Schrott	Rück Cr	Rück CrMo	Rück CrNiMo	Gussbruch	Restblöcke
All	0.6	19.8	0.5	0.0	0.3	0.1	0.0	0.6	0.0	0.0
Cluster 1	7.1	30.3	0.1	0.0	1.8	0.0	0.0	0.0	0.0	0.0
Cluster 2	0.0	24.5	0.0	0.0	0.0	0.1	0.0	0.0	0.0	0.0
Cluster 3	0.0	16.2	0.3	0.0	0.4	0.2	0.1	1.6	0.0	0.0
Cluster 4	0.0	13.2	1.9	0.0	0.1	0.0	0.0	0.2	0.0	0.0
Cluster 5	0.0	25.6	0.0	0.0	0.0	0.0	0.0	0.0	0.0	0.0

Table 7 shows the mean amounts of CO and H₂ in the off-gas together with the post-combustion degree. Cluster 3 and 4 show the largest amounts of unburnt chemical energy sources and the lowest PC-degree. These two clusters include also the largest amount of turnings in the scrap mix.

Table 7: Mean amounts of CO and H₂ in the off-gas for clustered scrap load of the second basket

	# heats	H ₂ / Nm ³	CO / Nm ³	PC-degree / %
All	3421	594	728	47
Cluster 1	266	424	572	54
Cluster 2	893	457	628	53
Cluster 3	1128	715	823	42
Cluster 4	752	710	813	43
Cluster 5	382	449	621	52

With the help of the cluster analysis the expected potential of available chemical energy sources in the off-gas can be estimated. From this information scrap cluster dependent operating patterns for the burners regarding overstoichiometric operation for post-combustion can be derived, see under Task 4.1.

Assessment of the scrap melting behaviour

Based on the information of the vibration sensors and the calculations with an energy and mass balance model, an on-line control model to determine the optimal time for charging the second basket was developed. An additional geometric measure for supporting this model calculation was derived from the position of the foot of the electric arc. This can be estimated from the electrode position, which is included in the set of furnace-specific process data already available at GMH, and the basket filling level derived from the image analysis, which gives an estimation of the starting height at arc ignition. The arc length, which can be determined by the actual arc voltage and current values using an established arc length model, has not been taken into account due to its minor contribution. In this way, the solid scrap height in the central area of the furnace may be described mainly corresponding to the electrode path.

The timely charging of the second basket is important to reduce energy losses due to insufficiently shielded arcs in the final meltdown phase of the first basket. On the other hand, if the second basket is charged too early it may not fit into the furnace and a time delay may occur due to the necessity of flattening the scrap. The basic principle of the model is to predict the free volume in the furnace vessel with respect to the melting progress of the first scrap basket, and to compare this

value to the volume required for the scrap load of the second basket. As a result, a model based on the vibration signals (P2) and supported by the position of the foot of the electric arc (P1) is defined as shown in **Figure 82**.

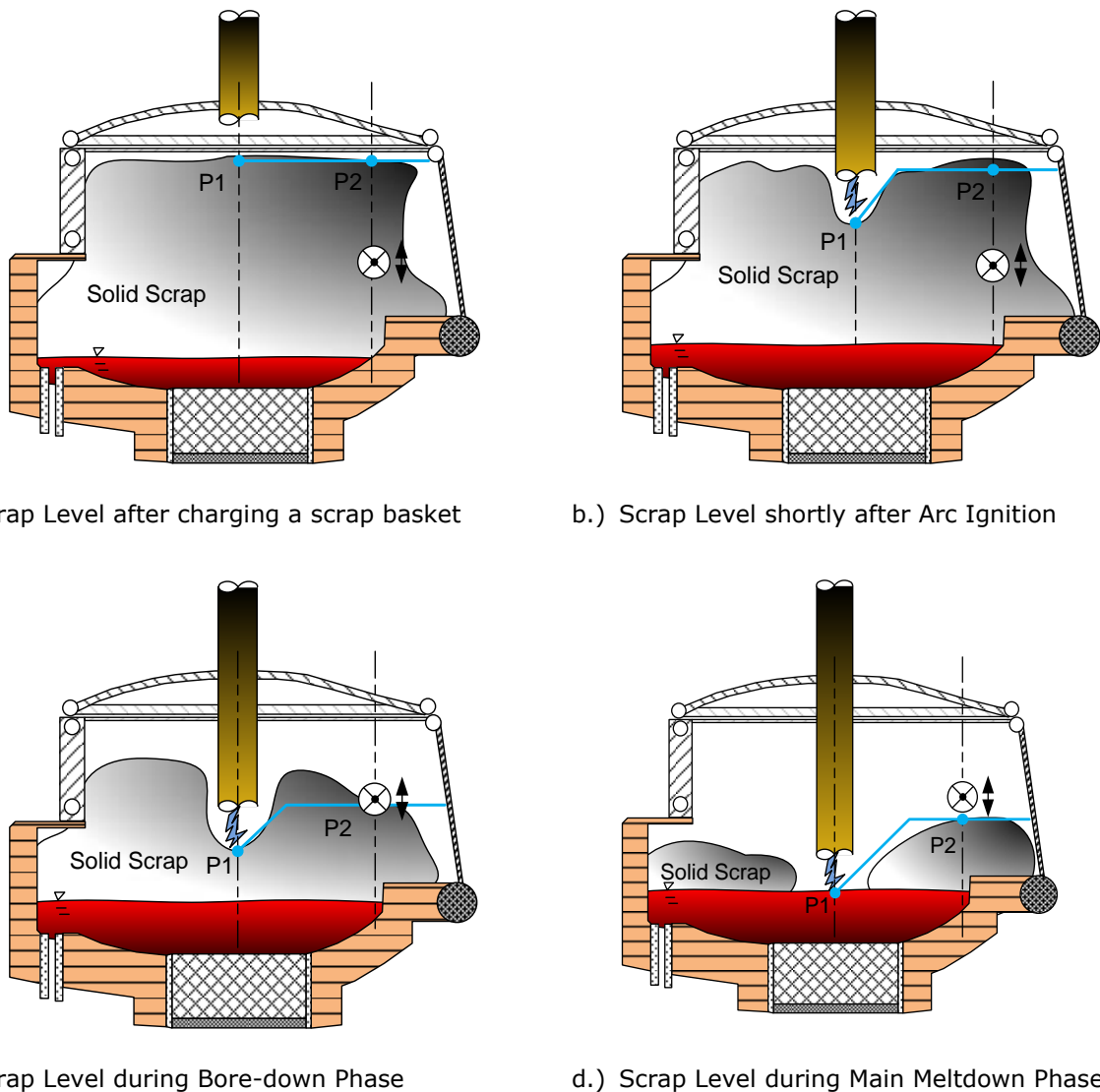


Figure 82: Exemplary States of Meltdown Progress Described by the Two-Point Solid Scrap Model

The two underlying scrap index estimation models are each designated as one point (P1 to P2) in a cross-section of the furnace, thus describing a height profile of the solid scrap still present in the furnace during the meltdown process. While the position of the electric arc's foot (P1) results from the underlying basic estimation principle, the vibration signal-based scrap height assessment (P2) cannot be assigned to a specific position directly. In this model it describes the solid scrap pile level in the remaining furnace area.

Thus, the two-dimensional slice of the furnace considered in this model extends from the centre of the electrode axis to the inner vessel wall. During the meltdown process, the scrap level estimated at each of the above mentioned two points will decline along the dotted lines as shown in the four partial images in Figure 82.

In this simplified approach however, a possibly irregular distribution of the remaining scrap is not taken into account. Further ideas to this end include considering the furnace's hot and cold spots. Information about their position and size could then be used to introduce appropriate weighting factors when calculating the solid scrap volume by rotational integration. A more detailed modelling

might also be achieved by installing additional vibration sensors in further positions, which each represent another slice of the furnace with a respective area of solid scrap to be considered in the volume integral.

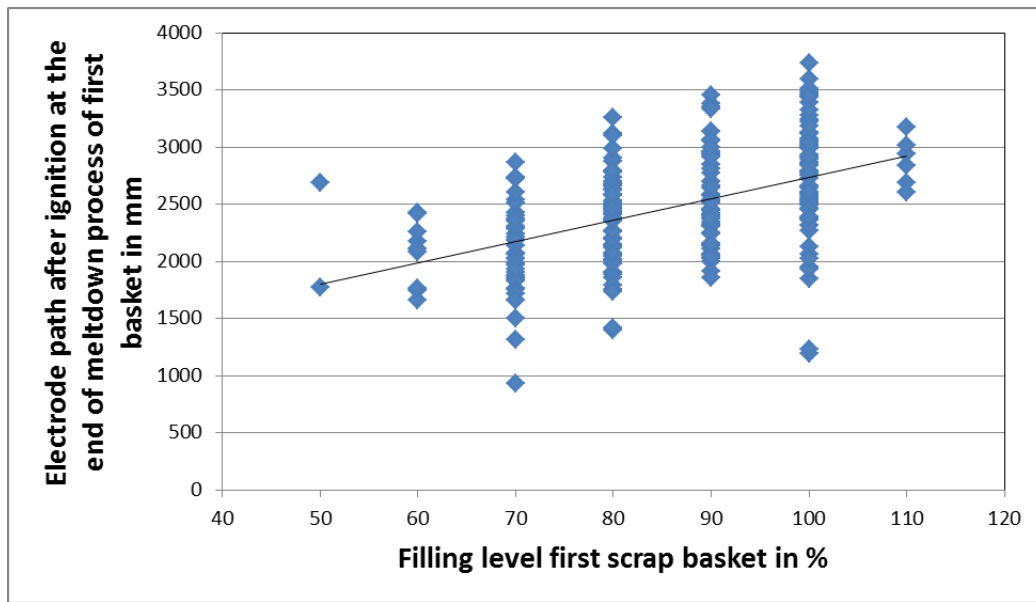


Figure 83: Correlation of Scrap basket filling level vs. electrode Path

Considering the position of the foot of the electric arc, **Figure 83** shows the correlation between electrode path after ignition (E_{Path}) and the filling level of the charged scrap basket (BFL). Usually, the electrode arrives at liquid bath level by the end of the meltdown process. Thus, the electrode path signal is used to formulate a correlation between basket filling level and resulting furnace filling level FFL_{Basket} . According to measurement results, the following approximation applies:

$$FFL_{Basket} = BFL * 22 + 600 + \text{Safety Factor}. \quad (1)$$

Reversely, the actual furnace filling level directly under the electrode (FFL_E) can be calculated by:

$$FFL_E = FFL_{Basket} - E_{Path}. \quad (2)$$

In **Figure 84**, the correlation between E_{Path} and the vibration level is illustrated.

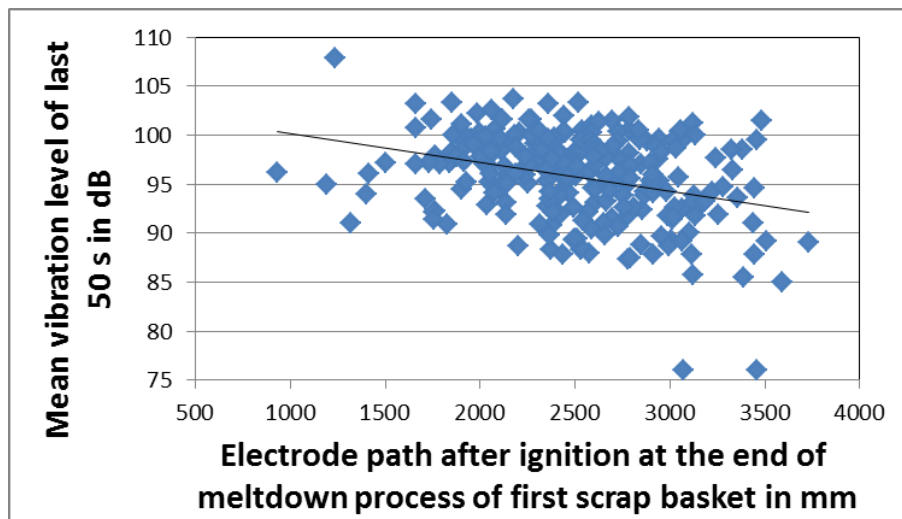


Figure 84: Correlation of Electrode Path vs. Vibration Level

Based on the expected mean vibration level, which linearly depends on the actual electrode path E_{Path} , the actual vibration level value can be classified as above or below expectation, yielding information about the actual arc shielding by scrap. A comparatively low vibration level indicates a good arc shielding. Consequently, a high scrap level between electrode and vibration sensor at the furnace wall is assumed. For high vibration levels, the scrap level around the electrode is considered to be the same as directly under the electrode. In order to evaluate the height of the scrap pile surrounding the borehole (FFL_S), the following model was found from measurements:

$$FFL_S = FFL_E + ((-0,003 * E_{Path} + 133 - Vib_{Level_{PT1}}) + O) * S \quad (3)$$

in which O is an offset and S a scaling factor. Thus, a vibration level-dependent addition is made to the scrap level detected directly under the electrode via the electrode path.

Two offline calculated trends of scrap levels as specified by the above models (FFL_E and FFL_S) during the meltdown process of the first scrap baskets are shown in **Figure 85** and **Figure 86**. The overall vibration level in Figure 85 is relatively low, so a large offset between FFL_E and FFL_S emerges. In contrast, the general vibration level of the process illustrated in Figure 86 is permanently high. Therefore, the offset between the two filling level indicators is much smaller.

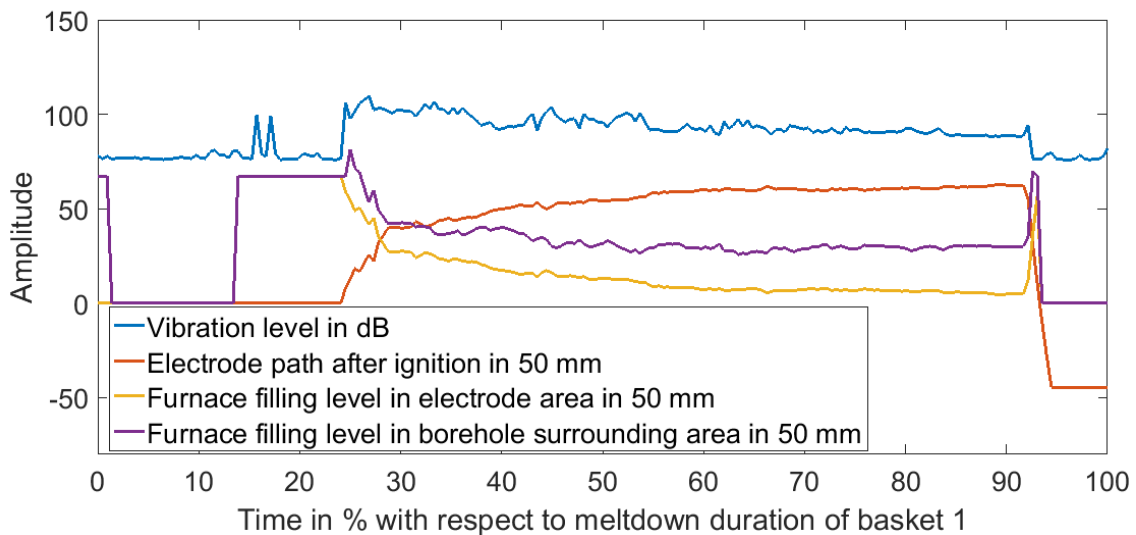


Figure 85: Trends of the Two-Point Scrap-Level-Model at low mean vibration levels

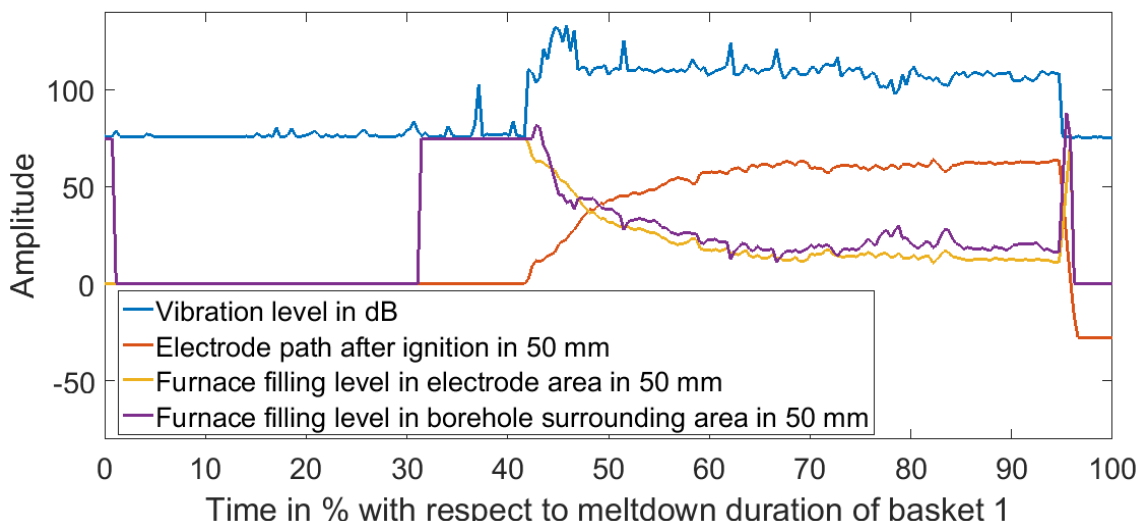
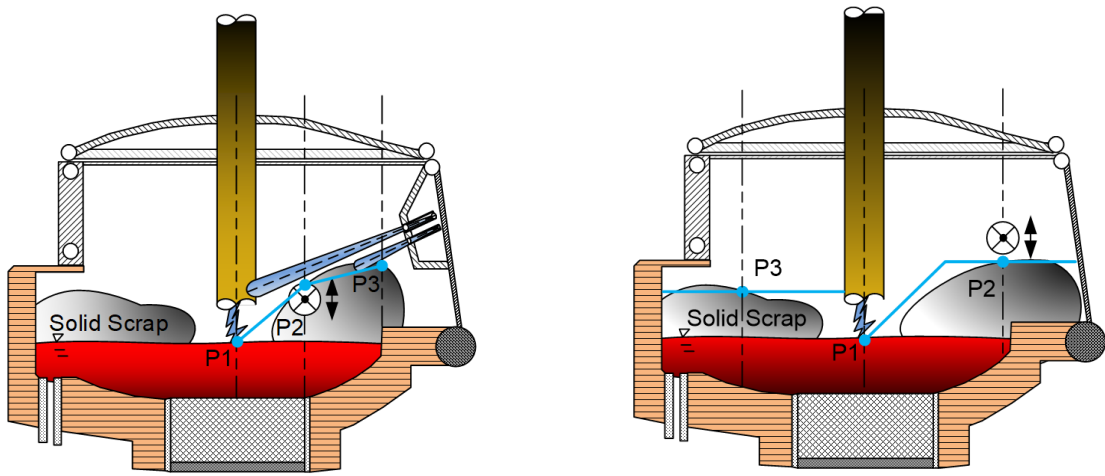


Figure 86: Trends of the Two-Point Scrap-Level-Model at high mean vibration levels



1. Additional spectrometer system

2. Additional energy information

Figure 87: Extension of the two point scrap index model

In **Figure 87** two different methods to expand the two point scrap index model are illustrated. The left picture demonstrates a model version using an additional spectrometer system. The two spectrometers are positioned one on top of the other and each of them can be used to detect solid scrap between electric arc and its corresponding lens in a light barrier fashion. Thus, a two-stage scrap level detection may be implemented based on the exact geometric conditions of the setup. With each transition from low to high level in spectrometer signals (P3), it may therefore be concluded that the scrap level has fallen below the index defined by the particular spectrometer's mounting position. This information could then be incorporated as a supporting point in the vibration-based model evaluation by immediately setting the model output to the defined index and continuing further calculation from this point. This kind of model was planned before the spectrometer system was removed from the furnace but could not be realised because of the spectrometers malfunction.

Supporting the described two-point-model, the scrap level is also estimated according to the energy balance of the process as illustrated in Figure 87 on the right. This model also takes into account the specific energy demand of different scrap mixes. The corresponding scrap filling level is marked as P3. As the two independent models are calculated on different data bases, an overall estimation of the solid scrap index remains possible even if a sensory input signal should experience a malfunction. Furthermore, weighting the model results according to their degree of influence is possible to constitute a single overall scrap index value. This is the result of the scrap filling level model development and was used as a basis for the following examinations.

The results of the two independently modelled scrap filling levels at the end of the first basket's meltdown process are shown in **Figure 88** and **Figure 89**.

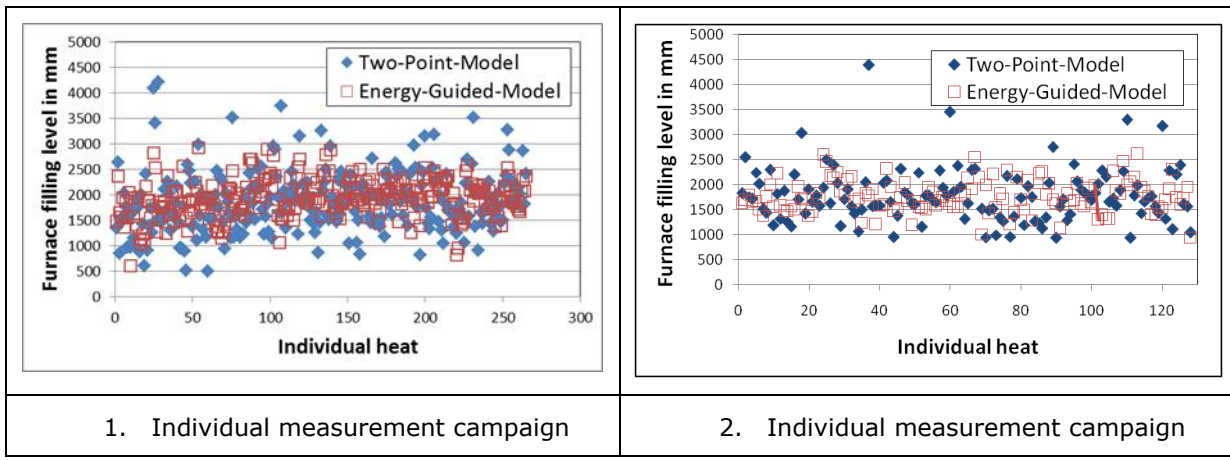


Figure 88: Results of two filling level models at the end of Basket 1 meltdown process vs. individual heats during two different measurement campaigns

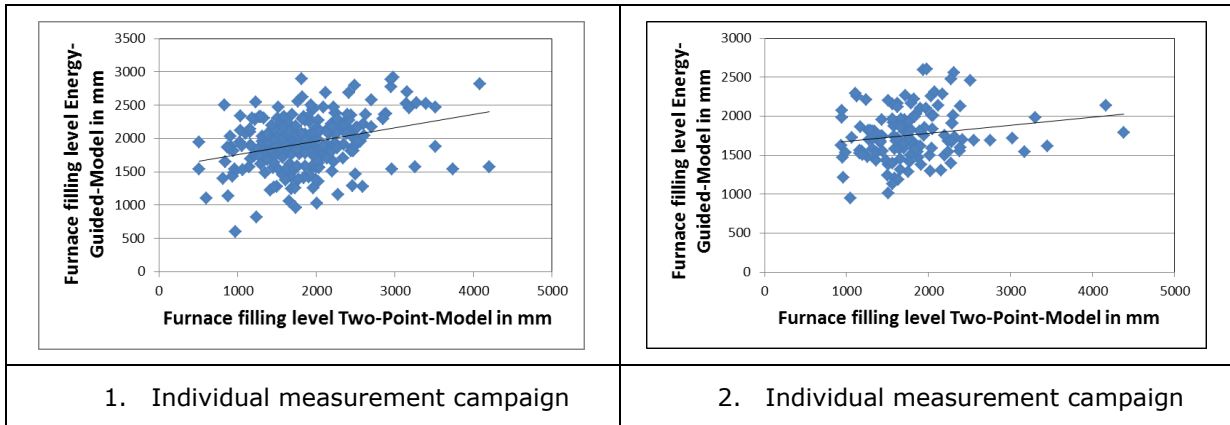


Figure 89: Correlation of both model estimations during two different measurement campaigns

Figure 88 illustrates the generally similar range of both model results. The maximum possible level at the furnace rim is in a range between 4500 mm to 5000 mm, depending on the wear of the bottom refractory over the furnace cycle. The estimated filling level values lie in a range of 1000 – 3000 mm, which seems to be plausible. Also, a similar tendency of both filling level predictions is observable, as shown in **Figure 89**.

Task 3.4: Implementation of a display for new measurements, enhanced modelling and melting yield results for the plant operators and engineers (BFI, GMH, HSU)

The result of the image analysis of the scrap baskets to determine the basket filling degree is displayed to the operators on a screen placed in the EAF control room. Two examples of different scrap filling degrees are shown in **Figure 90**.

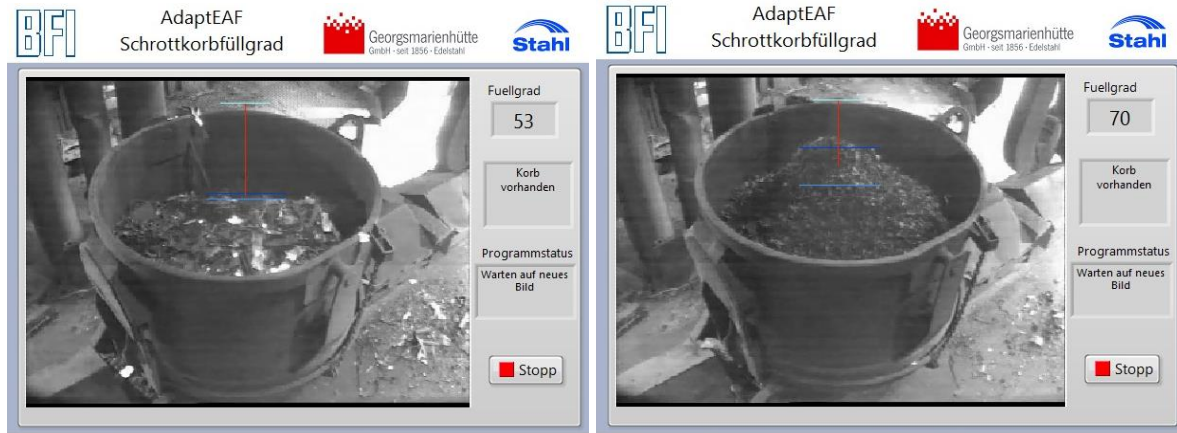


Figure 90: Display of scrap basket with detected filling degree in the EAF control room of GMH for two different examples

As can be seen in the upper right part, for every basket the filling degree is displayed. In the image the lines which were used to determine the filling degree are drawn. A cone in the scrap pile, as shown in the figure on the right hand side, is also considered.

To illustrate the data relevant to vibration analysis, generally two different screens are used. One display is installed in the vibration measuring-room, the other one is integrated in the EAF control room. The first display presents the user interface of the vibration signal analysis software, programmed in LabView. On the one hand it allows the local modification and extension of the program source code during recording interruption, on the other hand it shows the desired signals and model information in situ and offers the user the possibility of changing parameters. The graphical user interface is sectioned into several tabs.

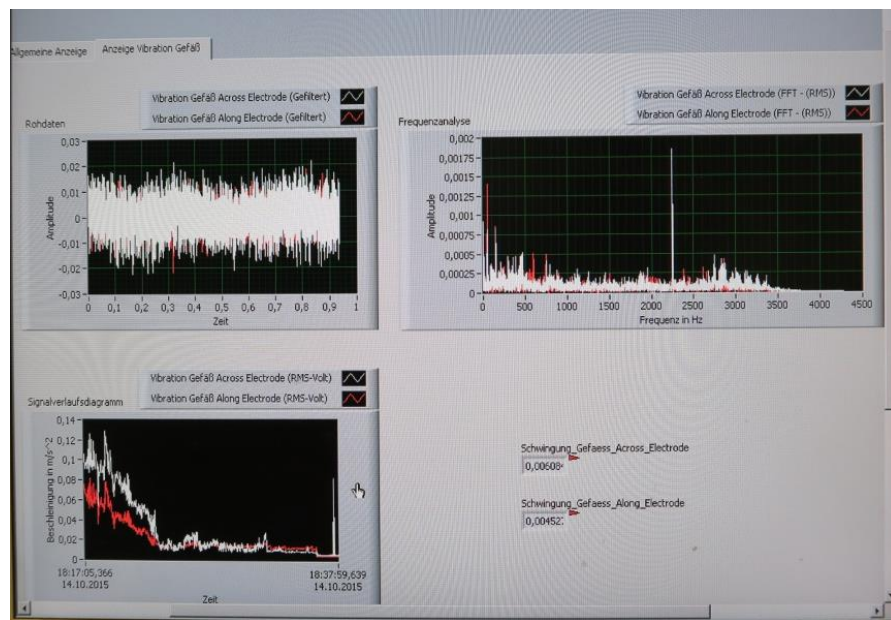


Figure 91: Display of the LabView On-Line Vibration Analysis-Software

Figure 91 shows one of the implemented tabs which presents the fundamental in situ numerical information of both incoming vibration sensor signals. The diagram on the upper left corner illustrates the incoming raw signals of the amplified sensor data. In the upper right corner, the spectral components of the raw data signals are shown. At the bottom left corner, the run of the resulting RMS signal is traced versus time elapsed. The actual numerical state of the RMS value is also displayed at the bottom right corner.

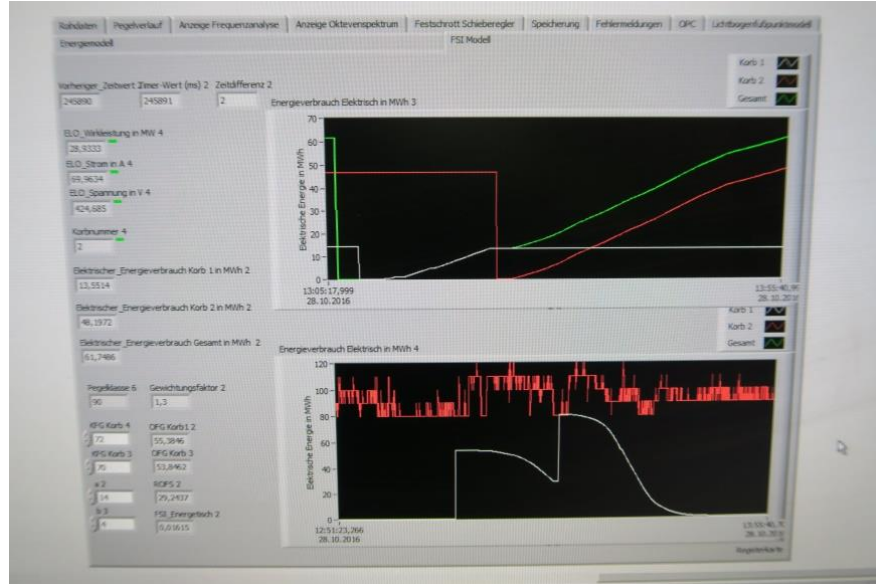


Figure 92: Model-Development Tab in On-Line Vibration Analysis-Software

Another tab of the vibration analysis program is depicted in **Figure 92**. This tab is used for in situ development, adaption and evaluation of dynamic process models, based on the vibration and further process data arriving from the PLC connected via the OPC-Client. The on-line trend in the lower pane shows the development status of the FFL (white graph). This was a principle trial of online model implementation. The run of this white line is based on the online measured vibration level signal combined with a fermi function limitation and the basket filling level. The latter was manually inserted by typing in the panel on the left border. In contrast to the 2 point model the electrode path after ignition was not used in this test. All these tabs can be modified and extended as needed.

The second display, installed in the furnace control room is shown in **Figure 93**. It is designated to display the current vibration level trend and the derived model results to the operator. In contrast to the former LabView based graphical user interface, this display is only installed to visualise the additional information of the furnace state, without any possibility of interaction. The charts presents the voltage (blue), the vibration level (red) and the formerly used spectrometer signals (green).



Figure 93: Display in the furnace control room

The results of the dynamic process model regarding the current melt state are displayed within the graphical user interface (GUI) of the Level-2 control system at GMH. Here the operator can select the different heat state parameters (melt temperature, steel and slag analysis) which are calculated continuously by the dynamic EAF process model, and can monitor their evolution over time in diagrams.

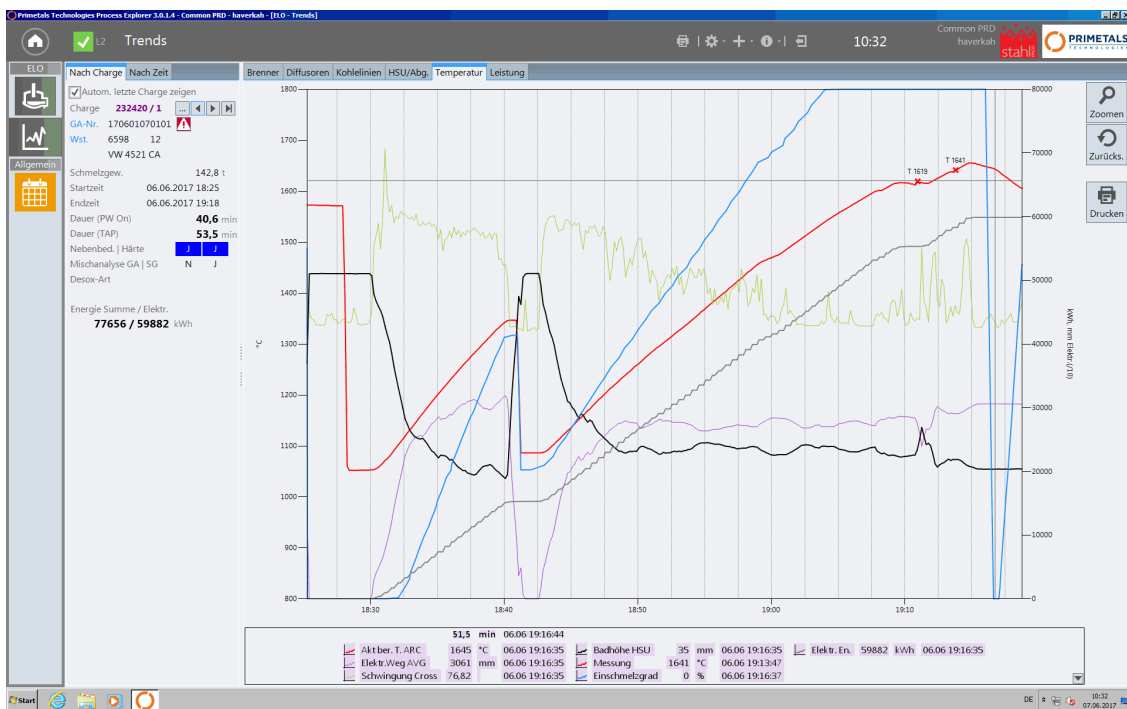


Figure 94: User interface of Level-2 process control system at the EAF of GMH

In **Figure 94** a detail of the user interface of the central Level-2 process control system is illustrated. In this program, all currently measured process states and derived model calculations are presented. On the illustrated tab, among other things the trend of the furnace filling level model is shown (black curve). The model is based on the basket filling level, the electrode path (violet curve) and the vibration level (green curve). The melt temperature calculated by the dynamic process model is shown together with thermocouple measurements in red. In this application the online monitoring of the actual melt is possible as well as the examination of previous melts by selecting the corresponding heat number.

2.2.4 WP 4: Application of process control tools based on newly implemented measurement systems and advanced dynamic process models

Task 4.1: Heat-individual control of the chemical energy inputs depending on scrap yield and melt status determined by model calculations and scrap characteristics (all partners)

To further investigate on the efficiency of the chemical energy input depending on the scrap mix, three trial campaigns with modified operating patterns for the different chemical energy inputs have been performed. The influence on the off-gas composition dependent on the individual scrap mix has been investigated and the energetic performance evaluated.

Furthermore an end point control has been developed to achieve the target tapping temperature and carbon content simultaneously.

Heat-individual control of chemical energy inputs depending on scrap mix

Within dedicated trial campaigns the operating patterns of two burners have been modified and tested in each case for about 20 heats. For the trials the oxygen input has been increased by higher flow rates during the meltdown phase of the two scrap baskets. The trials can be characterized in the following way:

- Trial 1: extended overstoichiometric operation of burner 4
- Trial 2: extended oxygen injection by burner 4
- Trial 3: extended overstoichiometric operation of burner 3

In a first step the analysed off-gas composition and the expected values on the basis of the investigations regarding the cluster analysis for the different basket loads described under Task 3.2 has been compared. The scrap loads of the trials have been assigned to the cluster division, and on the basis of the expected off-gas composition of each cluster the appropriate values have been determined for the trial heats. To compare these values to standard practice, the values of heats produced before and after the trials have been investigated, too. **Table 8** shows the expected off-gas composition together with the analysed values coming from the off-gas analysis system.

Table 8: Analysed and expected off-gas composition of first scrap basket

1. basket	analysed			expected from cluster analysis		
	H ₂ / Nm ³	CO / Nm ³	PC-degree / %	H ₂ / Nm ³	CO / Nm ³	PC-degree / %
standard practice	587	710	54	575	727	51
Trial 1	560	631	58	577	725	52
Trial 2	414	546	61	592	736	51
Trial 3	495	614	59	586	744	50
standard practice	535	652	57	548	698	53

For the three trial campaigns the measured PC-degree is significantly higher than expected, whereas for the heats produced under standard operating practice there is only a slight difference in the PC-degree. This demonstrates the positive effect of the additional oxygen input on the degree of the post-combustion reaction.

Table 9 shows the off-gas composition for the meltdown phase of the second basket. The observed PC-degree is higher than expected from the cluster analysis for the whole investigated time period. Especially for the trials 2 and 3 it is significantly higher.

Table 9: Analysed and expected off-gas composition of second scrap basket

2. basket	analysed			expected from cluster analysis		
	H ₂ / Nm ³	CO / Nm ³	PC-degree / %	H ₂ / Nm ³	CO / Nm ³	PC-degree / %
standard practice	695	722	51	598	727	47
Trial 1	434	577	55	483	633	51
Trial 2	575	571	57	622	743	46
Trial 3	564	571	56	645	769	45
standard practice	662	660	53	572	708	48

In the next step, BFI evaluated the data of these trial campaigns regarding the energetic performance of the DC furnace of GMH with the help of a model for calculating the electrical energy demand of EAFs by statistical analysis of the most relevant operational figures, which has been developed by BFI in previous EU projects [9-11]. With this statistical model, the electrical energy consumption of an EAF can be assessed in comparison to other furnaces, and variations of electrical energy demand at the same furnace can be analysed. The formula for calculating the electrical energy demand of EAFs with the parameter values determined in [11] is shown in **Table 10**.

Table 10: BFI formula for electrical energy demand of arc furnaces

$$\frac{W_R}{\text{kWh} / \text{t}} = 375 + 400 \cdot \left[\frac{G_E}{G_A} - 1 \right] + 80 \cdot \frac{G_{DRI} / HBI}{G_A} - 50 \cdot \frac{G_{Shr}}{G_A} - 350 \cdot \frac{G_{HM}}{G_A} + 1000 \cdot \frac{G_Z}{G_A} \\ + 0.3 \cdot \left[\frac{T_A}{^{\circ}\text{C}} - 1600 \right] + 1 \cdot \frac{t_S + t_N}{\text{min}} - 8 \cdot \frac{M_G}{\text{m}^3 / \text{t}} - 4.3 \cdot \frac{M_L}{\text{m}^3 / \text{t}} - 4.3 \cdot \frac{M_{LJ}}{\text{m}^3 / \text{t}} - 2.8 \cdot \frac{M_N}{\text{m}^3 / \text{t}}$$

G _A	Tap weight	t _S	Power-on time
G _E	Metallic charge weight	t _N	Power-off time
G _{DRI}	Weight of DRI	M _G	specific Burner gas
G _{HBI}	Weight of HBI	M _L	specific Lance oxygen
G _{Shr}	Weight of shredder scrap	M _{LJ}	specific Injector oxygen
G _{HM}	Weight of hot metal	M _N	specific Post Combustion (PC) oxygen
G _Z	Weight of slag formers	W _R	Calculated Electrical Energy demand
T _A	Tapping temperature		

The statistical model takes into account the specific consumption of total and several individual ferrous materials, slag formers, burner gas, oxygen for blowing by lances and injectors as well as for post-combustion, temperature before tapping and tap-to-tap time, divided in power-on and power-off time. All consumption values - also the actual electrical energy consumption W_E for comparison with the calculated demand W_R - are related to the tap weight.

In **Table 11** the average input values for the BFI statistical model are compiled for the three trial campaigns, and the periods before and after which were performed under standard operating practice.

Table 11: Average input values of GMH heats for calculation of electrical energy demand

	W_R	W_E	W_R-W_E	T_A	t_S	t_N	M_G	M_J	M_N
standard practice	365.4	450.8	-85.4	1631.6	40.1	18.0	3.6	25.6	9.6
Trial 1	382.4	439.5	-57.1	1638.2	40.2	26.1	3.6	21.0	12.3
Trial 2	373.2	436.1	-62.9	1628.8	38.9	23.9	3.4	25.3	9.7
Trial 3	370.5	436.2	-65.7	1628.4	38.7	18.1	3.6	22.3	10.8
standard practice	378.0	456.3	-78.3	1632.9	40.9	19.2	3.6	25.5	10.1

The difference between calculated demand and actually consumed electrical energy $W_R - W_E$ is a measure for the energetic performance of the furnace. Negative values indicate a worse energetic performance compared to the one which is expected according to the input values. This difference shows a lower negative value for the three trial campaigns with higher oxygen input during meltdown of the scrap baskets. This indicates an improved energetic performance of the furnace due to the improved post-combustion and thus an increased efficiency of the chemical energy input. In contrast to this, the values under standard operating practice show larger negative deviations between expected demand and actual energy consumption.

This result underpins the demand to adapt the operating patterns for the chemical energy input depending on the actual scrap mix. For each cluster a separate operating pattern for the burners regarding overstoichiometric operation for post-combustion shall be defined with respect to the energetic potential in the off-gas. Thus the oxygen input will be adjusted as needed for the expected chemical energy sources in the off-gas.

After filling a basket, the weights of all scrap types are known and the actual load can be assigned to the cluster where the scrap mix belongs to. For the meltdown process of the scrap basket the appropriate operating pattern will be selected. This procedure guarantees an optimal use of chemical energy inputs according to the actually charged scrap.

End-point control with respect to melt temperature and oxygen content

Besides the melt temperature also the carbon content in the steel is a target value which has to be adjusted during the refining treatment. As the dynamic process model also calculates the carbon content of the steel, the appropriate parameter for the decarburization rate of the injected oxygen can be determined. By knowing the current carbon content of the melt, the remaining treatment time needed for decarburization to reach the target carbon content can be predicted. Furthermore the chemical energy input by oxygen injection into the steel bath has to be considered for calculating the remaining time for reaching the target tapping temperature.

Figure 95 shows this concept for the end-point control at GMH. The initial conditions are defined by a melt temperature of 1550 °C and a steel carbon content of 0.09 %. To reach the target tapping temperature of 1650 °C and the aim carbon content of 0.06 %, a remaining treatment time of about 5 min is predicted. The expected progress regarding melt temperature and steel carbon content during refining treatment is proceeding along the drawn line. The remaining treatment time is marked in equidistant time steps of 1 minute.

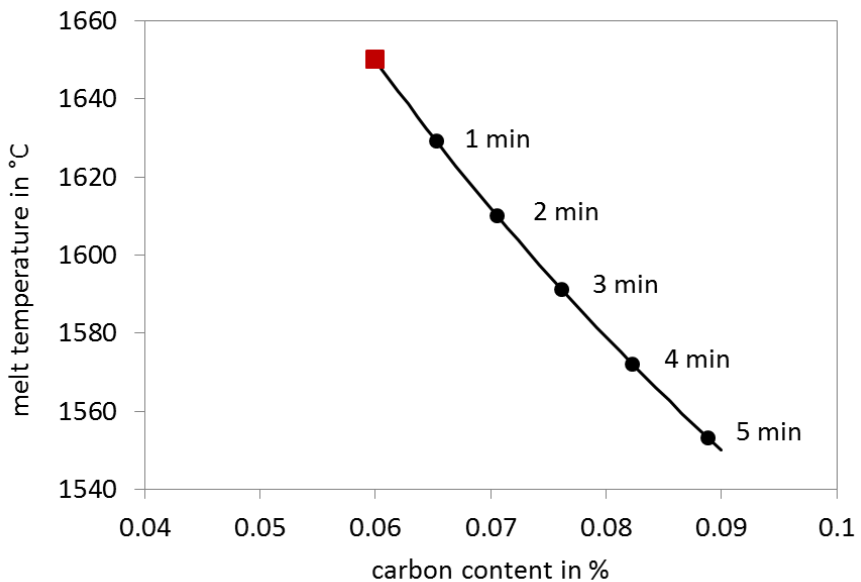


Figure 95: Evolution of end point control for reaching the aim tapping temperature and steel carbon content simultaneously

This end-point control concept is integrated within the dynamic process model. Based on the current melt status regarding carbon content and melt temperature, which is calculated by the model and adapted according to Celox measurements and steel analyses, heat individual set-points for the optimal input of oxygen and electrical energy are calculated to achieve the target values at the same time.

As the dynamic process model is fully integrated within the Level-2 control system of GMH, all its results can be provided and displayed to the operator. The set-points for electrical energy and oxygen input to achieve aim tapping temperature and the necessary decarburisation to achieve the aim carbon and oxygen contents are calculated cyclically on the basis of the currently calculated process state.

Task: 4.2 Determination of the optimal time for charging the second scrap basket depending on the information on scrap melting evolution and yield of the charge mix (all partners)

The specific objective of modelling the resulting furnace filling level at the end of the first basket meltdown, specified in WP 3, task 3.3, is to find the ideal point in time when to charge the second basket. Generally speaking, to decide if the next basket fits into the furnace, the filling levels of both baskets and the meltdown progress of the first scrap load are important.

Based on the information of the new sensors and the model calculations an on-line advisory concept to determine the optimal time for charging the second basket was developed. The timely charging of the second basket is important to reduce energy losses due to insufficiently shielded arcs in the final meltdown phase of the first basket. On the other hand if the second basket is charged too early it may not fit into the furnace and a time delay occurs by levelling the scrap. The basic principle of the model is to predict the free volume in the furnace vessel with respect to the melting progress of the first scrap basket, and to compare this value to the volume required for the scrap load of the second basket.

One possibility to examine whether the derived models are suitable for this purpose is to consider heats where the second basket did not fit into the furnace and therefore had to be flattened after charging. Thus, for a collective of about 300 recorded heats, the furnace filling level at the end of the first basket meltdown was calculated as a mean between the two model estimations (vibration-based and energy-based). The furnace filling level demand of the assigned second basket was then derived from the detected basket filling level. The sum of both thus indicates whether the maximum possible furnace filling level would be exceeded by charging the second basket. **Figure 96** shows the resulting filling level after basket one, the demand of the second basket and the estimated filling level after charging for all recorded heats. The heats where flattening of the second basket was necessary are depicted in **Figure 97**. The mean predicted filling level of all heats is 4232 mm, and 4592 mm in those cases where consequent flattening occurred. In view of the maximum possible filling level at the furnace rim of about 4500 mm after relining of the furnace, the models seem to be suited for detecting a possible overfilling of the furnace.

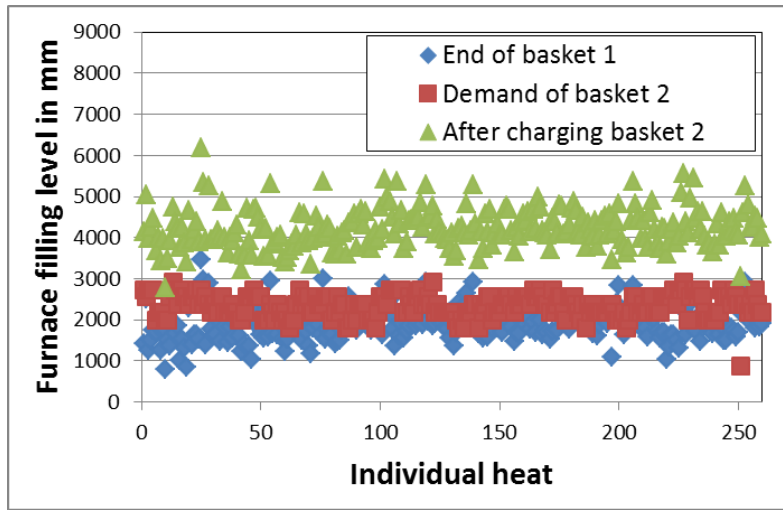


Figure 96: Prediction of furnace filling level after charging of second basket vs. individual heats

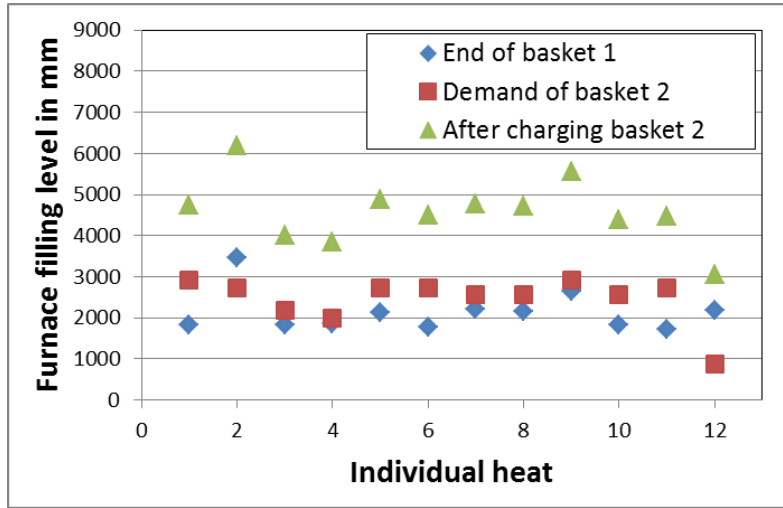


Figure 97: Prediction of furnace filling level after charging of second basket vs. individual heats with flattening of second basket

Another independent data analysis with reference to the furnace filling level and flattening events of the second basket was performed for one further set of observed heats. The corresponding results are shown in **Figure 98**, **Figure 99** and **Figure 100** and show large similarity to those depicted in Figure 96 and Figure 97. In this campaign, the flattening events were automatically registered when the furnace roof was not closed in a specified time after the charging signal. As a consequence, short flattening events where this critical time for closing the furnace roof was not ex-

ceeded could not be automatically detected in this way and were thus recorded by hand by the operator. The results of the automatically detected flattening events are shown in Figure 99 whereas Figure 100 depicts the filling levels of all flattening events, including the manually detected ones. In both cases, individual heats with flattening of the second basket have a model calculated mean value of approximately 4300 mm furnace filling level after charging the second basket.

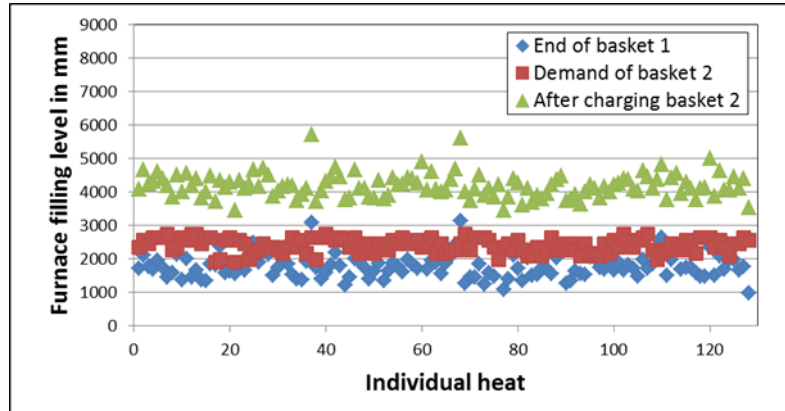


Figure 98: Prediction of furnace filling level after charging of second basket vs. individual heats

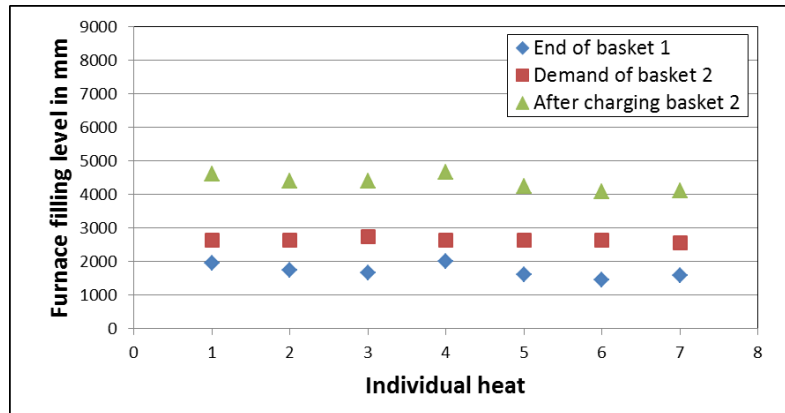


Figure 99: Prediction of furnace filling level after charging of second basket vs. individual heats with flattening of second basket

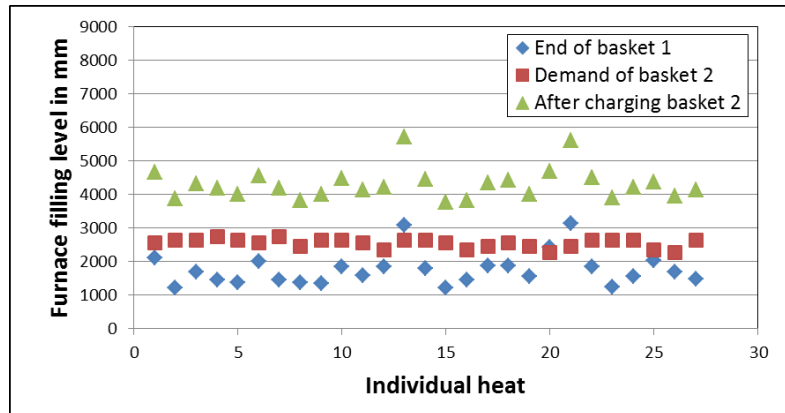


Figure 100: Prediction of furnace filling level after charging of second basket vs. individual heats with short flattening of second basket

From these results, a suggestion for charging the second basket can be derived for the operator, when the estimated filling level falls below a defined limit, e. g. 4300 mm. However, this limit value has to be carefully chosen in order to avoid the necessity of flattening the second basket on the one hand, and still charging the second basket as early as possible on the other hand. For a reliable trade-off between optimised energy efficiency and reduced process time through fewer interruptions, it is advisable to re-evaluate and adjust this limit value regularly.

Another evaluation approach examined in this project is a volume calculation, which indicates the free space in the furnace vessel, and thus allows the time when the next basket fits into the furnace to be estimated according to a mean melting rate. Also this model has been validated on the basis of irregular charging procedures which indicate a too early charging of the second basket. In normal operation about 20 % of the charging processes are delayed because the second basket does not fit into the furnace and has to be flattened. Although most of these flattening procedures do not lead to long and notifiable disturbances, it is advantageous to avoid or at least reduce the occurrence of them. For a trial campaign the flattening procedures which are not announced to the system has been notified by the operator if the second basket was charged too late, just right or did not fit into the furnaces and caused a flattening.

The two histograms in **Figure 101** show the calculated lack of space in the furnace for charging the second basket. The heats where the second basket fits into furnace are listed in the left diagram, heats with flattening of the second basket are shown in the right one. Negative values mean more free volume than needed, indicating a too late charging of the second basket. Positive values indicate that there is not enough free volume in the furnace for the scrap load of the next basket.

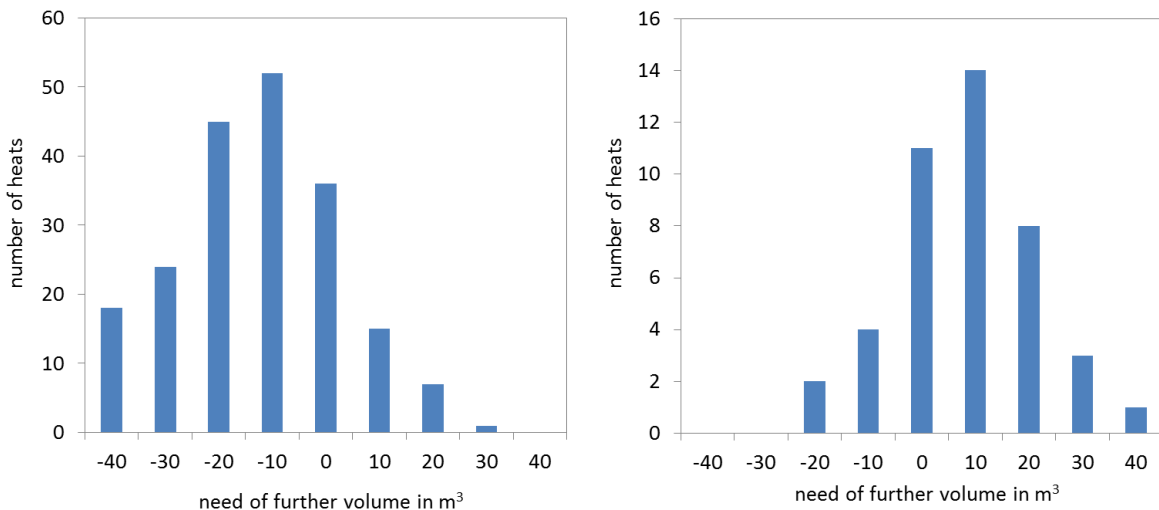


Figure 101: Histograms of calculated lack of volume for heats where the second basket fit into the furnace (left) and where the scrap has been flattened after charging (right)

About 80 % of the charging processes which required a flattening of scrap after charging are detected correctly by the model (**Figure 101**, right). For the heats without problems during the charging procedure the model predicts for about 75 % of the heats a negative volume which indicates an undisturbed charging procedure (**Figure 101**, left).

The determination of the optimal time for charging the second basket is integrated in the dynamic process model. The time when to charge the basket is calculated and can be displayed on the operator mask.

Task 4.3: Control of the steel bath level and remaining slag after tapping (GMH)

With the help of the dip sensor measurements the steel bath level can be controlled to an almost constant value, which guarantees a constant distance between the different injection lances and the bath surface and thus an optimal efficiency of the chemical energy inputs by burners and lances as well as of carbon blowing for foamy slag formation. Furthermore, the slag line remains in the same area of the furnace vessel where the refractory material is prepared for it. **Figure 102** shows

the dip-sensor measurements performed at the GMH furnace for about one year, covering in total three furnace campaigns.

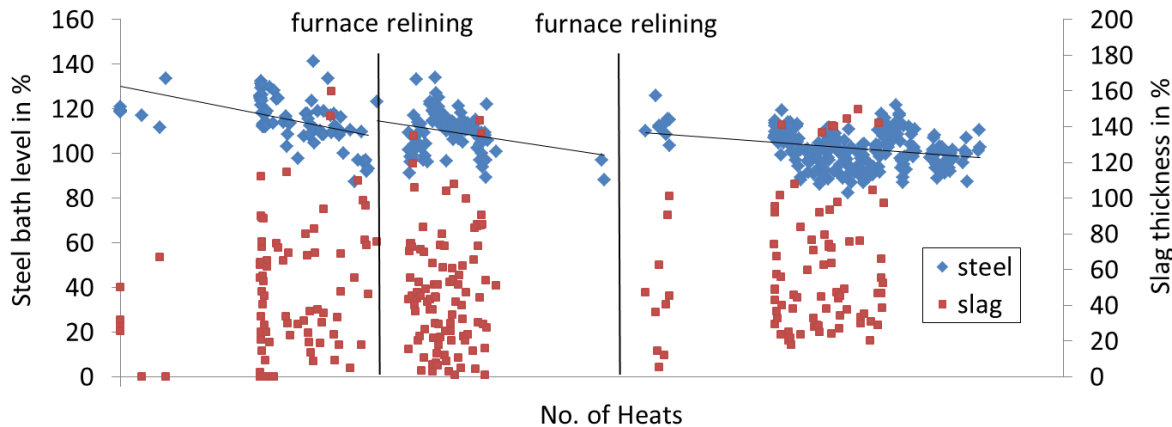


Figure 102: Dip sensor measurements for three furnace campaigns at GMH

The decreasing trend of the steel bath level due to the furnace wear, which was observed throughout the first two campaigns, has been reduced by an improved control of the steel bath level so that it was nearly constant during the last campaign. The operator uses the dip sensor information on the bath level to modify the scrap load and the tap weight if necessary. In contrast to that, the measured slag thicknesses still shows a wide scattering, as the deslagging process depends on other uncertainties.

Task 4.4: Consideration of quality-dependent constraints at EAF tapping (BFI, GMH)

The production portfolio of GMH covers a wide range of qualities with different requirements. Some constraints like the upper limit of carbon and phosphorous content have to be adjusted in the electric arc furnace, as a further lowering is not possible within the following secondary metallurgy treatment. But also the melt temperature is important for the metallurgical processes in the refining phase like dephosphorisation, as well as for the following treatment in the ladle furnace.

Figure 103 shows the histogram of the melt temperature at tapping for a longer production period at GMH. The temperature is calculated by the dynamic process model after adaption to previous thermocouple measurements.

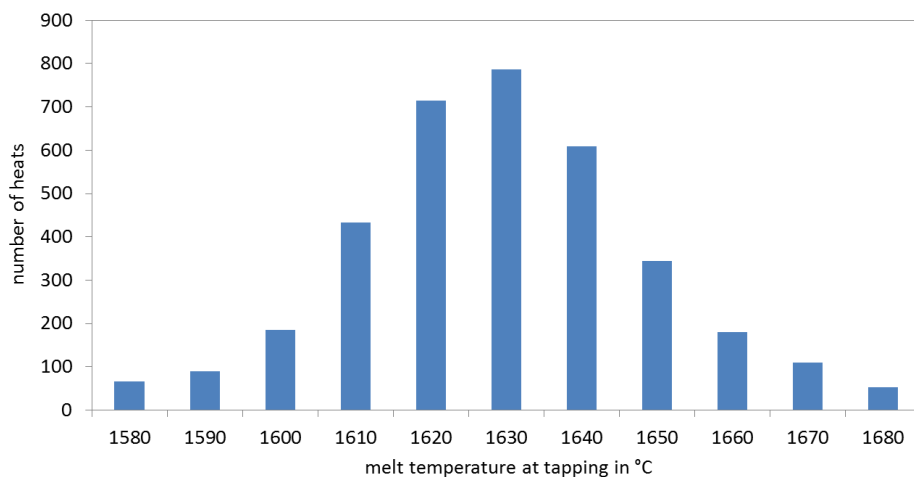


Figure 103: Histogram of melt temperature at tapping for GMH

The mean melt temperature at tapping is about 1630 °C but a wide scattering between 1600 °C and 1660 °C is obvious. In some quality dependent cases it is beneficial to build up an energy buffer before EAF tapping, if the addition of larger amounts of alloy materials at tapping or during secondary metallurgy treatment is necessary.

Figure 104 shows the histogram of the carbon content in the steel at tapping. For more than 20 % of the produced heats at GMH a steel sample is taken shortly before tapping and analysed in the laboratory.

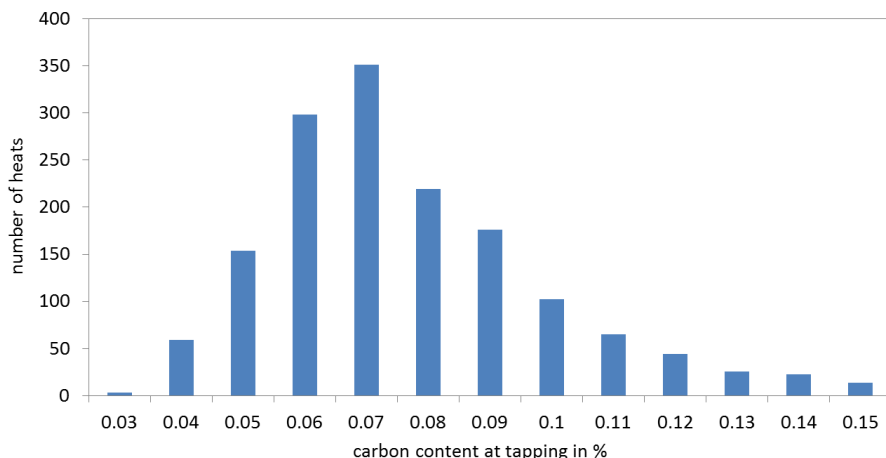


Figure 104: Histogram of carbon content at tapping for GMH

The mean carbon content in the steel at tapping is about 0.07 %. There is also a wide scattering of the content between 0.04 % and 0.1 %, whereby the contribution is very asymmetric. The quality-dependent carbon limit has to be adjusted in the EAF as its content cannot be further decreased during secondary metallurgy treatment.

The materials which are added during the tapping process depend on the produced steel quality. They comprise alloying and deoxidation materials as well as slag formers to prepare the further secondary metallurgy treatment. The total amount of material additions during tapping can vary between 1.5 and 8 t. For each material a fixed cooling factor defines its effect on the energy balance. Furthermore the reaction enthalpy occurring due to the addition of deoxidation materials has to be taken into account. The temperature loss according to the quality-dependent material additions can be estimated and considered for the adjustment of the aim tapping temperature. As described under Task 4.1 the end-point control is based on the aim tapping temperature and carbon content to reach both at the same time.

2.2.5 WP 5: Extensive plant trials for online test and evaluation of process control tools

Task 5.1 Long term plant trials for validation of the on-line adaptive control tools

The different components of the adaptive control tools, which have been set up in WP 4, have been tested in long term plant trials. The evaluated time period covers about 2500 heats produced in 2017.

Control of chemical energy input

The adaptive control function regarding chemical energy input, which was described under task 4.1, has been tested after the full integration of the extended dynamic process model within the Level-2 control system at the GMH furnace. With the help of the cluster analysis the scrap load of each basket has been assigned to an appropriate cluster. **Table 12** shows the number of assignments to each cluster together with the results of the off-gas measurements regarding average H₂ and CO content as well as Post-Combustion degree.

Table 12: Mean amounts of CO and H₂ in the off-gas for cluster assignment of the first basket

	# heats	H ₂ / Nm ³	CO / Nm ³	PC-degree / %
All	2339	41	48	51
Cluster 1	247	31	41	57
Cluster 2	1065	42	48	50
Cluster 3	451	42	51	48
Cluster 4	455	41	49	52
Cluster 5	121	45	54	46

The measured off-gas values show that clusters 3 and 5 still have the highest energetic potential, indicated by the rather low value for PC degree. These values are in accordance with the results in Table 4 of task 4.1 and point out the necessity to adapt the operating patterns for overstoichiometric operation of the burners. However, due to a limitation in the overall oxygen supply at the GMH furnace, it was not possible to apply an automatic adjustment of the overstoichiometric oxygen input according to the selected scrap mix cluster within the project duration.

Nevertheless, the efficiency of the injected oxygen into the steel bath to promote the decarburisation during the refining process has been improved significantly within the project duration. In **Table 13** the mean consumption of natural gas, oxygen and blow carbon per ton of liquid steel are listed for 2016 and 2017.

Table 13: Mean natural gas, oxygen and blow carbon consumption together with the achieved carbon content at tapping

	M _G	M _L	M _J	M _N	C _{blow}	C _{steel}
2016 II	3.5	14.4	10.3	9.9	14.2	0.083
2017 I	3.8	14.6	9.0	10.2	13.7	0.081
2017 II	3.9	14.5	7.6	10.4	9.8	0.082

At the turn of years to 2017 a further natural gas burner with integrated oxygen jet-function has been installed at the furnace of GMH. The natural gas consumption M_G has been increased by about 10 % and also the post-combustion oxygen M_N has been enhanced, whereas the oxygen consumption of the door lances M_L has been kept on a constant level. Significant savings have been achieved for the jet-oxygen M_J of the burners, although there was one burner more in operation. Besides the reduction of jet-oxygen also the consumption of blow carbon C_{blow} has been decreased by one third. These values indicate the substantial improvement of the decarburisation efficiency

during the refining phase of the EAF treatment, as the achieved carbon content at tapping C_{steel} , shown in the last column of Table 13, has been maintained on a constant level.

Monitoring of meltdown process and determination of optimal time for charging the second basket

The determination of the optimal time for charging the second scrap basket based on monitoring of the meltdown progress and the estimated scrap basket filling levels, as described under Tasks 1.3 and 3.3, has been validated with the same data basis. For this evaluation only the notifiable long disturbances in charging of the second scrap basket have been taken into account. About 10 % of the investigated heats have been disturbed by a long flattening of the second scrap basket.

As the automatic basket filling detection by image analysis was temporarily out of order during the evaluated period, the filling levels of the scrap baskets were estimated with the help of the calculated effective bulk density of each scrap type. As shown in task 1.3 these values can be determined with an error standard deviation of about 10 %.

The two histograms in **Figure 105** show the calculated lack of space in the furnace for charging the second basket. The heats where the second basket fits into the furnace are listed in the left diagram, heats with flattening of the second basket are listed in the right one. Negative values mean more free volume than needed, indicating a too late charging of the second basket. Positive values indicate that there was not enough free volume in the furnace for the scrap load of the next basket.

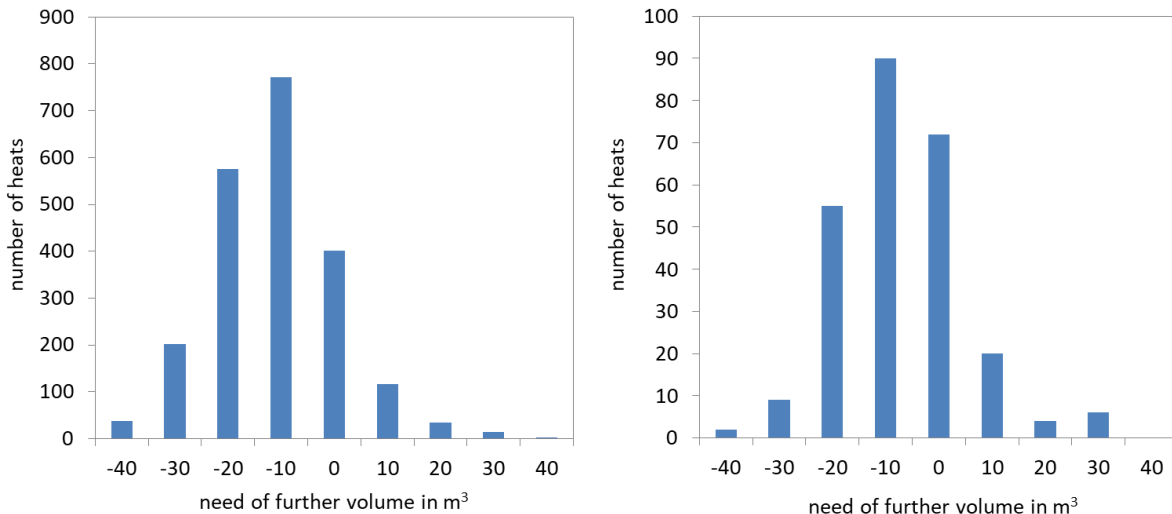


Figure 105: Histograms of calculated lack of volume for heats without or only with short disturbances (left) and where the flattening has led to a notifiable disturbance (right)

For this long time period only the notifiable disturbances were considered. The left histogram of Figure 105 shows that for 86 % of the heats with no notifiable disturbance the model recommendation was correct. The predicted negative volume indicates a fitting of the next scrap basket. When focussing on the about 230 heats with a rather large negative volume higher than 25 m^3 , it was found that in these cases the too late charging of the second basket resulted in an additional electrical energy demand of about 5 kWh/t, due to higher energy losses with less shielding of the arc by the scrap. This additional energy input could have been avoided when following the recommendation for the optimal charging time.

Furthermore this histogram contains some heats with short time flattening events, which were not notified. The investigations in task 4.2 have shown that about 10 % of the heats with a notifiable disturbance are performed with such a short flattening after charging the second basket.

The right histogram of Figure 105 shows that for 40 % of the heats with long disturbances by the need of flattening a positive volume was predicted by the model, which indicates a correct recommendation for a later charging of the second basket. In these cases the prolongation of the tap-to-tap time by about 2 minutes for flattening the scrap in the furnace after charging could have been avoided when following the recommendation for the optimal charging time.

For all heats in the diagrams the scrap basket filing levels were calculated with the help of the effective bulk density of each scrap type. The automatic basket filling detection by image analysis would improve the quality of the model recommendation, as the basket filling levels are estimated with an error standard deviation of about 10 % in comparison to the image analysis.

Control of steel bath level

The control of the steel bath level on the basis of the dip sensor measurements has become an established procedure at the GMH furnace. As shown in **Figure 106** the steel bath level was already nearly constant for the last two furnace campaigns in 2017.

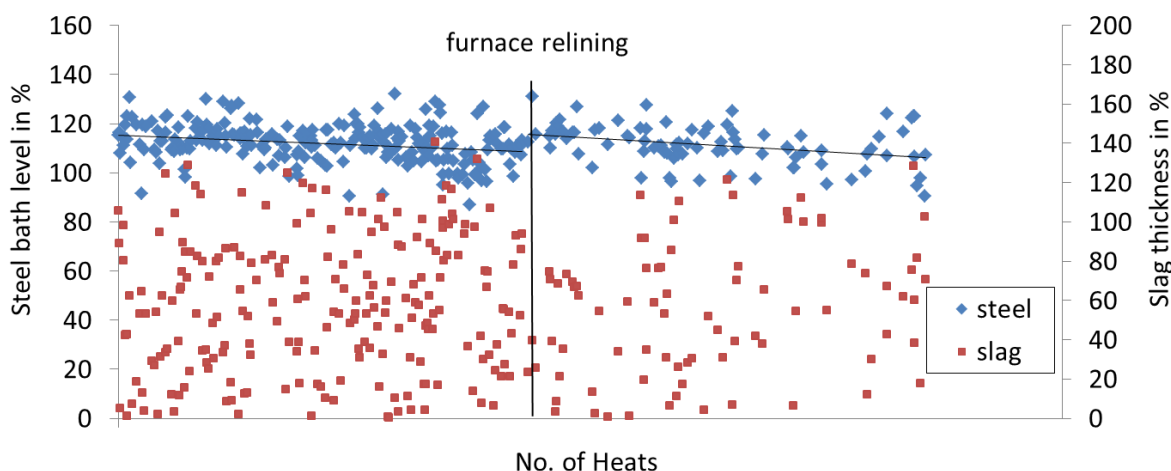


Figure 106: Dip sensor measurements for two furnace campaigns with nearly constant steel bath level

It can be stated that the efficiency improvement in injector oxygen and blow carbon input, which has been described above, can at least partly be explained by the nearly constant bath level and thus constant injection distance of both oxygen and carbon.

Consideration of quality-dependent constraints from secondary metallurgy

The quality-dependent constraints of the secondary metallurgy are considered by the dynamic model calculations for EAF end-point control. With the help of the calculated melt status at EAF tapping and the material additions for deoxidation and alloying, the steel temperature and analysis after tapping in the ladle has been calculated and compared to the first measurements in the ladle furnace. The left diagram of **Figure 107** shows the calculated melt temperature against the first measured one in the ladle furnace. The temperature is predicted with an error standard deviation of about 29 K. The mean duration of the tapping process is about 4 min. The first temperature measurement in the ladle furnace is performed after 35 min. These additional factors of uncertainty explain that the error standard deviation for the melt temperature in the ladle is higher than the one for the calculated temperature before EAF tapping (see Figure 72).

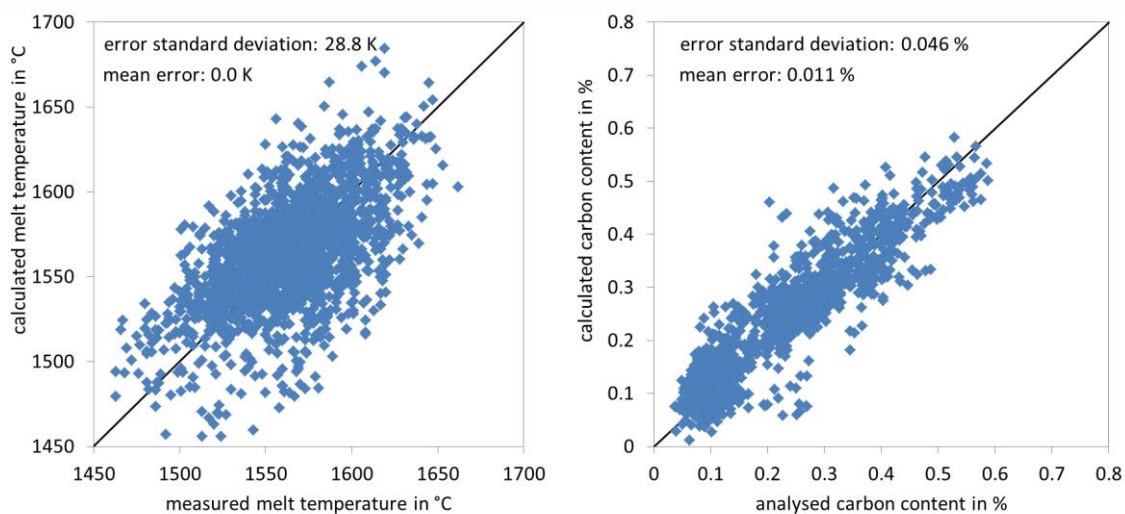


Figure 107: Comparison of calculated and first measured melt temperature (left hand-side) and calculated and first analysed carbon content (right hand-side) in the ladle

The right diagram of Figure 107 shows the calculated carbon content in the steel against the first analysed one in the ladle furnace. The carbon content is predicted with an error standard deviation of 0.046 %. The comparison with the first measurements in the ladle furnace confirms the good model accuracy regarding the calculated melt status at EAF tapping.

Task 5.2 Evaluation of performance of applied measurement techniques with regard to accuracy, availability and acceptance

A **dip sensor** was used to assess the liquid steel level and the slag thickness after deslagging, before EAF tapping. The commercial available Delta Dist sensor was connected to an already existing manipulator. The measurement accuracy for the steel bath level was estimated to be about 2.2 cm (corresponding to a weight accuracy of 2.2 t) and 65 mm for the slag thickness (corresponding to a weight accuracy of 3.3 t). The accuracy in measuring the steel bath level was found to be sufficient to control the bath level at a nearly constant value throughout the complete furnace campaign, as explained under Task 5.1. Using the installation at GMH one dip measurement causes a time delay for the production of about one minute. To reduce the effect on the production, the measurement was performed only for every third heat. Whereas the measurement of the liquid steel level works very reliable, the slag depth measurement is sensitive and sometimes does not provide a reasonable measurement value due to irregularities in the EAF slag. Meanwhile this commercial sensor is also tested and used by other steel shops to monitor the steel bath level in the EAF.

Furthermore the bath level was also monitored by a camera based technique. When the furnace roof is opened after tapping and before charging the first basket of the next heat, an image of the furnace interior with the hot heel is taken. An image analysis detects the borderline between slag and refractory and the distance between the upper furnace edge and the border line is evaluated. A comparison of the bath level before tapping and the **hot heel level** after tapping (taking into account the height change related to the tapping weight) showed a reasonable correlation, indicating a similar accuracy of both techniques. The accuracy of the imaging technique depends on the resolution of the optical system as well as the slag conditions, and how well the border line can be detected. The maintenance effort of this technique is very low, since the camera is well protected in an air cooled protection housing high above the furnace. The camera images are also routinely used by the operating personnel for visual inspection of the furnace interior with respect to slag

coverage, refractory defects and remaining unmolten scrap pieces, and have thus become an important tool for the EAF operators at GMH.

For monitoring of the **deslagging** of the furnace before tapping an IR camera was used with the intention to minimise steel losses. Steel and slag can be distinguished since they have a different emissivity in the IR spectral range, resulting in a lower radiation power of steel compared to slag at the same temperature. From the front view most of the metal is hidden by the slag, because the slag has a lower density and floats on the steel. Therefore the slag has to be monitored from the back and a position beneath the furnace was chosen. The video signal of the IR camera is transferred onto a monitor which is helpful for the operators. However automatic detection of steel running based on image analysis to stop deslagging automatically is a very challenging task since the slag flow is not a compact stream but is usually very fragmented.

The **filling level of the scrap basket** was analysed by two different techniques: a laser scanner and a camera based technique. The trials with installation of the laser scanner were not successful, since the programming and data evaluation was time consuming and complex, and the camera system seemed more promising. Using a conventional CCD camera, images of the scrap baskets in the transfer cars were acquired in the furnace hall before they were taken by the crane. The scrap was detected automatically by image analysis and the height with respect to the upper basket edge was evaluated. The reliability of this system is high and requires little maintenance since the camera is well protected in a protective housing. The accuracy of the image analysis is high and shows a good correlation to operator estimations. The results are more objective compared to the subjective estimation of the different operators. The filling level for each basket is automatically determined and stored for later analysis, and is also provided to a model to determine the optimum time for charging the second basket.

The scrap meltdown behaviour is analysed based on two **vibration sensors** which are installed at the furnace shell at the level of the water cooled panels. It was observed that during meltdown the fraction of unmolten scrap correlated with a decline in the vibration amplitude. The sensors are well protected and are working reliably for about two and a half years now. The vibration measurement gives a valuable indication of the meltdown degree, which can be used to determine the optimal time for charging the second basket, but it is clearly not a precise measurement.

Two **spectrometers** were installed inside a water cooled protection box inside one cooling panel of the furnace. They were used to follow the scrap meltdown progress by detecting the time when the electric arc is not fully covered any more by scrap. However the maintenance and repair effort was too high such that the devices were dismounted. Since the signals were not available for further analysis, the **electrode path** after ignition was used for further analysis and modelling. This distance measurement system is commercially available and is in general permanently installed at the electrode arm of modern EAFs, operating with a high reliability and accuracy. In connection with the vibration measurement and an energy and mass balance calculation, the electrode path was used as input for a model to determine the optimal time for charging the second basket.

Task 5.3 Assessment of benefits of the on-line application of the adaptive EAF process control

The overall benefits of the adaptive EAF process control have been investigated with the help of the average consumption values and the results of the statistical model for calculating the electrical energy demand of arc furnaces, as already described under task 4.1. The energetic performance of the furnace has been evaluated for different time intervals covering the whole time period of the

project. In **Table 14** the average consumption values and the calculated electrical energy demand W_R are compiled for different time periods of the project. Roman numeral one means the first half of a year before the summer break and roman numeral two the second half after the break.

Table 14: Average consumption values and calculated electrical energy demand covering the whole time period of the project

	W_R	W_E	$W_R - W_E$	G_A	g_{scrap}	T_A	tap-to-tap	M_G	M_L	M_J	M_N	C_{blow}
2014 II	385.1	450.5	-65.4	138.1	1097.8	1643.1	59.8	3.4	12.5	10.6	8.1	15.8
2015 II	388.7	463.7	-74.9	137.2	1123.1	1644.0	61.6	3.6	13.8	11.9	9.0	14.6
2016 I	379.8	448.2	-68.4	137.0	1114.8	1642.3	59.7	3.6	14.6	10.6	10.4	16.4
2016 II	383.1	438.3	-55.2	137.4	1103.6	1649.6	57.6	3.5	14.4	10.3	9.9	14.2
2017 I	382.5	440.5	-57.9	136.2	1103.6	1651.9	57.1	3.8	14.6	9.0	10.2	13.7
2017 II	384.7	439.5	-54.8	136.2	1108.3	1653.1	57.0	3.9	14.5	7.6	10.4	9.8

The difference between calculated demand and actually consumed electrical energy $W_R - W_E$ decreases during the progress of the project, which means that the overall energetic performance of the GMH furnace has been improved. But not only the difference between expected and actually consumed electrical energy has been reduced, but also the absolute specific electrical energy consumption has been decreased by about 10 kWh/t of liquid steel.

Besides the energetic performance also the productivity has been improved significantly during the project progression. The tap-to-tap time has been reduced by about 5 % from 60 min to 57 min. This means an increase in production of more than one heat per day.

A further significant process improvement has been achieved regarding the decarburisation during the refining phase. The efficiency of the oxygen injection into the steel bath has been increased with the effect of a reduced consumption of about one third. As described in task 5.1 the achieved carbon content in the tapped steel has been held nearly constant, with significant consumption savings in oxygen and blow carbon.

Of course it cannot be claimed that this overall improvement regarding decrease of energy and resource consumption and increase of productivity can be fully explained by the introduction of the adaptive process control tools, as surely other measures were taken during the project period. Nevertheless the developments of the AdaptEAF project certainly have provided a significant contribution to achieve these savings.

Also it has to be mentioned that not all functions of the adaptive process control have been put into on-line operation up to the end of the evaluation period. As shown above, a further decrease of about 5 kWh/t in electrical energy consumption and of 2 minutes in tap-to-tap time can be achieved when applying the recommendation for the optimal time of charging the second scrap basket.

Task 5.4 Review of the tracking of characteristics of each scrap quality

The characteristics of the different scrap types were determined as described under task 3.2 with the help of statistical tools which were developed in a first version within the previous RFCS project Flexcharge [6]. To improve the reliability of these scrap property values the heat-individually estimated hot heel amount, determined as described under Task 2.1, was additionally taken into account. By this measure, a significant improvement has been achieved in prediction of the metallic yield of each scrap type. To determine the individual metallic yield of each scrap type, conventional statistical calculations use the measured tap weight in the ladle as the aimed liquid steel weight. The heat individual change in the hot heel has been so far not considered as this value was in general not available. The left diagram of Figure 108 shows one example regression calculation without

consideration of a varying hot heel amount. The measured tap weight can be predicted from the effective yield values for the different scrap types with an error standard deviation of 5.2 t. A similar result for the scrap types in use at GMH has already been shown in Figure 65.

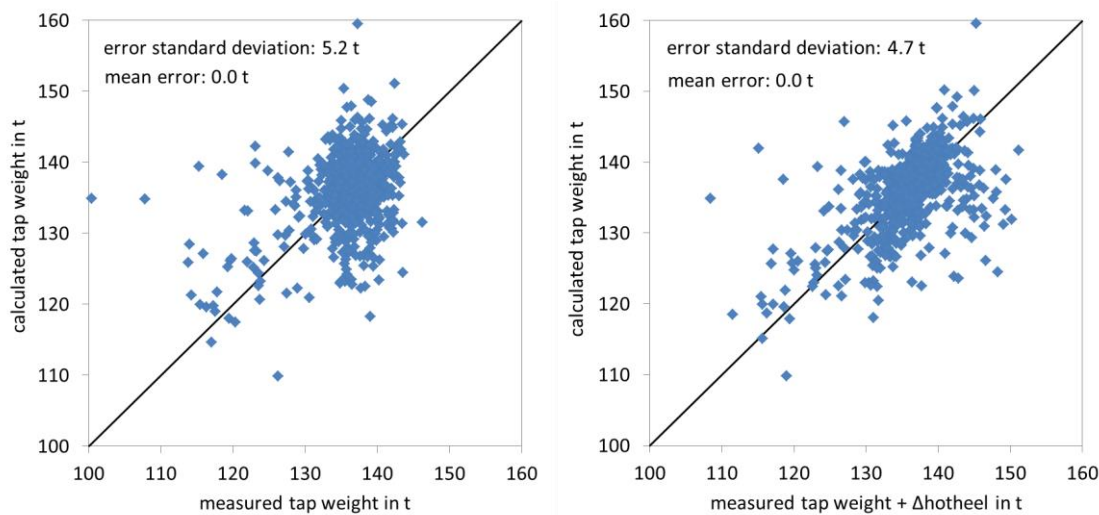


Figure 108: Result of a conventional regression calculation for predicting the measured tap weight (left) and improved calculation considering the change in the hot heel amount (right)

The right diagram of Figure 108 shows the result of the same regression calculation, but here the achieved liquid steel amount is corrected by the heat-individual change in the hot heel amount, as determined by the approach based on the Delta Dist bath level measurement. The error standard deviation for the calculated tap weight has been reduced by 10 %, and especially the misalignment of the values relating to the angle bisector has been reduced significantly, which means that the yield parameters of the individual scrap types can be determined with higher reliability when considering the heat-individual change of the hot heel amount.

The influence of the hot heel amount on the calculation of the element-wise yield of each scrap type has been investigated, too. However it was found that for this calculation it is sufficient to take the analysis of the previous heat with a constant hot heel amount into account, as the variation in the steel composition is not so large. The same applies for the influence of the varying hot heel amount on the heat-individual dynamic energy balance calculation. The temperature of the hot heel at the beginning of a heat is similar to the first measured value after meltdown, and the energy balance, from which the meltdown energy demand of each scrap type is derived, is validated with the help of these measurements.

Task 5.5 Definitions of guidance rules for transfer of the project results for further EAF plants

The main project results concern the development and implementation of new sensors and measurement devices as well as the application of extended process models, for acquisition of additional process information and for use in adaptive EAF process control tools.

The Delta Dist dip sensor for bath level measurement can be easily applied at further EAFs which are already equipped with a lance manipulator for thermocouple measurements and steel sampling. In the meantime this device has already been used in further EAFs for bath level measurement, which is of practical use not only for DC EAFs with a strongly varying hot heel amount.

The camera system for monitoring the furnace interior was found to be very useful for inspection of the furnace regarding refractory wear, slag shielding and unmolten scrap. Its installation and

maintenance is easy when an appropriate distance of the protected cameras to the furnace can be ensured.

The imaging system for detection of the scrap basket filling degree was found to be an important tool for determining the optimal time for charging the second scrap basket. If a free view on the basket volume can be ensured, it can be easily installed and maintained, either in the furnace hall or at the scrap yard.

The follow-up of the scrap meltdown process can be performed in a simple and reliable way with the help of an energy and mass balance model. Additionally the information from the measured electrode path can be evaluated, which is normally assessed at a modern EAF by a distance measurement. An additional vibration measurement at the furnace shell provides further information, but needs of course a higher installation and maintenance effort.

Finally, the developed and extended statistical models for determining the scrap type properties and the dynamic process model are already applied at several EAFs. For transfer to further plants, a configuration to the furnace equipment and the available input data as well as an adaptation of the model parameters is required. However, this adaption procedure is a rather simple task and is already supported by self-adaptive algorithms.

The evaluation of the results of the statistical model showed that the consideration of a heat-individual amount of the hot heel, as determined with the help of the Delta Dist measurement, allows to improve especially the accuracy and reliability in determining the metallic yield of the different scrap types. The error standard deviation can be reduced by about 10 %, and a systematic error can be removed almost completely. However, as described under Task 5.4, no significant improvement of the accuracy in determining the element-wise yield of the scrap types and also of the dynamic process model for predicting the melt temperature was found.

On the basis of applicable measurement systems and process models also the corresponding process control tools for chemical energy input, optimal charging time for the second scrap basket as well as end-point control and bath level control can be easily applied at further EAF plants.

In general it can be stated that the application of new sensors and measurement devices as well as of the extended process models, for acquisition of additional process information and for use in adaptive EAF process control tools, is not limited to DC EAFs. The technologies developed within the project can be easily transferred to AC EAFs, as they are not based on any plant components or functions available only at DC furnaces.

Finally the required investment and operating costs for the measurement equipment and process models were compared to the expected benefits in terms of reduced production costs.

For implementation of the bath level measurement based on the Delta Dist sensor, a lance manipulator for temperature measurement and sampling, which is already installed at modern EAFs, has to be revamped. For this measure, costs of about 35.000 € have to be considered. The costs for one Delta Dist probe are around 10 €.

The costs for the camera system to monitor the furnace interior are around 40.000 €, and for monitoring the basket filling degree about 10.000 €. The installation and maintenance costs of the vibration sensors to support the monitoring of the scrap meltdown behaviour are around 50.000 €.

The consideration of the new measurement information within existing dynamic process models induces only costs for software adaptation which can be estimated to be around 10.000 €.

Thus the CAPEX costs for investments needed for application of the different measures sum up to around 115.000 €, and the OPEX costs for maintenance and additional probes sum up to around 40.000 € /a.

These OPEX/CAPEX costs have to be compared to the cost savings in electrical energy, which are estimated to 95.000 €/a, and to the cost savings due to increased productivity, which are estimated to 200.000 €/a. Thus the amortisation time for the total costs of all measures performed within the project is well below one year.

3. Final conclusions

Within the project, different novel and existing sensors were installed and applied at the EAF of GMH to acquire additional process information. For determination of steel, hot heel and slag amounts a dip sensor to measure steel and slag levels was implemented and enabled for permanent operation. Due to the measurement duration of about 1 min, the sensor was used before tapping only for every third heat, which nevertheless allows following the evolution of the hot heel level. In addition an imaging system to monitor the bath level in the furnace after tapping was installed, which can be used for determination of the hot heel amount for every heat. In combination with a simple refractory wear model, the results of the dip sensor measurement and the image analysis system were used to determine and to follow the amount of the hot heel. The results of both measurement systems were found to be comparable.

The overflow of liquid steel and slag via the slag door was monitored with the help of an IR imaging system. Steel carry-over during deslagging can in principle be detected to minimise yield losses. However the results of an appropriate image analysis for metal detection in the slag stream were not reliable enough to create a signal for automatic back-tilting of the furnace.

To estimate the filling level of the scrap baskets just before charging into the EAF, a camera system together with an automated image analysis was developed and applied. The image analysis provides objective results and compared well with operator estimations. An alternative detection of the filling level via a laser scanner turned out to be not reliable enough and implementation was too time consuming. From the image analysis the effective density of the scrap mix and the different scrap types were derived.

For monitoring of the scrap melting progress, a vibration sensor system was installed at the furnace shell and used for long term campaigns. Based on the sensor signals appropriate indexes were defined to characterise the meltdown behaviour of the charged scrap mix. To support this work, further process data like the electrode path and offgas analysis values were evaluated. In addition a spectrometer system was installed in a water cooled box in one cooling panel of the furnace for monitoring of the arc shielding and thus scrap meltdown behaviour. Despite promising results it was later removed due to high maintenance and repair effort.

The additional process information coming from the measurement systems and the corresponding signal evaluation have been integrated in the EAF process data base at the GMH furnace for modelling and validation purposes. Existing dynamic and statistical process models were enhanced on the basis of the additional process information, especially with respect to a slag balance calculation. Furthermore a new model approach was developed to assess the scrap melting behaviour on the basis of additional process information coming from the evaluation of vibration measurement, electrode path, offgas values as well as energy and mass balance model calculations. Finally, methods to display the new process information and the enhanced model calculations to the plant engineers and the operators were developed.

Several adaptive process control tools based on the newly implemented and already existing measurement systems and advanced process models were developed, applied and tested at the GMH furnace. Adapted operating diagrams for control of the chemical energy input depending on the actually charged scrap mix were defined, and a strategy for end-point control for steel temperature and carbon content based on the dynamic model calculations was developed which also considers quality dependent restrictions. A procedure to determine the optimal point of time for charg-

ing the second scrap basket based on the evaluation of vibration measurement, electrode path and energy and mass balance model calculations was set up and validated. The steel bath level can be controlled to a nearly constant value on the basis of the Delta Dist dip sensor measurement.

Finally plant trials with extensive process data collection over a longer period of time were performed and used for on-line test and validation of the enhanced process control tools. It was found that significant savings in electrical and chemical energy consumption of about 10 kWh/t can be achieved, and the productivity of the EAF can be improved by decreasing the tap-to-tap time by about 3 minutes. Consequently the production costs can be reduced by around 300.000 €/a, which means that the amortisation time for the measures needed to enhance the EAF process control is well below one year.

The accuracy, reliability and acceptance of the new measurement systems was evaluated, and guidelines for transfer of the project results to further EAF plants have been defined.

4. Exploitation and impact of the results

Actual applications

Due to the nature of a Pilot & Demonstration project, new sensors, measurement systems and dynamic on-line models were already applied during the project duration under the industrial conditions of the DC EAF of GMH. Both sensors and models can easily be applied to other EAF plants, as explained in detail under WP 5.

Technical and economic potential for the use of results

Applying the developed adaptive on-line control tools allows to adapt the operating conditions of the EAF process to the strongly varying properties of the actually charged materials. The economic potential for the use of the project results lies mainly in savings of chemical and electrical energy input as well as in the improvement of productivity by reduced tap-to-tap times.

Publications and conference presentations

Parts of the project results regarding the EAF slag balance calculation have been included in a paper submitted for the European Electric Steelmaking Conference (EEC 2016), which took place in Venice from 25th to 27th of May 2016. The paper is entitled "Modelling of EAF slag properties for improved process control". Authors are R. Pierre and B. Kleimt (BFI), L. Schlinge (GMH) and I. Unamuno and A. Arteaga (Sidenor).

First overall project results were presented in a paper at the 3rd European Steel Technology & Application Days (ESTAD 2017), held in Vienna from 26th to 29th of June 2017. The paper is entitled "Adaptive EAF online control based on innovative sensors and comprehensive models". Authors are T. Rekersdrees, H. Snatkin and L. Schlinge (GMH), R. Pierre, B. Kleimt and T. Kordel (BFI), and S. Gogolin and V. Haverkamp (HSU).

Patents

Patents have not been submitted.

Any other aspects concerning the dissemination of results

Results of the project have been disseminated during seminars and workshops in the framework of the VALEAF Dissemination project [12].

5. List of figures

Figure A:	Sketch and measurement procedure of the Delta Dist sensor	6
Figure B:	View from the position of camera no. 3 into the furnace shell with hot heel level	6
Figure C:	Position of IR camera for slag tapping supervision and example IR image	7
Figure D:	Image of scrap baskets with detection of filling degree	7
Figure E:	Positions and mounting of the vibration sensors at the GMH furnace	8
Figure F:	Observation of the meltdown progress using a spectrometer system	8
Figure G:	Follow-up of liquid steel and hot heel amount at the GMH furnace	9
Figure H:	Hot heel level measurement with Delta Dist sensor and image analysis	9
Figure I:	Evolution of the remaining slag in the furnace for a trial campaign	9
Figure J:	Vibration Levels (left), spectrometer signal (right) and Active Power during an EAF melt	10
Figure K:	Vibration level for one heat and mean value level during first basket meltdown process	10
Figure L:	Vibration Level and Electrode Path during First Basket Meltdown Process	11
Figure M:	Calculated Cr and slag Cr_2O_3 , CaO and FeO content evolution for example heat of GMH	11
Figure N:	Two point scrap index model and correlation to energy balance	12
Figure O:	Display for scrap basket filling level and model results	12
Figure P:	Evolution of end-point control for tapping temperature and steel carbon content	13
Figure Q:	Histograms of calculated lack of volume for heats where the second basket fits into the furnace (left) and where the scrap has been flattened after charging (right)	13
Figure R:	Dip sensor measurements for three furnace campaigns at GMH	14
Figure 1:	Photo and sketch of the Delta Dist Dip sensor of Heraeus Electronite [1]	18
Figure 2:	Measurement procedure with the Delta Dist sensor	18
Figure 3:	Measurement of the slag level by electrical contact at the tip of the Delta Dist sensor	19
Figure 4:	Measurement of the liquid steel level by eddy current change in a coil inside the sensor	19
Figure 5:	Operating screen for the lance manipulator at the GMH furnace	20
Figure 6a:	Plant trials with Delta Dist measurement of steel bath (blue) and slag level (red) for consecutive GMH heats	21
Figure 6b:	Plant trial with 4 consecutive Delta Dist measurements of steel bath (blue) and slag level (red) for one GMH heat	16
Figure 7:	Schematic drawing of the EAF with the camera positions	22
Figure 8:	Camera at position no. 3 installed above the EAF	22
Figure 9:	View into the open and empty furnace with hot heel by all three cameras.	23
Figure 10:	View from the position of camera no. 3 down to the furnace shell with hot heel. Colour lines from image analysis are superimposed	24
Figure 11:	View of camera no. 3 into the open furnace before and after charging of the second basket for two different heats.	24
Figure 12:	IR image during slag tapping without steel encountered	25
Figure 13:	IR image during slag tapping with significant steel overflow	25
Figure 14:	Previous position (from the front) and improved position (from the side) of IR camera for monitoring of steel running during slag tapping	26
Figure 15:	Images of IR camera during deslagging: only slag (left), slag accompanied by steel (right)	26
Figure 16:	Timing of steel / slag sampling for a GMH example EAF heat	27
Figure 17:	Functional principle of Bulkscan® Sensor [2] and installation in the scrap hall of GMH	28
Figure 18:	Schematic drawing of the scrap filling level measurement setup with line scanner	29
Figure 19:	Image of a scrap basket on the transfer vehicle with loaded scrap	30
Figure 20:	Manual adaption of an ellipse to the edge of a scrap basket (left) and 3D plot of the correlation between image and reference ellipse (right). The sharp and high peak in the plot denoted the centre of the basket which can be determined.	30
Figure 21:	Images of the scrap basket with overlay for a cone shaped scrap pile.	31
Figure 22:	Scrap basket filling level of images in Figure 19 by novel image analysis	31

Figure 23:	Comparison of image analysis results and operator estimations for the scrap basket filling level	32
Figure 24:	Mean density of the loaded scrap in the basket versus the loaded scrap mass for the first and the second basket	32
Figure 25:	Estimated basket filling level based on the effective scrap density of the individual loaded scrap types versus the detected basket filling level	33
Figure 26:	Vibration Sensor Configuration at an AC Furnace	34
Figure 27:	Vibration Sensor Installation Positions at the Main Cooling Water Pipes	35
Figure 28:	Schematic Top View of Vibration Sensor Positions at the GMH DC Furnace	35
Figure 29:	Generally Possible Positions for New Vibration Sensors	36
Figure 30:	Design Principle of a Shear-Type Vibration Sensor	36
Figure 31:	Temporary Vibration Measurement Setup	37
Figure 32:	Vibration Measurement Signals of the First 10 Minutes into the Meltdown Process	38
Figure 33:	Long-Term Installation of the Vibration Sensors at the Furnace Vessel	38
Figure 34:	Calibration of Vibration Sensors	39
Figure 35:	Signal Routing inside the Vibration Measurement Room	40
Figure 36:	Observation of the Meltdown progress using a Spectrometer System	40
Figure 37:	Process and Spectrometer Data during a Two-Basket Heat	41
Figure 38:	Spectra of a High Resolution Spectrometer, Installed in the Upper Position	42
Figure 39:	Spectra of a Broadband Spectrometer, Installed in the Lower Position (with Clipping Effect)	42
Figure 40:	Spectra of a Broadband Spectrometer, Installed in the Lower Position	43
Figure 41:	Original Design of a Lens Adapter	44
Figure 42:	Geometric models of lens adapters for use of spectrometers at the GMH EAF	44
Figure 43:	Subdivision of the vessel volume of the GMH furnace into an upper and bottom part	46
Figure 44:	Histogram of measured steel bath level (left) and estimated liquid steel weight (right)	47
Figure 45:	Follow-up of liquid steel and hot heel amount for one trial campaign at GMH	47
Figure 46:	Images of camera 1 and 2 of the inner furnace with results of image analysis	48
Figure 47:	Schematic drawing of the electric arc furnace illustrating the height as measured by the Delta Dist sensor before tapping (left) and the filling level as determined by image analysis after tapping (right)	48
Figure 48:	a) Dip sensor measurements for selected heats and b) comparison of hot heel level based on dip sensor measurements and image analysis from two different cameras (NO, NW)	49
Figure 49:	Histogram of the calculated slag weight for the examined heats at GMH	50
Figure 50:	Histogram of the measured slag weight for the examined heats at GMH	50
Figure 51:	Histogram of the variation in the slag amount for the examined heats at GMH	51
Figure 52:	Evolution of the remaining slag in the furnace for a consecutive sequence of 30 heats	51
Figure 53:	Evolution of the remaining slag in the furnace for a trial campaign	52
Figure 54:	Vibration Levels and Active Electric Power during a Melt	53
Figure 55:	Correlation of the Vibration Level Signals Picked Up in Different Directions of Sensitivity	54
Figure 56:	Vibration Level Trend goes along with Fine Coal Injection	55
Figure 57:	Vibration level during one complete heat	55
Figure 58:	Distribution of mean vibration level during first basket meltdown process	56
Figure 59:	Typical Vibration and Irradiance Level during one complete Meltdown-Cycle	57
Figure 60:	Vibration Level and Electrode Path during First Basket Meltdown Process	57
Figure 61:	Correlation of vibration level vs. electrode path	58
Figure 62:	Calculated volume of CO (left diagram) and H ₂ (right diagram) against measured one during the meltdown process of the first scrap basket	59
Figure 63:	Correlation between amounts of CO and H ₂ in the off-gas during the meltdown process of the first scrap basket	59
Figure 64:	Data exchange network at GMH	60
Figure 65:	Determination of the scrap-individual metallic yield at GMH	62
Figure 66:	Determination of the scrap-individual yield parameters for the Cu content at GMH	63
Figure 67:	Determination of the scrap-individual Cr content at GMH	63
Figure 68:	Evolution of the metallic yield over time for scrap type E5M	64
Figure 69:	Evolution of the Cu content over time for scrap type E5M	64
Figure 70:	Structure of the BFI dynamic process model for the EAF	65

Figure 71: Calculated melt temperature and comparison with measurements for one example heat of GMH	66
Figure 72: Model accuracy of melt temperature calculation for GMH (Left: First measurement; Right: Further measurements after adaption to first one)	66
Figure 73: Calculated carbon and oxygen content evolution for one example heat of GMH	67
Figure 74: Model accuracy of steel oxygen (left-hand side) and carbon content (right-hand side)	67
Figure 75: Calculated slag and steel weight evolution for one example heat of GMH	68
Figure 76: Calculated CaO and FeO content evolution for one example heat of GMH	68
Figure 77: Model accuracy of slag CaO (left-hand side) and FeO content (right-hand side)	69
Figure 78: Calculated Cr and Cr ₂ O ₃ content evolution for one example heat of GMH	69
Figure 79: Model accuracy of Cr content in the steel (left-hand side) and Cr ₂ O ₃ content in the slag (right-hand side)	70
Figure 80: Follow-up of the hot heel amount and measured weights derived from Dip sensor measurements for a longer time period	71
Figure 81: Mean vibration levels at the end of first basket meltdown process vs. first basket filling level	73
Figure 82: Exemplary States of Meltdown Progress Described by the Two-Point Solid Scrap Model	75
Figure 83: Correlation of Scrap basket filling level vs. electrode Path	76
Figure 84: Correlation of Electrode Path vs. Vibration Level	76
Figure 85: Trends of the Two-Point Scrap-Level-Model at low mean vibration levels	77
Figure 86: Trends of the Two-Point Scrap-Level-Model at high mean vibration levels	77
Figure 87: Extension of the two point scrap index model	78
Figure 88: Results of two filling level models at the end of Basket 1 meltdown process vs. individual heats during two different measurement campaigns	79
Figure 89: Correlation of both model estimations during two different measurement campaigns	79
Figure 90: Display of scrap basket with detected filling degree in the EAF control room of GMH for two different examples	80
Figure 91: Display of the LabView On-Line Vibration Analysis-Software	80
Figure 92: Model-Development Tab in On-Line Vibration Analysis-Software	81
Figure 93: Display in the furnace control room	82
Figure 94: User interface of Level-2 process control system at the EAF of GMH	82
Figure 95: Evolution of end point control for reaching the aim tapping temperature and steel carbon content simultaneously	86
Figure 96: Prediction of furnace filling level after charging of second basket vs. individual heats	87
Figure 97: Prediction of furnace filling level after charging of second basket vs. individual heats with flattening of second basket	87
Figure 98: Prediction of furnace filling level after charging of second basket vs. individual heats	88
Figure 99: Prediction of furnace filling level after charging of second basket vs. individual heats with flattening of second basket	88
Figure 100: Prediction of furnace filling level after charging of second basket vs. individual heats with short flattening of second basket	88
Figure 101: Histograms of calculated lack of volume for heats where the second basket fit into the furnace (left) and where the scrap has been flattened after charging (right)	89
Figure 102: Dip sensor measurements for three furnace campaigns at GMH	90
Figure 103: Histogram of melt temperature at tapping for GMH	90
Figure 104: Histogram of carbon content at tapping for GMH	91
Figure 105: Histograms of calculated lack of volume for heats without or only with short disturbances (left) and where the flattening has led to a notifiable disturbance (right)	93
Figure 106: Dip sensor measurements for two furnace campaigns with nearly constant steel bath level	94
Figure 107: Comparison of calculated and first measured melt temperature (left hand-side) and calculated and first analysed carbon content (right hand-side) in the ladle	95
Figure 108: Result of a conventional regression calculation for predicting the measured tap weight (left) and improved calculation considering the change in the hot heel amount (right)	98

6. List of tables

Table 1:	Calculated effective bulk density for some often used scrap types	33
Table 2:	Model accuracy regarding slag components.....	70
Table 3:	Cluster analysis of the scrap load for the first basket.....	72
Table 4:	Mean amounts of CO and H ₂ in the off-gas for clustered scrap load of the first basket	72
Table 5:	Analysis of mean vibration level and charged scrap cluster.....	73
Table 6:	Cluster analysis of the scrap load for the second basket.....	74
Table 7:	Mean amounts of CO and H ₂ in the off-gas for clustered scrap load of the second basket	74
Table 8:	Analysed and expected off-gas composition of first scrap basket	83
Table 9:	Analysed and expected off-gas composition of second scrap basket.....	84
Table 10:	BFI formula for electrical energy demand of arc furnaces	84
Table 11:	Average input values of GMH heats for calculation of electrical energy demand	85
Table 12:	Mean amounts of CO and H ₂ in the off-gas for cluster assignment of the first basket	92
Table 13:	Mean natural gas, oxygen and blow carbon consumption together with the achieved carbon content at tapping	92
Table 14:	Average consumption values and calculated electrical energy demand covering the whole time period of the project.....	97

7. List of References

- [1] Internal brochure from Heraeus Electro Nite: The Delta Dist L Sensor, 2006
- [2] Homepage Fa. Sick www.sick.com
- [3] Dittmer, B.; Krüger, K. et al.: Structure-Borne Sound Assisted AC-EAF Power Control. METEC InSteelCon, EECR Steel, Düsseldorf 2011
- [4] Haverkamp, V. et al.: Spectrometer-Based Real-Time Measurement of the Electric Arc Radiation in a DC-EAF. 30th Journées Sidérurgiques Internationales, Paris 2012, France
- [5] Deng, J.; Dettmer, B. et al.: Continuous Off-Gas Analysis System TETHYS-GASCON at the DC-Electric Arc Furnace of GMH. METEC InSteelCon, EECR Steel, 2011
- [6] RFCS-CT-2007-00008: "Cost and energy effective management of EAF with flexible charge material mix FLEXCHARGE", 7/2007 - 6/2010
- [7] ECSC 7210-PR/328 "Development of operating conditions to improve chemical energy yield and performance of dedusting in airtight EAF" 7/2002 - 6/2005
- [8] RFS-CR-03031 "Dynamic control of EAF burners and injectors for oxygen and carbon for improved and reproducible furnace operation and slag foaming" 9/2003 - 2/2007
- [9] Köhle, S.: Improvements in EAF operating practices over the last decade. Proc. 57th Electric Furnace Conference, Pittsburgh 1999, p. 3-14
- [10] Köhle, S.: Recent improvements in modelling energy consumption of electric arc furnaces. Proc. 7th European Electric Steelmaking Conf., Venice, 2002, p. 1.305 – 1.314
- [11] Improving the productivity of electric arc furnaces. Final Report for ECSC Project 7210-PR/132 (1999-2002), Report EUR 20803, 2003
- [12] RFSR-CT-2014-0002: "Valorisation and dissemination of EAF technology" (VALEAF), 7/2014 – 12/2015

Getting in touch with the EU

In person

All over the European Union there are hundreds of Europe Direct information centres. You can find the address of the centre nearest you at: https://europa.eu/european-union/contact_en

On the phone or by email

Europe Direct is a service that answers your questions about the European Union. You can contact this service:

- by freephone: 00 800 6 7 8 9 10 11 (certain operators may charge for these calls),
- at the following standard number: +32 22999696 or
- by email via: https://europa.eu/european-union/contact_en

Finding information about the EU

Online

Information about the European Union in all the official languages of the EU is available on the Europa website

at: https://europa.eu/european-union/index_en

EU publications

You can download or order free and priced EU publications at:

<https://publications.europa.eu/en/publications>. Multiple copies of free publications may be obtained by contacting Europe Direct or your local information centre (see https://europa.eu/european-union/contact_en).

EU law and related documents

For access to legal information from the EU, including all EU law since 1952 in all the official language versions,

go to EUR-Lex at: <http://eur-lex.europa.eu>

Open data from the EU

The EU Open Data Portal (<http://data.europa.eu/euodp/en>) provides access to datasets from the EU. Data can be downloaded and reused for free, for both commercial and non-commercial purposes.

The objective of the pilot and demonstration project AdaptEAF was to complement modern EAF process control by integrating novel sensor data and advanced process modelling tools, and to test and evaluate this adaptive EAF process control under industrial conditions at the 140 t DC Electric Arc Furnace of Georgsmarienhütte (GMH).

Novel sensors were installed at the EAF of GMH, aiming to provide additional process information for online control. For determination of steel, hot heel and slag amounts a dip sensor to measure steel and slag levels was implemented, and an imaging system to monitor the bath level in the furnace was installed. An imaging system was also used to estimate the filling level of the scrap baskets. Vibration sensors at the furnace vessel were applied to monitor the scrap melting progress.

The additional process information was integrated in the EAF process data base and operator display and used as inputs for extension of process models and development of control tools. Adapted operating diagrams for control of the chemical energy input depending on the actually charged scrap mix were defined, and quality dependent strategies for end-point control were developed. A procedure to determine the optimal point of time for charging the second scrap basket was set up and validated. The steel bath level is controlled on the basis of the dip sensor measurement. Finally plant trials for online test and validation of the enhanced process control tools have been performed and evaluated in terms of achieved savings in energy input and treatment time.

Studies and reports

